Ollscoil na hÉireann, Corcaigh

National University of Ireland, Cork

ucc

Coláiste na hOllscoile Corcaigh, Éire
University College Cork, Ireland

CT Dose Optimization with Model Based Iterative Reconstruction

Thesis presented by

Fiachra Gerard Moloney

MB BCh BAO, BMedSc, MRCPI,

FFR RCSI, FRCPC, EDiR

For the degree of

Doctor of Medicine

University College Cork

School of Medicine

Head of School: Professor Fergus Shanahan

Supervisors: Professor Michael Maher, Dr. Owen O' Connor

January 2019

Table of Contents

Chapter III

Low-dose carotid CT angiography using pure iterative reconstruction

Chapter IV

Low-dose CT imaging of the acute abdomen using model based iterative reconstruction: a prospective study

Chapter V

Low-dose chest CT using pure iterative reconstruction at chest radiography dose levels: a prospective study in patients with cystic fibrosis undergoing treatment with Ivacaftor (Kalydeco)

Chapter VI

Declaration

This is to certify that the work I am submitting is my own and has not been submitted for another degree, either at University College Cork or elsewhere. All external references and sources are clearly acknowledged and identified within the contents. I have read and understood the regulations of University College Cork concerning plagiarism.

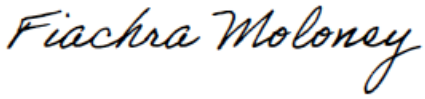

Publications Arising From This Thesis

1. Low-dose CT imaging of the acute abdomen using model-based iterative reconstruction: a prospective study. **Moloney F**, James K, Twomey M, Ryan D, Grey TM, Downes A, Kavanagh RG, Moore N, Murphy MJ, Bye J, Carey BW, McSweeney SE, Deasy C, Andrews E, Shanahan F, Maher MM, O'Connor OJ. *Emerg Radiol*. 2018 Nov 17.
2. Determination of a suitable low-dose abdominopelvic CT protocol using model-based iterative reconstruction through cadaveric study. **Moloney F**, Twomey M, Fama D, Balta JY, James K, Kavanagh RG, Moore N, Murphy MJ, O'Mahony SM, Maher MM, Cryan J, O'Connor OJ*. J Med Imaging Radiat Oncol.* 2018 Oct;62(5):625-633.
3. Low-dose carotid computed tomography angiography using pure iterative reconstruction. **Moloney F**, Murphy KP, Twomey M, Crush L, Canniffe EM, McLaughlin PD, Moore N, O'Keeffe M, O'Neill S, Manning BM, Wyse G, Fanning N, O'Connor OJ, Maher MM. *J Comput Assist Tomogr.* 2016 Sep-Oct;40(5):833-9. PMID: 27331923.

Acknowledgements

I wish to sincerely thank my supervisors and colleagues, Professor Michael M Maher and Dr Owen J O'Connor for their time and help in undertaking this research thesis. I am also very grateful to Ms Marian Bourke for her assistance and dedication to UCC radiology.

I would also like to give a special mention to our two committed research radiographers at Cork University Hospital, Niamh Moore and Mary-Jane Murphy, without whose dedication, good will and patience, none of this research would have been possible.

I am also very grateful to Ms Jackie Bye and her CT specialist colleagues at General Electric Healthcare for their invaluable advice with regard to protocol design and image acquisition.

Several of my radiology colleagues have also been of great help to me. I would like to give a special thanks to Doctors Sean McSweeney, Kevin Murphy, and Lee Crush. In addition, Tyler Grey and Daniel Fama were also of great assistance. Many thanks to you all.

I am very grateful to my clinical colleagues Professor Fergus Shanahan, Dr Barry Plant and the General Surgeons of Cork University Hospital for assisting with patient recruitment. Their assistance was essential to completion of this thesis.

I would also like to thank the Consultant Radiologists of Cork University and Mercy University Hospitals for their help, advice and guidance during my time on the Diagnostic Radiology training scheme. Finally, I would like to express my eternal gratitude to my wife and colleague Maria, and to my beautiful daughter Muireann, for their never-ending love and support.

Abbreviations

AEC	**Automated exposure control**
ALARA	**As low as reasonably achievable**
ASiR/ASIR	**Adaptive Statistical Iterative Reconstruction**
BMI	**Body mass index**
CF	**Cystic fibrosis**
CD	**Conventional dose**
CED	**Cumulative effective dose**
cm	**Centimetre**
cm^2	**Centimetre squared**
CNR	**Contrast-to-noise ratio**
CAT	**Computed axial tomography**
CCA	**Common carotid artery**
CT	**Computed tomography**
CTA	**Computed tomography angiography**
$CTDI_{vol}$	**Computed tomography dose index for the imaged volume**
DLP	**Dose-length product**
ED	**Effective dose**
FBP	**Filtered back projection**
FOV	**Field of view**
Gy	**Gray**
HU	**Hounsfield unit**

ICRP	**International Commission on Radiological Protection**
ICA	**Internal carotid artery**
IR	**Iterative Reconstruction**
kV	**Tube voltage**
LD	**Low-dose**
mA	**Tube current**
MBIR	**Model-Based Iterative Reconstruction**
MDCT	**Multi detector computed tomography**
mGy	**Milligray**
mGy.cm	**Milligray-centimetre**
MRA	**Magnetic resonance angiography**
MRI	**Magnetic resonance imaging**
mSv	**Millisievert**
PFTs	**Pulmonary function tests**
RERF	**Radiation Effects Research Foundation**
ROI	**Region of interest**
SD	**Standard Deviation**
SNR	**Signal to noise ratio**
SSDE	**Size-specific dose estimate**
Sv	**Sievert**
mSv	**Millisievert**
TAP	**Thorax, abdomen and pelvis**
UCC	**University College Cork**
US	**Ultrasound**
USA	**United States of America**

Chapter I

General Introduction

History of CT

Computed tomography (CT), also know as 'CAT' scanning (computed axial tomography), derives its name from the Greek word 'tomos' meaning 'slice' or 'section' and 'graphia' meaning 'describing'. CT was invented in 1972 by a British engineer Sir Godfrey Hounsfield of EMI Laboratories, England and by South Africa-born physicist Allan Cormack of Tufts University, Massachusetts who were jointly awarded the 1979 Nobel Prize in Physiology or Medicine for their work.

Early commercial CT scanners installed between 1974 and 1976 were dedicated to head imaging alone, but larger bore systems to facilitate body imaging were developed in 1976. The first CT scanner developed by Hounsfield in his lab took several hours to reconstruct a single axial image from the raw data. Since this time, significant technological advances have made CT an invaluable imaging modality with faster scanning times, higher contrast and spatial resolution, and less artifacts, enabling the acquisition of diagnostic quality images at lower radiation doses.

The technology utilizes computer-processed combinations of multiple X-ray images acquired at different angles to produce cross-sectional (tomographic) images or virtual slices of a specific body part. The emitter of X-rays rotates around the patient and the detector, which is diametrically opposed, picks up the

image of a body section. Cross sections are then reconstructed from the measurement of attenuation coefficients of X-ray beams in the volume studied. The attenuation coefficient quantifies how easily the X-ray beam can penetrate a material and thus enables the calculation of the density of the tissue traversed by the beam. The density of the tissue within each pixel of an image is given by the Hounsfield Unit (HU), a quantitative scale for describing radiodensity on CT images. It is calculated relative to the radiodensities of water and air, which have a HU value of 0 and -1000, respectively. Other tissues have the following approximate HU values: lung: -500 HU; fat: -60 to -120 HU; soft tissue: 30 to 100 HU; bone: 700-3000 HU.

Increasing use of CT

Medical imaging has become the largest source of radiation exposure for humans other than natural background radiation.[1] In Ireland, the average person receives approximately 4mSv of radiation per annum of which 86% (3.48mSv) is attributable to natural sources such as radon in homes, cosmic rays, gamma radiation in the environment, and radioactivity in food. Radon is the principle source of radiation in Ireland, representing just over 55% (2.1mSv) of the radiation dose received by the Irish population.[2] For reference, the radiation dose incurred by a passenger on a trans-Atlantic flight is 0.5mSv per 100 hours of flying.[3]

The availability of and improvements in diagnostic imaging have led to a sevenfold increase in the use of radiological imaging modalities over the past 30 years.[4] This is especially true for CT, with studies reporting a 7.8% annual increase in the use of CT from 1996 to 2010, representing an overall doubling of

the mean per capita effective dose of ionizing radiation[5] (Figure 1.1[6]). It was estimated that approximately 62 million CT scans were performed in the Unites States of America (USA) in 2007, compared to 3 million in 1980,[7] with CT contributing to 24% of the total population dose in 2009.[8] The increased use of CT may be attributable to new CT scan indications, an increase in the availability of CT scanners, increasing population, and perhaps a need for increased diagnostic certainty by physicians in the current medico-legal climate.

The major concern associated with the widespread uptake of CT is the parallel increase in radiation exposure incurred by patients. CT is a high dose procedure in comparison with other conventional radiology examinations that contributes a disproportionately large amount towards total collective patient dose from diagnostic imaging. This is particularly true in certain patient groups with documented high cumulative radiation doses from radiological imaging, primarily attributable to CT. These include patients with cystic fibrosis[9], Crohn's disease[10], end-stage kidney disease[11], and testicular cancer.[12]

CT currently imparts more than 75% of all radiation exposure from diagnostic imaging while still only accounting for 11% of all diagnostic examinations that utilize ionizing radiation.[13] The dramatic increase in the use of CT is further compounded by the expansion and increased use of fluoroscopic and interventional procedures that further increase the radiation dose delivered to the population during diagnostic imaging.[14]

Quantifying the radiation dose incurred by patients during medical imaging is gaining increasing traction in clinical practice. This is evident from the recent development of automated dose monitoring software systems by industry with eight countries currently planning to introduce national patient dose tracking

programs.[15] These systems facilitate the monitoring of cumulative effective dose in individual patients, the optimization of CT protocols, and audit of practice. While dose limits and reference standards exist for those occupationally exposed to radiation, currently there is no legal requirement to monitor cumulative radiation dose from medical imaging in patients.

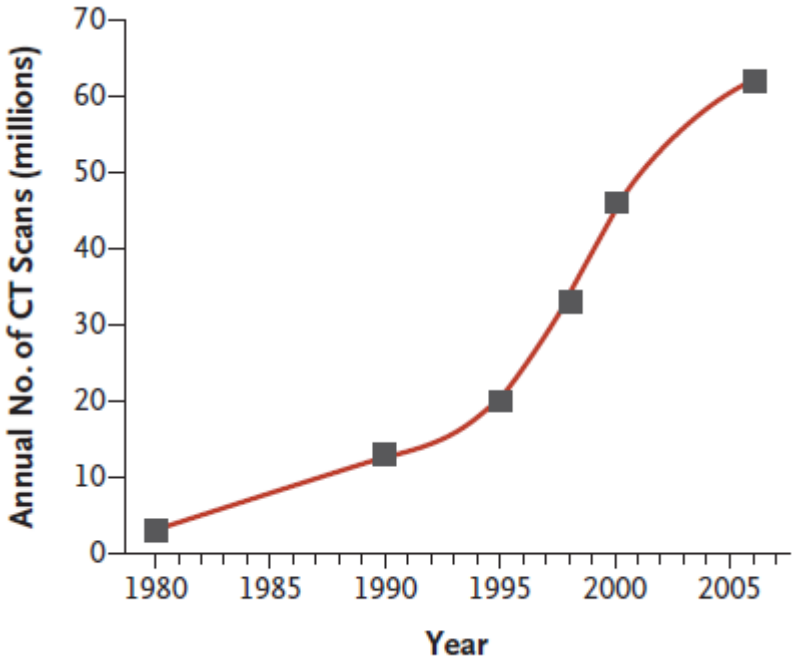

Figure 1.1 Estimated number of CT scans performed annually each year in the United States (image taken directly from Brenner et al. 2007).[4]

Biological effects of exposure to ionizing radiation

Radiation damage at a cellular level can be caused by the direct or indirect action of radiation on DNA molecules. In the direct action, the genetic material in the nucleus is struck directly by the radiation particle or photon, disrupting the molecular structure. Such structural change leads to cell damage or cell death.

Damaged cells that survive may later induce carcinogenesis or other abnormalities. In the more frequently encountered indirect action, the radiation ionizes water molecules in the cytoplasm, leading to the production of free radicals such as hydroxyl and alkoxy, which in turn cause cellular or nuclear damage.

Tissue damage from radiation can also be divided into deterministic and stochastic effects. Deterministic effects are predictable complications and have a threshold below which no effect will be observed. However, once the threshold is exceeded, the severity of an effect increases with dose. These complications are rarely observed in the diagnostic imaging setting with the exception of extended fluoroscopic intervention procedures. Examples include skin erythema, hair loss, and cataracts. Conversely, stochastic effects occur by chance, have no lower threshold, and the risk of occurrence increases with dose. Cancer induction is the primary stochastic effect of concern.

Risk of cancer induction from radiation exposure

The relationship of radiation exposure to a quantifiable risk of cancer induction remains a controversial topic. It is widely accepted that exposure to large doses of ionizing radiation places an individual at an exponentially increased risk of developing cancer in their lifetime, but the association between the relatively low levels of radiation exposure incurred during diagnostic imaging and carcinogenesis remains unclear.

Several studies have demonstrated a dose-dependent correlation between radiation exposure and cancer incidence following protracted exposure to low-level ionizing radiation.[16, 17, 18] Many of these studies have been largely based on

extrapolated data from studies of survivors of the atomic bombs dropped in Hiroshima and Nagasaki in 1945. The International Commission on Radiological Protection (ICRP), as well as the National Academy of Sciences Committee on Biological Effects of Ionizing Radiation have estimated cancer risks associated with protracted exposures to low-dose ionizing radiation by extrapolating from published data of the Japanese atomic bomb survivors who had, in large part, acute exposures to high doses of radiation.[2] Using this method of extrapolation, where small hypothetical risks are multiplied by large patient numbers, Brenner et al estimated that 1-2% of all future cancers in the USA would be attributable to diagnostic radiation exposure.[4] Similarly, a study conducted in 2009 predicted that as a result of the increased use of ionizing radiation examinations, 29,000 additional cancers and 14,500 additional deaths could be expected each year.[19] Epidemiological studies have also provided evidence of increased cancer-related mortality following exposure to low levels of ionizing radiation from diagnostic imaging.[20, 21] Other efforts to quantify the cancer risk from low-dose radiation exposure have focused on the cancer incidence among radiation workers in the nuclear industry. A retrospective cohort study examining the effects of low-dose protracted exposures to ionizing radiation in 15 countries involving almost 600,000 workers demonstrated a dose-related increase in all cancer mortality.[22] However, use of data generated from atomic bomb survivors and nuclear industry workers to estimate cancer risk from diagnostic radiology examinations is not ideal and remains controversial,[23] with the American Association of Physicists in Medicine stating that 'predictions of hypothetical cancer incidence and deaths in patient populations exposed to low-doses are highly speculative and should be discouraged'. Other authors have even suggested that exposure to

low levels of ionizing radiation may stimulate an immune response that protects an individual from carcinogenesis, a concept known as hormesis.[24]

The *linear no-threshold model* associated with high-dose exposures, whereby even low doses of radiation are associated with a risk of carcinogenesis with the risk increasing linearly with dose, is also assumed to apply to low-dose exposures. However, the validity of this model has come under scrutiny in recent years with many authors arguing that a practical threshold exists below which the risk of cancer induction is no greater than an individual's background spontaneous risk.[18, 25]

The results of a study of the Radiation Effects Research Foundation (REFR) data (collected from the Japanese atomic bomb survivors) was more consistent with a *threshold-quadratic model* of radiation-induced cancer than with the *linear no-threshold model*.[26] The authors compared the incidence of colon cancer (commonly used as a cancer indicator in the Japanese population) in Hiroshima and Nagasaki with other Japanese cities not affected by the nuclear bombings and found that its incidence was not increased in those who received radiation doses of less than 100mSv. It is now felt by many that ascribing cancer risks to radiation exposures of less than 100mSv is confounded by other risk factors for malignancy within an individual population[18], with the Health Physics Society stating that at doses below 50-100mSv, 'the risks of health effects are either too small to be observed or are non-existent'.[27]

There are other factors that need to be taken into consideration when assessing the effects of radiation exposure in the pediatric population. Children receive greater organ doses during CT.[28] The effective dose delivered to a neonate during a CT scan can be double that received by an adult for the same examination.[29]

Children are also at greater risk due to increased cell sensitivity to ionizing radiation due to rapid tissue growth, as well as having more subsequent years of life in which to develop a radiation-induced cancer.

A prospective study of a large cohort of pediatric patients who had undergone at least one CT examination before the age of 22 years reported a linear association between radiation dose to the brain and brain tumor risk and radiation dose to the bone marrow and subsequent development of leukemia (Figure 1.2).[30] They found that cumulative radiation doses from CT scans in excess of 50mGy and 60mGy, would triple the risk of developing leukaemia and brain cancer, respectively. The absolute risk was low however, at approximately one excess case per 10,000 CT studies, as both neoplasms are rare. This was one of the first prospective studies to suggest a link between diagnostic radiation exposure and cancer induction that did not rely on extrapolated data from high dose exposures. A further study conducted in 2013 reported a 24% increase in cancer incidence rates in children exposed to a CT scan more than one year before any cancer diagnosis, compared to unexposed individuals.[31]

While it remains ambiguous if the results of these studies can be applied to adult patients, it seems a simple dismissal of the *linear no-threshold model* in pediatric patients may be premature, especially as the greatest growth in the use of CT is occurring in the pediatric population. Between the years 1991 and 1994, the use of CT has increased by 63% in patents younger than 15 years of age.[32]

In the case of adult patients, it now seems that a threshold–model of cancer risk might be more appropriate with the risk increasing exponentially with cumulative radiation doses in excess of 75 to 100mSv. The International Agency for Research on Cancer has concluded that a cumulative effective dose (CED) in

excess of 75mSv results in a 7% increase in the risk of cancer induction when compared with the general population.[20] Although such high cumulative doses may not be encountered routinely in clinical practice, it is increasingly recognized that certain patient groups, particularly those with chronic diseases who may have a requirement for repeated imaging, are at risk of incurring cumulative radiation doses in excess of 100mSv. A previous study of 399 patients with Crohn's disease conducted at our institution found that 16% of patients received a CED in excess of 75mSv over a 15 year period from medical imaging.[8] Similarly, CEDs exceeding 75mSv were documented in 13% and 10.4% of patients with cystic fibrosis[7] and chronic renal disease[9], respectively. A more recent study of 120 young patients undergoing surveillance for testicular cancer found that 77.5% of these patients received a CED exceeding 75mSv over a median follow-up of 4.4 years.[10]

Given these findings, acceptance of the *threshold model* of cancer risk does not allow complacency when considering the need to perform an imaging investigation that utilizes ionizing radiation. Physicians are beholden to keep radiation doses from diagnostic imaging as low as reasonably practical as the doses incurred by each examination can quickly accumulate, especially in patients with chronic medical complaints, resulting in a potential increase in the risk of cancer induction.

The use of CT during pregnancy requires special consideration as the fetus, with a greater sensitivity to radiation than the mother, is also exposed to radiation and is directly in the beam when performing abdominopelvic CT. In a recent study assessing fetal dose from abdominopelvic CT, the average fetal dose was 24.8mGy with 12.5% (7 cases) of examinations being classified as high dose (>30

mGy) and a single examination exceeding the 50mGy threshold for an increased risk of childhood cancer.[33] Nevertheless, CT is an invaluable diagnostic tool in pregnancy in certain scenarios such as trauma and in the acute abdominal setting, and indeed the use of CT in pregnancy has increased in recent years, in line with the overall trend towards an increased use of CT.

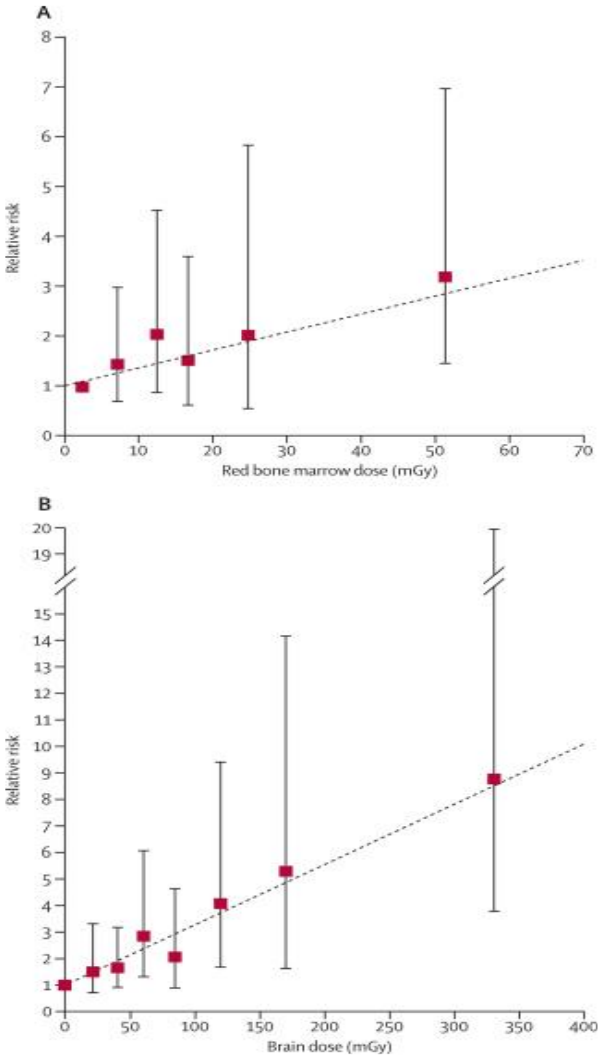

Figure 1.2 Relative risk of leukaemia & brain tumour in relation to estimated radiation dose from CT scans in childhood (image taken directly from Pearce et al).[28]

Measuring CT radiation dose

Several different measures of CT radiation dose exist. When assessing the dose to a patient from a CT scan, several factors can to be taken into consideration including the radiation output from the scanner, the length of body region scanned, and patient size.

Volume CT dose index (CTDIvol) is a measure of the radiation output of the CT scanner. Its units are milligray (mGy). It is measured by using a pencil ionization chamber placed in a standard circular polymethyl methacrylate phantom. Dose measurements are made at the center and at the periphery, and these values are combined using a weighted average to produce a single estimate of radiation dose to the cylinder. Two sizes of phantoms are used to measure CTDIvol: a 16-cm phantom for adult head and paediatric head and torso calculations and a 32-cm phantom for adult torso measurements. The method for calculating CTDIvol is standardized across all CT manufacturers and models using these two reference phantoms. Thus, CTDIvol is one of the key radiation dose descriptors in CT and can be used for comparing different scanner outputs from different imaging protocols and for comparing the same protocol on different CT machines. CTDIvol is dependent on the technical parameters selected for the CT scan and independent of patient size and length of region scanned.[34]

Dose-length product (DLP) is a second key patient dose descriptor in CT.

It describes the linear extent of the exposure to the patient indicated by the average CTDIvol and is calculated simply by measuring the CTDIvol by the length of the scanned range in cm; hence the units of DLP are mGy-cm.

Absorbed dose describes the amount of energy (joule) that is deposited by ionizing radiation per unit mass (kilogram) of tissue. The unit of measurement is the Gy, where one Gy equals one joule of energy per kilogram of tissue, although in practice, the milligray is more commonly used.

If a standard CTDIvol setting is used to scan two different sized patients, the absorbed dose in the smaller patient will be greater as the larger patient will have a more diluted deposition of absorbed dose (the same dose distributed over a larger mass) than the smaller patient.

Effective dose (ED) is an estimation of dose that reflects the sensitivity of the organs or tissue types involved. Effective dose incorporates the absorbed dose (in milligrays) in its derivation, but also includes the relative radio sensitivity of the exposed organs. Tissues and organs are most sensitive to radiation when they are immature, undifferentiated or rapidly dividing. As cells mature they become less sensitive to the ill effects of radiation, which is reflected in the tissue weighting factors. For example, the bone marrow, stomach, lung, and breast have the highest tissue weighting factor of 0.12, while the gonads have a tissue weighting factor of 0.08 and the skin a tissue weighting factor of 0.01.[35] The unit of ED is the Sievert (Sv), although the millisievert (mSv) is more commonly used in practice.

Effective dose is practical because it allows comparison of different radiologic modalities on a common scale. It also allows comparison of dose from medical examinations to other forms of radiation such as cosmic rays, radon, and

occupational radiation exposure. This is particularly helpful when discussing the risks of a CT examination with patients and referring physicians.

The DLP from a given CT examination is often multiplied by conversion factors to estimate the ED.[36],[37] Conversion factors can vary however leading to discrepancies, and DLP is more often used as a more comparable and reproducible measure of patient dose in the research setting.

More recently, *size specific dose estimation (SSDE)* has been recommended as a more accurate measurement of patient radiation dose. Calculation of SSDE involves multiplying CTDIvol by a conversion factor (fSSDE), which relates to patient size (effective diameter). SSDE was validated as a measure of radiation dose exposure by the American Association of Physicists in Medicine Report 204[38], due to inclusion of patient size in its calculation, allowing more accurate estimation of radiation dose than CTDIvol, or DLP.[39] The advantage of SSDE over CTDIvol was shown by Christner et al. using an automated exposure control system, which adjusted CT scanner output depending on patient size while performing CT of thorax or abdomen-pelvis.[40] Patient size and scanner output measured using CTDIvol were related in a linear manner, but after substitution of CTDIvol with SSDE, scanner output was found to be independent of patient size. The use of CTDIvol to infer patient radiation dose was shown to potentially underestimate effective dose by a factor of between two and three. This is especially relevant with the changing body habitus and increasing obesity rates we are observing in society today with high BMI associated with significantly higher radiation doses when performing CT.[41]

Dose optimization strategies

The system of radiation protection used throughout Europe is based on the recommendations of the International Commission for Radiological Protection. The core principles of radiation protection are justification, optimization and dose limitation. The principle of *Justification* requires that exposure to radiation results in more benefit to the exposed individual than harm. The principle of *optimization* requires that the magnitude of individual doses should be kept 'as low as reasonably achievable' (ALARA principle). Dose limits are set for workers and the general public and do not apply to patients. The principles are embodied in various European directives, most notably the Basic Safety Standard 96/29/EURATOM and the Medical Exposures Directive 97/43/ EURATOM. The Basic Safety Standard was transposed into Irish legislation by statutory instrument (SI) 125 (2000), whereas the Medical Exposures Directive 97/43 EURATOM was transposed by SI 478 (2002), with associated amendments SI 303 (2007) and SI 459 (2010). The Medical Exposure Directive 97/43 EURATOM is the main legal instrument for the protection of patients undergoing diagnostic and therapeutic procedures using ionizing radiation.

As a large proportion of collective patient dose is attributable to CT scanning, strategies to reduce overall patient dose from medical imaging should be targeted at minimizing the dose from CT. It must be stated that CT is a useful and often invaluable diagnostic tool when used judiciously in many patients and most CT examinations are associated with a very favorable ratio of benefit to risk. CT has reduced the proportion of patients requiring inpatient admission, reducing the need for emergency surgery from 13% to 5%, and has replaced many exploratory surgical procedures.[42,43]

Technological advances in CT over the past few decades have enabled a substantial reduction in the doses delivered to patients; the dose of an abdominopelvic CT has decreased by a factor of between two and three since the early 1980s.[44] However, due to differences in CT vendor technology and scanning protocols and techniques, there still exits significant variation in the average reported dose for a given examination both between and within institutions.[45]

Several dose optimization strategies may be employed when performing low-dose CT. These include:

Limiting the scan range and judicious protocoling: The scan range is directly related to the total radiation dose delivered to the patient. The scan range should be kept as small as possible but as large as necessary for diagnostic purposes in order to avoid direct radiation exposure to any region of the body not necessary for diagnosis. A retrospective study of 106 patients undergoing abdominopelvic CT reported instances of unnecessary 'over scanning' above the diaphragm in 97% (103/106), and below the pubis symphysis in 94% (100/106) of patients.[46] CT protocols should be tailored to the clinical question and unnecessary, non-contributory phases must be avoided. Indeed, protocol manipulation may have a greater impact than parameter modification on radiation dose.

Patient centering: Accurate patient centering is another important and often overlooked dose reduction strategy. Inaccurate patient centering has been shown to increase dose significantly[47], with variance from the isocenter by 6 cm leading to an approximately 50% increase in dose in one study.[48] Furthermore, poor patient centering results in increased image noise[49], as well as affecting the

efficacy of bow-tie filters and automatic exposure control systems in reducing dose.[50]

Tube current modulation and automatic exposure control: A common method to optimize radiation dose is to adjust the tube current based on the patient's size or weight and determine the appropriate amperage from a technique chart.[51] For example, paediatric patients will not need as high a tube current level as adults to acquire diagnostic quality images, while obese patients will require a higher amperage setting to maintain image quality.

A more advanced technique is automatic exposure control (AEC), which automatically modulates the tube current to accommodate differences in attenuation due to patient anatomy while maintaining a pre-defined level of image quality or noise index. The tube current may be modulated as a function of the projection angle (angular modulation), the longitudinal location along the patient (z-axis modulation), or both. The noise index is a threshold level of image noise or 'graininess' deemed acceptable for diagnostic purposes that aids in the difficult task of balancing image quality with radiation exposure. This may be varied depending on the CT manufacturer as the use of a constant noise target may lead to unacceptable image quality in small patients and excessive radiation dose in large patients.[46] AEC has been shown to be most effective in patients of average or low body mass index (BMI) achieving mean dose reductions in the order of 10-20%.[52] Overall, AEC facilitates delivery of the optimal dose to achieve optimal diagnostic image quality.

Optimal tube potential: Automated tube-voltage (kV) selection uses an attenuation-based calculation from planning radiographs to determine the optimal kV for the patient and body part being scanned.[53] The technique has

achieved dose reductions of approximately 70% and 40% in chest and abdominopelvic CT, respectively.[54]

Lower kV selection is reportedly superior for studies with iodinated contrast medium due to the increased attenuation of iodine at lower tube potentials than at higher tube potentials. Despite the resultant increase in image contrast, images obtained at a lower tube potential tend to be noisier due to the greater absorption of low-energy photons in the patient. This is especially true for patients with a high BMI. There is therefore a tradeoff between image noise and contrast enhancement, and if the patient size is above a particular threshold, increased noise levels can often negate the benefit of improved contrast enhancement.[46]

Gating: The use of electrocardiogram gating can decrease dose in cardiac CT by 50% or more. Gating involves varying the tube current output in synchrony with the patient's electrocardiogram to reduce radiation during phases in the cardiac cycle when the heart is moving more dynamically and image quality would be suboptimal.[55]

Shielding: Shields made of thin sheets of flexible latex impregnated with bismuth can be used to cover the lens of the eye, thyroid, or breasts during CT exams. Dose savings to these superficially located target organs when using such shields have been reported to be 40% to 67% for adults and 30% to 40% for children.[56] It should be noted that the majority of studies using such shields report artifacts around the shields.

Other: Additional dose optimization techniques include the use of noise reduction filters[57], integrated circuit detectors[58], slice spacing techniques[59], and adaptive collimation.[60]

Consideration should also be given to imaging modalities that do not involve exposure to ionizing radiation such as magnetic resonance imaging (MRI) and ultrasound (US). However, this may not be possible in many cases due to the lack of availability of MRI at some institutions, prolonged imaging times of MRI compared to CT, patient contra-indications to MRI, and the sub-optimal diagnostic capabilities of MRI compared to CT in certain clinical scenarios.
Clinical decision support tools are another more recent development that have helped many hospitals reduce unnecessary tests. These tools are designed to help referring clinicians to adhere to evidence-based practice guidelines, eliminate inappropriate procedures, and identify patients at-risk of duplicate examinations, and high cumulative radiation doses from diagnostic imaging. Furthermore, these systems record data that can be mined for information, such as benchmarking to target education and quality improvement, or to assess patterns of use.
The development of *iterative reconstruction* techniques (discussed below) has been one of the most significant advances in CT dose reduction in recent years.

Assessment of image quality

The challenge when performing low-dose CT is to keep radiation exposure as low as reasonably possible while still maintaining diagnostic image quality.
As radiation dose is reduced, the number of photons reaching the detector reduces, resulting in increased levels of image noise. Noise or image 'graininess' refers to unwanted signal that leads to a random variation in image brightness or the grey-scale appearance of the image that is not an accurate reflection of the true image. Noise in CT has two principal sources: quantum noise and electronic

noise. The quantum noise is determined by the number of photons incident and collected by the detector. The electronic noise is the result of fluctuation in the electronic components of the data acquisition system.

Image quality can be assessed both quantitatively and qualitatively, both in phantom and patient studies, with the use of several metrics including image noise. Objective image noise assessment is most frequently performed by calculating the standard deviation (SD) of the voxel values on a CT image of a homogenous water phantom. When a homogenous water phantom is imaged, each pixel should have a HU value of zero, hence any deviation from this is a reflection of image noise. This deviation can be measured on a standard workstation using a region of interest (ROI) tool that measures the standard deviation of the mean HU value within the voxels in the ROI. The signal-to-noise ratio (SNR), where the signal is a true representation of the imaged area, can also be derived from this.[61] Subjective image noise assessment is often performed in conjunction with objective assessment by experienced readers who score the presence of image noise at various anatomical levels.

High-contrast spatial resolution is another metric of image quality that quantifies the minimum size of a high-contrast object that can be resolved. Low-contrast spatial resolution quantifies the minimum size of a low-contrast object that can be differentiated from the background. This relates to both the contrast of the material and the noise-resolution properties of the system.

Spatial resolution assessment is typically performed with the use of 'modulation transfer function' in phantoms or subjectively from patient images. High spatial resolution scores indicate better edge definition and better delineation between adjacent objects.

Contrast resolution refers to the ability to distinguish between differences in image intensity or brightness. This can be assessed subjectively with the use of a specially made phantom or from patient CT images. Contrast-to-noise ratio (CNR) is another common metric to quantify the overall image quality.
Low radiation dose images generally contain more artifacts with localized imperfections, not true representations of the object being imaged.
The presence of artifacts such as streak artifact (abnormal linear streaks in an image due to alteration in photon number and energy adjacent to high density objects), and photon starvation (loss of image quality due to too few photons reaching the detectors), can also be scored when performing image quality evaluation.

Iterative reconstruction techniques

Image reconstruction has a fundamental impact on image quality and therefore on radiation dose. Image reconstruction is a mathematical process whereby images are generated from the acquired X-ray projection data. The aim is to reconstruct images with the lowest possible noise and highest possible image accuracy and spatial resolution. Thus, reconstruction algorithms that improve image quality can be translated into a reduction in radiation dose as images of acceptable diagnostic quality can be acquired at lower dose settings.
Reconstruction techniques in CT include both analytical and iterative reconstruction (IR) algorithms. Filtered back projection (FBP) is one such analytical algorithm that has served the CT community for the past 40 years. The technique involves 'smearing' or projecting back a function defined on each line in the reconstruction plane over the line of acquisition. This process is then

repeated over several imaging projections and computationally efficient inversion formulas then reconstruct the image from the points where the back-projection lines meet, with filters being used to 'smooth' the final image.

The performance of traditional FBP has been questioned in recent years with the current industry drive to reduce radiation doses in CT. In order to minimize reconstruction times, FBP ignores key information about the x-ray photon statistics, such as the Poisson distribution of photons and system hardware details including focal spot size, active detector area, and image voxel shape. For example, the x-ray source and the individual cell on the detector are considered to be infinitely small and each voxel has no shape or size. These false assumptions compromise the truthfulness of the final images. Consequently, at reduced radiation doses, FBP is associated with high levels of image noise and artifacts.

To address this need to reduce radiation dose without sacrificing image quality, manufactures introduced new IR algorithms into clinical practice in 2009.

IR techniques use an initial FBP image to create an image model of the object, which subsequently undergoes a forward projection creating an artificial model 'raw projection data'. This in turn is compared with the original data, enabling identification and elimination of noise and artifacts with the aid of modeled noise and artifact statistics. This noise elimination step is repeated through several iterations until a final image is created. The process is much more computationally intense than traditional FBP requiring longer reconstruction times and more robust computers.

CT manufacturers have adopted different algorithmic approaches to iterate different components of the image reconstruction algorithm. However, the

common endpoint of all IR algorithms is the production of images with reduced levels of image noise and higher resolution through the preservation of edges and reduction of artifacts.[62] Low-dose CT can be achieved by modifying the scanning parameters such as tube current potential with the concurrent application of IR techniques to improve the image quality.

Hybrid or 'blended' IR algorithms are the most studied IR techniques to date and have been introduced into clinical practice in many centers. The final image represents a distinct percentage or 'blend' of both IR and FBP and the number of iterations performed is pre-defined according to the percentage of IR in the blend. Examples of hybrid iterative reconstruction include Adaptive Statistical iterative Reconstruction (ASiR, GE Healthcare, GE Medical Systems, Milwaukee, WI), Image Reconstruction in Image Space (IRIS, Siemens Healthcare, Erlangen, Germany), Sinogram-Affirmed Iterative Reconstruction (SAFIRE, Siemens Healthcare), Advanced Modeled Iterative Reconstruction (ADMIRE, Siemens Healthcare), Adaptive Iterative Dose Reconstruction 3D (AIDR, Toshiba Medical Systems, Tokyo, Japan) and iDose (1 to 5) (Philips Healthcare, Eindhoven, The Netherlands). Hybrid IR techniques incorporate modeling of photons and electric noise in the CT system, and are not too computationally intense or time-consuming to perform on today's CT computer systems. They have been used with success to acquire diagnostic quality CT images of the head and neck[63], chest[64,65] and abdomen[54, 66] at substantially reduced radiation doses.

Pure IR is a newer IR technique that in addition to incorporating modelling of photon and noise statistics, also models system optics, to create the final image. The process is mathematically more complex but reportedly more accurate than hybrid IR. Examples include Model-Based Iterative Reconstruction (MBIR, Veo,

GE Healthcare, GE Medical Systems, Milwaukee, WI) and Iterative Model Reconstruction (IMR, Philips Healthcare, Eindhoven, The Netherlands).

Recent studies of MBIR have consistently shown improved image quality and reduced image noise compared to both FBP and hybrid IR for chest[67], abdominal[68], and head and neck CT.[69] MBIR seems to have had the greatest success to date in the field of cardiac imaging achieving dose reductions of up to 82%.[70] High computation load remains one of the greatest challenges for pure IR impeding its use in many clinical settings. However, further advances in computational technology may lead to incorporation of pure IR techniques into routine clinical practice in the future.

Careful clinical validation of MBIR as a dose reduction technique is essential to determine its most appropriate uses and to identify any potential limitations, thereby ensuring the safe introduction of MBIR into clinical practice. The aim of this thesis is to assess the feasibility of using MBIR to achieve diagnostic quality images at substantially reduced radiation doses for a variety of CT protocols including neck, chest, and abdominopelvic studies.

In chapter 2, we conduct preliminary phantom and cadaveric studies to examine the performance of MBIR at different radiation dose levels in the thorax and abdomen. We also aim to determine the dose level at which MBIR has the greatest efficacy for noise reduction. Chapter 3 examines the diagnostic performance of a modified low-dose carotid angiography protocol compared to a conventional dose protocol. Chapter 4 assesses the use of low-dose CT with MBIR in patients presenting with acute abdominal symptoms. Achieving diagnostic quality low-dose abdominopelvic CT images is particularly challenging, as the abdominopelvic region does not lend itself as well to low-dose

scanning as the thorax. Good image contrast is essential to resolve pathological changes within the solid abdominal viscera. Subtle changes in attenuation values that represent pathology can be obscured by increased image noise more so than in the thorax, where tissues have greater inherent contrast due to the large difference in their densities. Chapter 5 combines MBIR with a modified chest CT protocol acquired at the dose of a chest radiograph in patients with cystic fibrosis. These patients undergo repeated chest CT from a young age and with an increasing life expectancy, it is essential to keep CED from repeated CT imaging as low as possible.

Chapter II

Determination of suitable low-dose chest and abdominopelvic CT protocols using model based iterative reconstruction through phantom and cadaveric studies

Introduction

The exponential increase in the use of CT in recent years has lead to growing concerns among physicians and patients regarding the risk of cancer induction.[4] The risk of cancer linked to radiation exposures in the diagnostic imaging range remains a controversial topic with some opinions suggesting that up to 2% of all incident cancer cases in the USA may be attributable to CT.[4] However, protracted exposure to low-level ionizing radiation is widely believed to be associated with an increased risk of malignancy[14, 16, 24], and given the uncertainty, dose optimization without loss of diagnostic performance is essential to good practice when performing CT. This is especially true for abdominopelvic CT as it accounts for 50% of total CT collective dose[71], and dose reduction strategies in this area will therefore have a significant impact on the overall population dose from diagnostic imaging.

Potential dose reduction techniques that may be employed when performing chest or abdominopelvic CT include automatic exposure control[72], low tube

voltage techniques[73], scan range control[41], adaptive collimation[53], judicious protocoling, and ensuring that every CT study is justified. These strategies however, have a limited effect on radiation dose reduction due to the innate limitations of the traditional analytical reconstruction algorithm, FBP, currently installed on most CT systems. This technique has the intrinsic problem of high levels of image noise and consequently poorer image quality at reduced radiation doses.[74]

Advanced IR algorithms that reduce image noise facilitating the generation of diagnostic quality images at reduced radiation doses have received much attention in the literature recently. These techniques incorporate statistical information of the CT system including photon statistics and electronic acquisition noise to reduce image noise.[75] ASIR is the most studied iterative algorithm in chest and abdominopelvic CT to date with studies reporting dose reductions in the order of 25% to 74% with preserved image quality and diagnostic value.[54, 76]

MBIR is a more computationally intense pure IR algorithm that incorporates optical models and advanced modeling of system statistics into its iteration process to enable greater noise reduction. The exact mechanism by which the MBIR algorithm operates is proprietary and generally unknown. It therefore essential to evaluate the diagnostic quality of images reconstructed with MBIR before introduction of the technique into widespread clinical practice.

Several strategies may be used to compare the efficacy of reconstruction techniques in noise reduction including technical and anthropomorphic phantoms[77], the split-dose technique[54] or the artificial addition of image noise to conventional dose images to simulate low-dose images.[78]

Technical and anthropomorphic phantoms provide a safe, objective and reproducible method of assessing the image quality of different reconstruction algorithms over a range of radiation dose levels. Preliminary phantom experiments with MBIR report a significant reduction in image noise and streak artifact, with significant improvements in image quality compared to FBP and ASIR.[70, 73] Many phantom models do not accurately reflect the complex relationship that exits between anatomical variability and image quality, and the results of phantom studies may not be entirely applicable to the clinical setting. However, patient studies to assess the performance of reconstruction algorithms at different dose levels can often be problematic to implement, as imaging large numbers of patients at different dose settings introduces confounding and imaging one patient at different dose settings is ethically prohibited. To date, clinical studies assessing the use of MBIR in chest and abdominopelvic CT are limited.[79,80]

The use of radiological images acquired from cadavers for research[81], teaching[82], and training[83] purposes has been well described in the literature. Cadavers also provide an excellent model with which to compare reconstruction algorithms by facilitating the repeated scanning of one subject over a range of radiation dose settings. To the best of our knowledge, this is the first study to assess the image quality of cadaveric abdominopelvic CT scans reconstructed with MBIR.

The purpose of this anthropomorphic phantom study was to compare the image quality of chest and abdominopelvic CT scans reconstructed with MBIR with those reconstructed with FBP and hybrid IR over a range of radiation dose levels. We performed a concurrent cadaveric study assessing the image quality of abdominopelvic CT scans reconstructed with MBIR. In addition, we aimed to

determine the dose range at which MBIR had the greatest efficacy for noise reduction. The results of this study were subsequently used to guide the development of modified low-dose chest and abdominopelvic CT protocols for clinical studies in patients.

Materials and methods

CT torso phantom

The CT torso phantom used for the study was a one-piece anthropomorphic torso phantom (CT Torso Phantom CTU41, Kyoto Kagaku, Fushimi-ku, Kyoto, Japan). The phantom has full internal organs embedded with a HU, which simulates the anatomy of the human body. The soft tissues and bones are composed of a urethane base resin (SZ-50) and an epoxy base resin is used for the synthetic bones (Figure 2.1).

Figure 2.1 CT Torso Phantom (CTU41, Kyoto Kagaku, Fushimi-ku, Kyoto, Japan). Single axial images of the chest and upper abdomen are shown.

Cadaveric subjects

The study was conducted under the auspices of a 'License to Practice Anatomy' granted to the Chair of the Department of Anatomy and Neuroscience of our institution under the Anatomy Act 1832. Donors premorbidly signed written consent for the use of their bodies for the purposes of education and research. 5 human cadavers (4 male, 1 female) were included in the study. The median time from death to CT scanning was 38 days (range, 8 to 180). The cadavers were fresh frozen at -4°C and thawed for the purpose of the study.

Phantom CT technique

The torso phantom was scanned with our clinical scanner, a 64-slice GE Discovery 750HD CT scanner (General Electric Healthcare, Waukesha, WI, USA). The phantom was scanned in the supine position in the isocenter of the gantry. Our standard departmental CT thorax and CT abdomen protocols were used but tube current was altered to achieve a range of dose levels. CT thorax and CT abdomen series were acquired separately at tube currents of 400, 200, 100, 50, and 10mA.

DLP and CTDIvol values for the CT thorax series were 866.68mGy.cm (25.13mGy), 443.25mGy.cm (12.58mGy), 221.69mGy.cm (6.29mGy), 110.77mGy.cm (3.14mGy), and 22.15mGy.cm (0.63mGy) respectively. DLP and CTDIvol values for the CT abdomen series were 1037.54mGy.cm (27.99mGy), 560.03mGy.cm (12.68mGy), 279.92mGy.cm (6.34mGy), 140.02mGy.cm (4.85mGy), and 25.32mGy (0.63mGy).

The tube voltage (120kVp), gantry rotation time (0.8 seconds), collimation (40 x 0.62mm), pitch factor (0.98), and acquisition thickness (0.625 mm) were kept constant for all acquisitions.

Cadaver CT technique

Each cadaver was scanned without intravenous or oral contrast in the supine position enclosed in a body bag without any metallic fasteners.

The standard departmental abdominopelvic protocol was employed with varying tube voltage (kV) and current (mA) settings of 80kV/225mA, 120kV/100mA, 100kV/225mA, and 120kV/200mA, resulting in mean DLP/size

specific dose estimates (SSDE) of 630.9±32.7mGy.cm/14.17±1.64mGy, 447.2±23.35mGy.cm /10.04±1.16mGy, 315.5±16.4mGy.cm /7.09±0.82mGy, and 238.7±12.41mGy.cm/5.36±0.62mGy, respectively. We focused on abdominopelvic structures alone for the cadaveric studies as the abdomen and pelvis represents the greatest challenge to dose reduction owing to subtle differences in attenuation observed between abdominal and pelvic structures, and furthermore, the subtle differences in attenuation that can represent pathology. The radiation exposure resultant from the CT localizer radiographs was excluded from the dose calculations.

The 120kV/200mA protocol was used as a reference conventional dose (CD) following a review of the radiation dose of 100 standard abdominopelvic CT studies performed at our institution (mean DLP of 640.4±272.8mGy.cm). The 80kV/225mA, 120kV/100mA, and 100kV/225mA lower radiation dose levels were termed low-dose (LD) 1, LD2, and LD3 respectively (Figure 2.2). The gantry rotation time (0.8 seconds), collimation (40 x 0.62mm), pitch factor (0.98), and slice thickness (0.625 mm) were kept constant for all acquisitions.

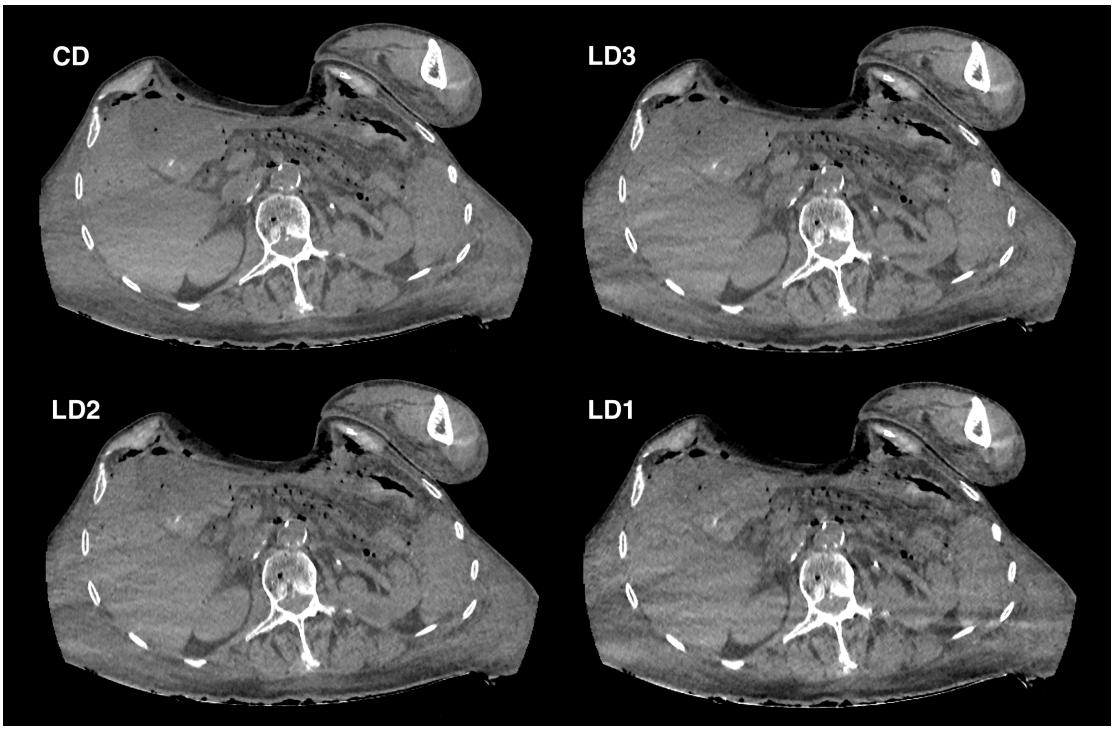

Figure 2.2 Axial CT images acquired in a cadaver at the level of the porta hepatits with varying tube voltage and current settings to give a reference conventional dose and three low-dose datasets. The images are reconstructed with MBIR.

CT image reconstruction

All images were reconstructed from the raw-data acquisitions. Each data set (400, 200, 100, 50, and 10mA) from both the CT thorax and CT abdomen series were reconstructed using three different reconstruction techniques: FBP; our standard departmental reconstruction technique hybrid iterative reconstruction (60% FBP and 40% ASIR), labeled ASIR40; and pure iterative reconstruction (MBIR). The MBIR software offers two reconstruction algorithms for chest CT: MBIR RP05 and MBIR RP20, and two algorithms for abdominal CT: MBIR RP05 and MBIR NR05. The chest and abdominal data sets were reconstructed with both to allow for a comparison between the two MBIR data sets. A data set was created for each radiation dose level and reconstruction algorithm resulting in a

total of 40 data sets for analysis (20 CT thorax and 20 CT abdomen). Images were reconstructed from an acquisition thickness of 0.625mm to a final slice thickness of 1.25mm for all data sets.

The cadaveric data sets were reconstructed from the raw-data acquisitions using FBP, ASIR40, and MBIR (Figure 2.3). A series was generated for each imaging protocol and reconstruction algorithm resulting in a total of 12 series per cadaver.

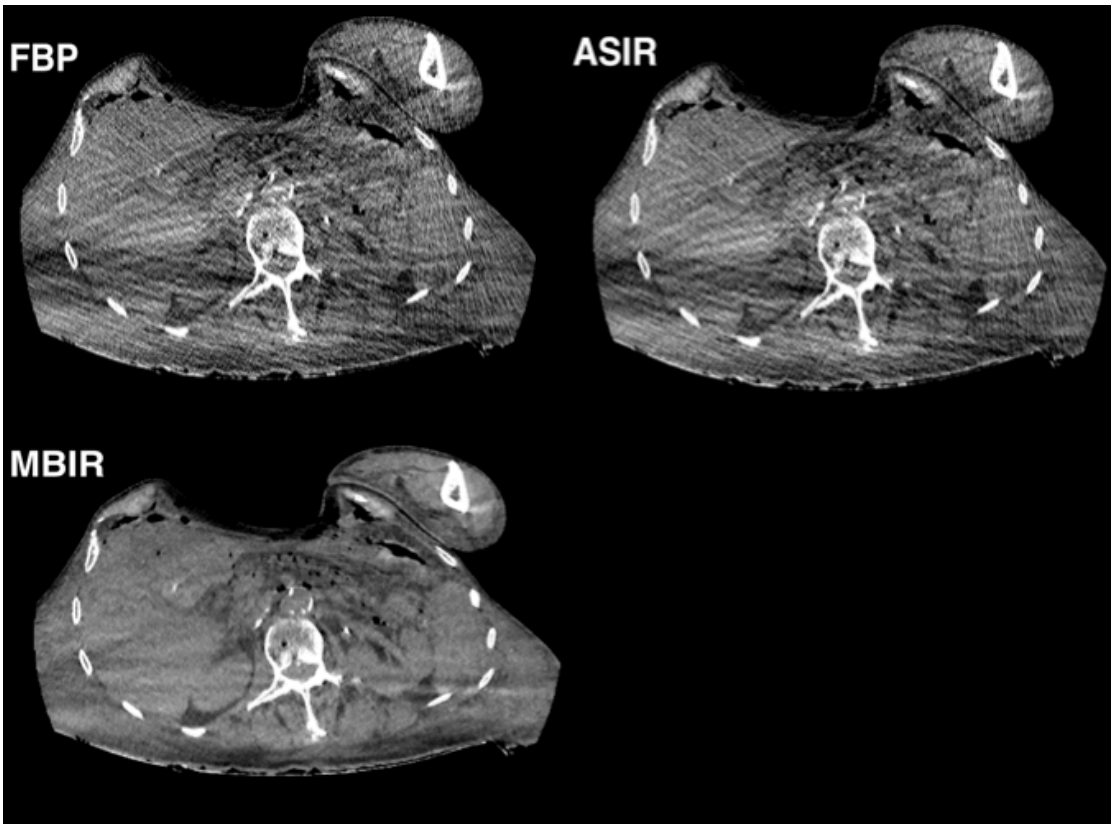

Figure 2.3 Axial cadaveric CT images at the level of the porta hepatits reconstructed with FBP, ASIR40 and MBIR.

CT dose measurement

DLP and CTDIvol tolerances were verified using a standard 32cm perspex phantom and a 10cm ionization chamber with a Victoreen NERO mAx unit (Fluke Biomedical, OH, USA). The 32cm phantom was imaged at tube currents of 40mA and 50mA with a 32cm field of view (FOV). Radiation measurements were taken with the pencil chamber inserted at central and peripheral locations. Three measurements at each location were averaged and used to calculate corresponding CTDI values which were subsequently converted to a weighted CTDI. The displayed CTDI and DLP values of the CT console were recorded and percentage error calculated using ionization chamber measures. Calibration of the CT unit was performed once per week in accordance with the manufacturer's instructions.

Image quality

Quantitative analysis of image noise

Objective image quality analysis was performed independently on a dedicated workstation (Advantage Workstation VolumeShare 2, Version 4.4, GE Medical Systems, Milwaukee, WI) by the author (6 years experience) and a second operator with 7 years experience. For the phantom chest images, attenuation values were measured in HU at three levels: the aortic arch, the carina, and the maximum cardiac diameter. Measurements were recorded by placing spherical histograms of equal size (diameter, 10mm; volume, 519 mm^3) in the descending aorta and paraspinal muscles of the posterior chest wall at each level.[84]

For the phantom abdominal images, attenuation values in HU were measured at five levels using spherical histograms of equal size (diameter, 10mm; volume,

519 mm^3). The ROIs were placed in the following anatomical structures: liver parenchyma at the level of the right hemi-diaphragm; liver parenchyma at the level of the porta hepatis; the spleen at the level of the splenic hilum; the body of the pancreas at the superior mesenteric artery origin; and the right kidney at the level of the renal hilum.

For the cadaveric abdominal images, ROIs were placed in the following anatomical structures: liver parenchyma at the level of the right hemi-diaphragm; liver parenchyma at the level of the porta hepatis; erector spinae at the right renal hilum; psoas muscle at the iliac crest; and gluteus maximus muscle at the roof of the acetabulum.[54]

The ROIs were placed in as homogenous an area as possible, taking care to avoid fat planes and blood vessels. Soft tissue interfaces were avoided to allow standardized comparisons between studies. A diameter of 10 mm was used for all ROIs, selected following review of prior studies[47, 54], although the result obtained should not differ with the size of the ROI if the tissues being assessed are homogenous. The standard deviation of the mean attenuation in the ROI served as an objective measure of image noise.[85] The signal-to-noise ratio of each ROI was calculated by dividing the mean HU by its standard deviation.[77]

Measurements were taken three times by each operator to reduce error and the mean was recorded. The mean of both operators' measurements was used for analysis. The operators were blinded to the scanning protocol and reconstruction technique used and the order of the data sets was randomized.

Qualitative analysis

Subjective image quality assessment was performed on the Advantage Workstation by two experienced readers in consensus. Image noise (grade 1, major, unacceptable; grade 2, substantial, above average; grade 3, moderate, average; grade 4, minor, below average; grade 5, absent) and overall image quality (grade 1, bad, no diagnosis possible; grade 2, poor, diagnostic confidence substantially reduced; grade 3, moderate, but sufficient for diagnosis; grade 4, good; grade 5, excellent) were rated at six different levels in the chest of the phantom: the lung apices, the aortopulmonary window, the carina, below the pulmonary hila, and at the widest cardiac and thoracic diameters.[77, 86]

For the phantom abdominal images, image noise and overall image quality were rated using the same scoring systems at five levels: the right hemi-diaphragm; the porta hepatis; the splenic hilum; the superior mesenteric artery origin; and the level of the right renal hilum.

Subjective image noise, diagnostic acceptability, and contrast resolution were graded on a 10-point scale at 5 anatomical levels in the cadaveric abdominal CTs: right hemi-diaphragm, porta hepatis, right renal hilum, iliac crest, and roof of the acetabulum. Image noise was graded as acceptable (score of 5) if average graininess was seen with satisfactory depiction of small anatomical structures such as blood vessels and tissue interfaces, unacceptable (score of 1) if graininess interfered with structure depiction, and excellent (score of 10) if there was no appreciable mottle. Diagnostic acceptability was graded as acceptable (score of 5), unacceptable (score of 1), or excellent (score of 10) if depiction of solid organs, large bowel, small bowel, peri-colonic fat, and peri-enteric fat for diagnostic interpretation and degree of image degradation by beam hardening artifacts was satisfactory, unsatisfactory or considerably

superior, respectively. Contrast resolution was also graded at the liver, spleen and buttock musculature using a 10-point scale in which a score of 10 represented superior contrast between different abdominal soft tissues, a score of 1 indicated the poorest contrast, and a score of 5 indicated acceptable contrast. Streak artifact was also graded at each level using a 3-point scale: 0, no streak artifact present; 1, streak artifact present but not interfering with image interpretation; and 2, streak artifact present and interfering with image interpretation. The parameters of image quality were selected on the basis of previous studies and the *European Guidelines on Quality criteria for Computed Tomography*.[87, 88, 89] The authors had used these methods previously and trained the other readers before analysis with a set of 5 practice scans.[47]

The order of all data sets was randomized and the readers were blinded to the scanning protocol and reconstruction technique. The readers used a combination of axial and coronal reformats for interpretation and altered the CT level and window width at their discretion.

Catphan

A Catphan 600 phantom (The Phantom Laboratory, Greenwich, NY, USA) was scanned over its entire length using the same scan parameters and reconstruction techniques as the torso phantom. Images were reconstructed from an acquisition thickness of 0.625mm to a final slice thickness of 1.25mm to give a total of 20 data sets for analysis.

The Catphan consists of several modules that may be used to evaluate spatial resolution, low contrast detectability, and CNR. All Catphan analyses were performed independently by two readers. The Catphan contains a high-

resolution test gauge with 1 through 21 spaced aluminum line pairs that facilitates the quantification of spatial resolution in the transverse plane. The highest line pair set with distinguishable line pairs was recorded by both readers in consensus.

The low contrast modulus of the phantom contains several sets of cylindrical low-contrast objects with varying contrast levels (1%, 0.5%, and 0.3%). The 40mm long supra-slice (targets with a z axis dimension longer than most maximum slice widths) objects with a 1% contrast level and varying diameters (2, 3, 4, 5, 6, 7, 8, 9, and 15mm) were used for analysis. A side-by-side analysis was performed whereby spherical ROIs of equal size (diameter, 10mm; volume, 519 mm3) were placed in the 15mm low contrast object and in the nearby phantom background. The side-by-side analysis ensured that the ROIs were placed in the same position in each data set. The CNR was calculated by subtracting the mean HU measured in the nearby phantom background from the mean HU measured in the 15mm object and dividing the result by the standard deviation of the pixels in the 15mm object.[90] The mean CNR of both readers was used for analysis.

For the subjective assessment of low contrast detectability, the readers rated the visibility of the low contrast objects using a three-point scale: grade 1 indicated the object was clearly visible; grade 0.5 indicated the object was partially visible; and grade 0 indicated the object could not be seen. The grade assigned to each data set was then summated and the mean of both readers was used for analysis. Each dataset was viewed independently by both readers in a randomized and blinded fashion.

Statistical analysis

Data was exported from Microsoft Office Excel 2010 (Microsoft Corporation, CA, USA) into GraphPad Prism version 6.0 (GraphPad Software Incorporated, San Diago, USA) and Statistical Package for the Social Sciences (SPSS) version 22 (IBM, Chicago, Illinois, USA) for further analysis. Distribution of variables was assessed using D'Agostino-Pearson omnibus normality test. Inter-observer concordance was assessed with Cohen's k test.

One-way analysis of variance was used to compare three or more unmatched groups of parametric indices. Dunn's or Tukey's multiple comparisons test was used to assess differences between the reconstruction algorithms at each tube current level for quantitative and qualitative parameters. Mean differences between reconstruction algorithms and their 95% confidence intervals were calculated at each tube current level. Percentage noise reduction compared to FBP and ASIR40 was determined for each of the MBIR data sets. Dunnett's test was used to compare the quantitative and qualitative parameters of the low-dose MBIR cadaveric series with the CD ASIR40 series. P values less than 0.05 were considered to be statistically significant.

Results

Phantom chest CT

Quantitative analysis of image noise

Objective image noise was significantly different across all dose levels ($p<0.0001$) with the greatest levels of noise observed in the 10mA reconstructions.

Figure 2.4 demonstrates the variation in objective image noise with choice of reconstruction algorithm at the different dose levels. MBIR RP05 reconstructions had significantly lower measures of objective image noise compared to FBP reconstructions at tube current levels of 200, 100, 50, and 10mA with the greatest mean difference at the 10mA level ($p<0.0001$). This equated to percentage noise reductions of 34.3%, 44.9%, 58%, and 74% at each of these tube current levels respectively.

MBIR RP20 reconstructions had significantly lower measures of objective image noise compared to FBP reconstructions at tube current levels of 50 and 10mA with the greatest mean difference at the 10mA level (noise reduction of 60%)($p<0.0001$).

MBIR RP05 had significantly lower measures of objective image noise compared to ASIR40 at tube current levels of 50 and 10mA with the greatest mean difference at the 10mA level ($p<0.0001$). See Table 2.1 for a comparison of all reconstruction algorithms.

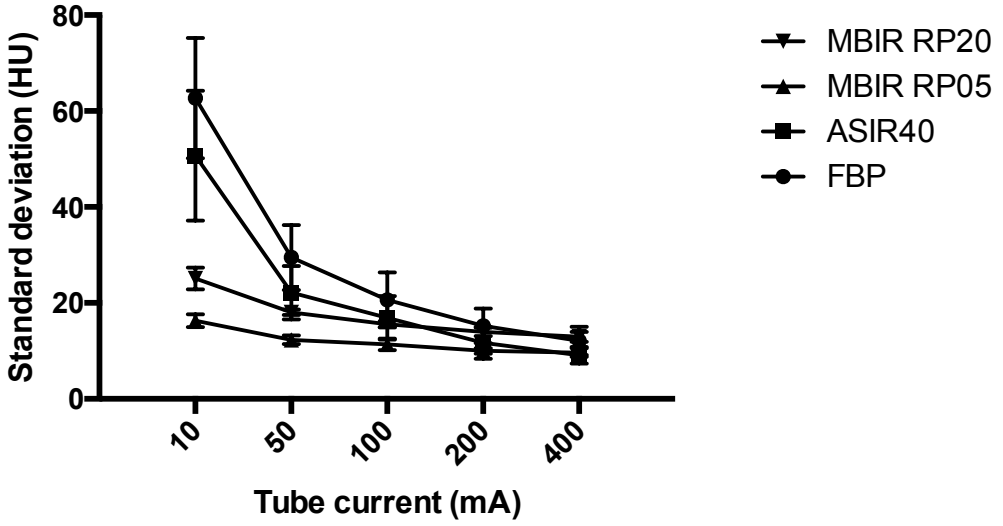

Figure 2.4 Variation in standard deviation of Hounsfield units (HU)(objective image noise) with choice of reconstruction algorithm at different dose levels for the CT thorax data sets. Data are plotted as mean and standard deviation.

	400mA		200mA		100mA		50mA		10mA	
	Mean diff.	95%CI	Mean diff.	95%CI	Mean diff.	95%CI	Mean diff.	95%CI	Mean diff.	95% CI
FBP v ASIR40	3.02*	0.062 to 5.97	3.53	-0.522 to 7.59	3.77	-2.22 to 9.75	7.32*	0.194 to 14.44	12.02	-3.02 to 27.05
FBP v MBIR05	2.45	-0.51 to 5.40	5.23**	1.18 to 9.29	9.28**	3.3 to 15.27	17.13***	10.01 to 24.26	46.40***	31.36 to 61.44
FBP v MBIR20	-0.83	-3.78 to 2.12	1.27	-2.79 to 5.32	5.08	-0.91 to 11.07	11.40**	4.28 to 18.53	37.62***	22.58 to 52.65
ASIR40 v MBIR05	-0.56	-3.52 to 2.38	1.70	-2.36 to 5.76	5.52	-0.472 to 11.50	9.82**	2.69 to 16.94	34.38***	19.35 to 49.42
ASIR40 v	-3.85**	-6.81 to -	-2.27	-6.32 to 1.79	1.32	-4.67 to	4.08	-3.04 to	25.60***	10.56 to

MBIR20		0.90				7.30		11.21		40.64
MBIR05 v MBIR20	-3.28*	-6.24 to -0.33	-3.97	-8.02 to 0.088	-4.20	-10.2 to 1.79	-5.73	-12.86 to 1.4	-8.78	-23.82 to 6.252

Table 2.1 Comparison of objective image noise between each reconstruction algorithm at each dose level for the CT thorax data sets. Given is the mean difference between reconstruction techniques with their 95% confidence intervals. The significance level of Dunn's multiple comparisons test is indicated by *.

Mean SNR of MBIR RP05 reconstructions was significantly higher than FBP and ASIR40 reconstructions at the 10 mA level (P<0.01). All other comparisons were non significant (Figure 2.5).

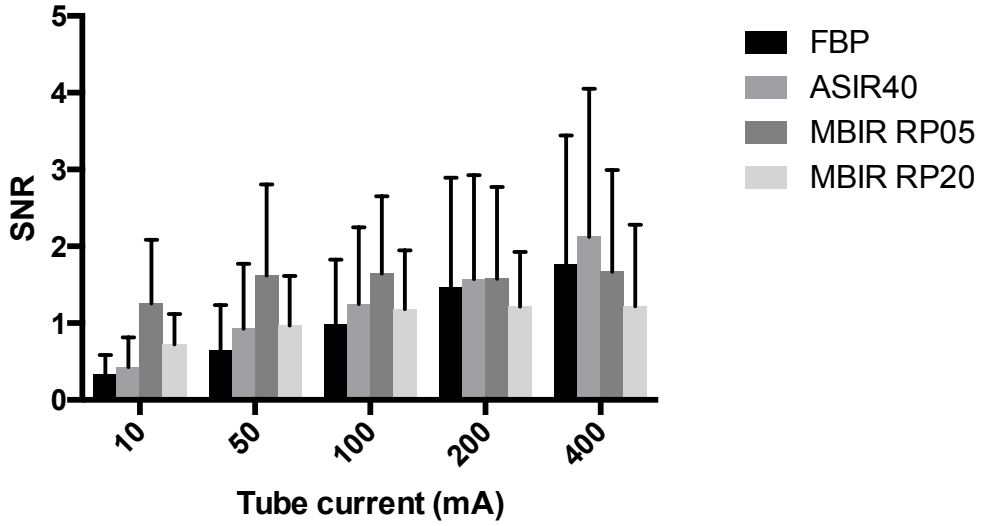

Figure 2.5 Variation in signal-to-noise ratio (SNR) with choice of reconstruction algorithm at different dose levels for the CT thorax data sets. Data are plotted as mean and standard deviation.

Qualitative analysis

Subjective image noise scores were significantly higher for both MBIR RP05 and MBIR RP20 reconstructions compared to FBP reconstructions at all dose levels with the greatest mean difference observed for both at the 10mA level ($p<0.0001$)(Figure 2.6). Subjective noise scores were also significantly higher for both MBIR RP05 and MBIR RP20 reconstructions compared to ASIR40 reconstructions at the 400, 200, 50, and 10mA dose levels with the greatest mean difference at the 10mA level ($P<0.0001$). No significant difference was observed between the two MBIR reconstruction algorithms at all levels.

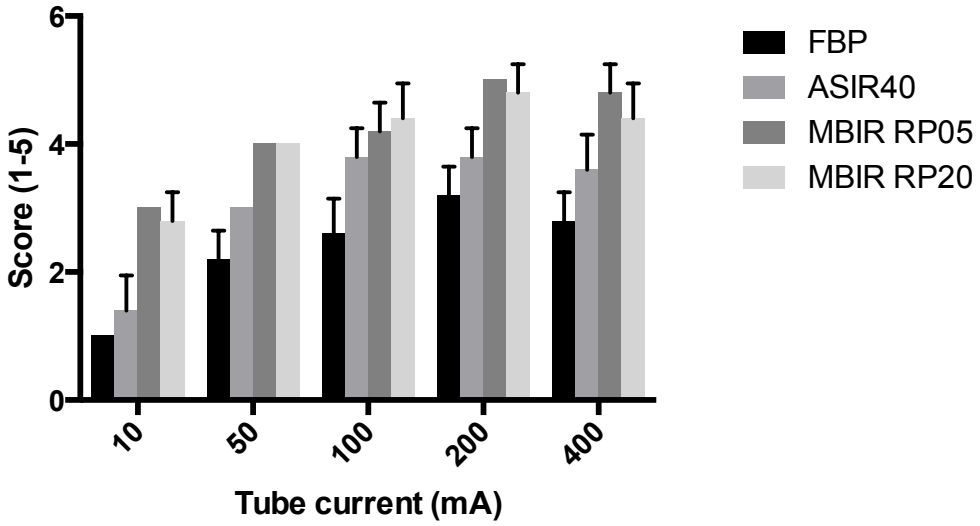

Figure 2.6 Variation in subjective noise scores with choice of reconstruction algorithm at different dose levels for the CT thorax data sets. Data are plotted as mean and standard deviation.

Subjective image quality scores were significantly higher for both MBIR RP05 and MBIR RP20 reconstructions compared to FBP reconstructions at all dose levels except 200mA with the greatest mean difference at the 10mA level ($p<0.0001$)(Figure 2.7). Image quality scores were also significantly higher for both MBIR RP05 and MBIR RP20 reconstructions compared to ASIR40 reconstructions at the 10mA dose level ($P<0.001$). No significant difference was observed between the two MBIR reconstruction methods at all levels.

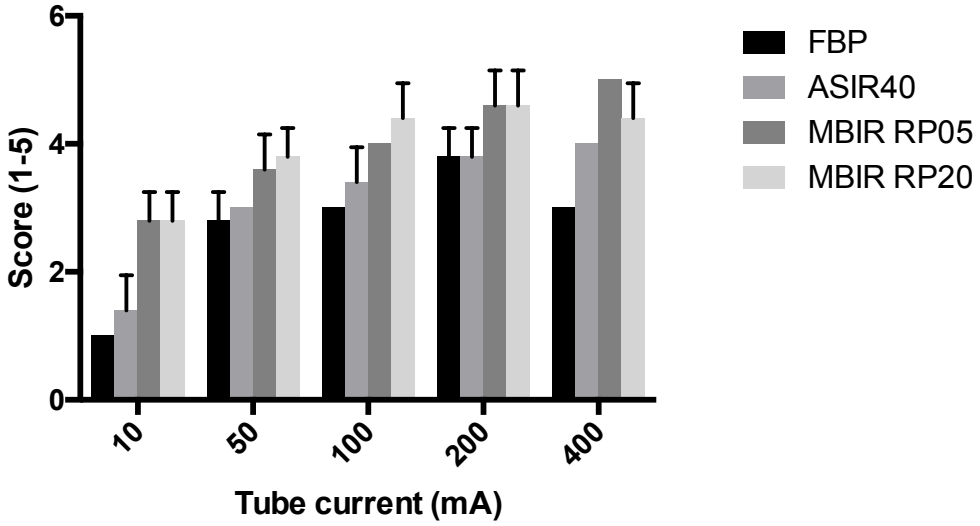

Figure 2.7 Variation in image quality scores with choice of reconstruction algorithm at different dose levels for the CT thorax data sets. Data are plotted as mean and standard deviation.

Phantom abdominal CT

Quantitative analysis of image noise

Objective image noise was significantly different across all dose levels ($p<0.0001$) with the greatest levels of noise observed in the 10mA reconstructions.

Figure 2.8 demonstrates the variation in objective image noise with choice of reconstruction algorithm at the different dose levels. Both MBIR RP05 and MBIR NR05 reconstructions had significantly lower measures of objective image noise compared to FBP reconstructions at all tube current levels with the greatest mean differences observed for both at the 10mA level ($p<0.0001$).

This equated to percentage noise reductions of 44%, 53.4%, 61.7%, 71.2%, and 76.5% for MBIR RP05 and 52.7%, 63.8%, 68.7%, 75%, 86.9% for MBIR NR05 compared to FBP at tube levels of 400, 200, 100, 50, and 10 respectively.

Both MBIR RP05 and MBIR NR05 reconstructions had significantly lower measures of objective image noise compared to ASIR40 reconstructions at all tube current levels with the greatest mean differences being observed for both at the 10mA level ($p<0.0001$). See Table 2.2 for a comparison of all reconstruction algorithms.

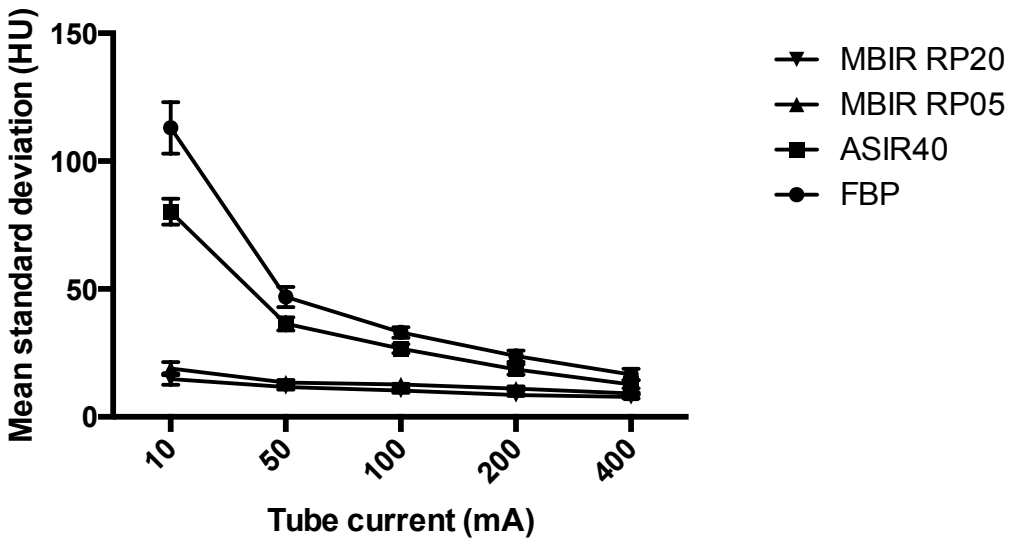

Figure 2.8 Variation in standard deviation of Hounsfield units (HU)(objective image noise) with choice of reconstruction algorithm at different dose levels for the CT abdomen data sets. Data are plotted as mean and standard deviation.

	400mA		200mA		100mA		50mA		10mA	
	Mean diff	95% CI	Mean diff	95% CI	Mean diff	95% CI	Mean diff	95% CI	Mean diff	95% CI
FBP v ASIR40	3.88**	1.34 to 6.43	5.24**	2.44 to 8.04	6.32****	3.77 to 8.87	10.48**	6.03 to 14.93	32.78**	22.11 to 43.45
FBP v MBIR05	7.38***	4.84 to 9.93	12.70**	9.89 to 15.50	20.36**	17.81 to 22.91	33.40**	28.95 to 37.85	94.12**	83.45 to 104.8
FBP v MBIR20	8.76***	6.22 to 11.30	15.18**	12.38 to 17.98	22.70**	20.15 to 25.25	35.16**	30.71 to 39.61	98.24**	87.57 to 108.9
ASIR40 v MBIR05	3.50**	0.95 to 6.05	7.46****	4.66 to 10.26	14.04**	11.49 to 16.59	22.92**	18.47 to 27.37	61.34**	50.67 to 72.01
ASIR40 v MBIR20	4.88***	2.34 to 7.43	9.94****	7.14 to 12.74	16.38**	13.83 to 18.93	24.68**	20.23 to 29.13	65.46**	54.79 to 76.13
MBIR05	1.38	-1.17	2.48	-	2.34	-0.21	1.76	-	4.12	-6.55

5 v	to	0.324	to	2.688	to
MBIR2	3.93	to	4.89	to	14.79
0		5.29		6.21	

Table 2.2 Comparison of objective image noise between each reconstruction algorithm at each dose level for the CT abdomen data sets. Given is the mean difference between reconstruction techniques with their 95% confidence intervals. The significance level of Dunn's multiple comparisons test is indicated by *.

Mean SNR of MBIR NR05 reconstructions was significantly higher than FBP and ASIR40 reconstructions at the 200, 100, 50, and 10 mA levels with the greatest mean difference at the 10mA level (P<0.001). Mean SNR of MBIR RP05 reconstructions were significantly higher than FBP and ASIR40 reconstructions at the 50 and 10mA levels with the greatest mean difference at the 10mA level (P<0.01). All other comparisons were non significant (Figure 2.9).

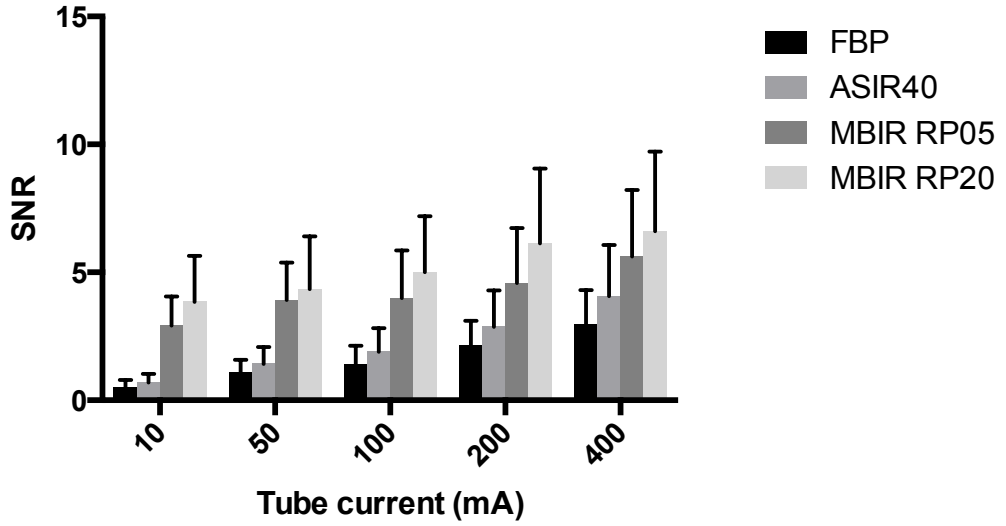

Figure 2.9 Variation in signal-to-noise ratio (SNR) with choice of reconstruction algorithm at different dose levels for the CT abdomen data sets. Data are plotted as mean and standard deviation.

Qualitative analysis

Subjective image noise scores were significantly higher for MBIR RNR05 reconstructions compared to FBP and ASIR40 reconstructions at all dose levels with the greatest mean difference observed at the 10mA level ($p<0.0001$)(Figure 2.10). Subjective noise scores were significantly higher for MBIR RP05 reconstructions compared to FBP and ASIR40 reconstructions at the 200, 100, 50, and 10mA dose levels with the greatest mean difference at the 10mA level ($P<0.0001$). No significant difference was observed between the two MBIR reconstruction methods at all levels.

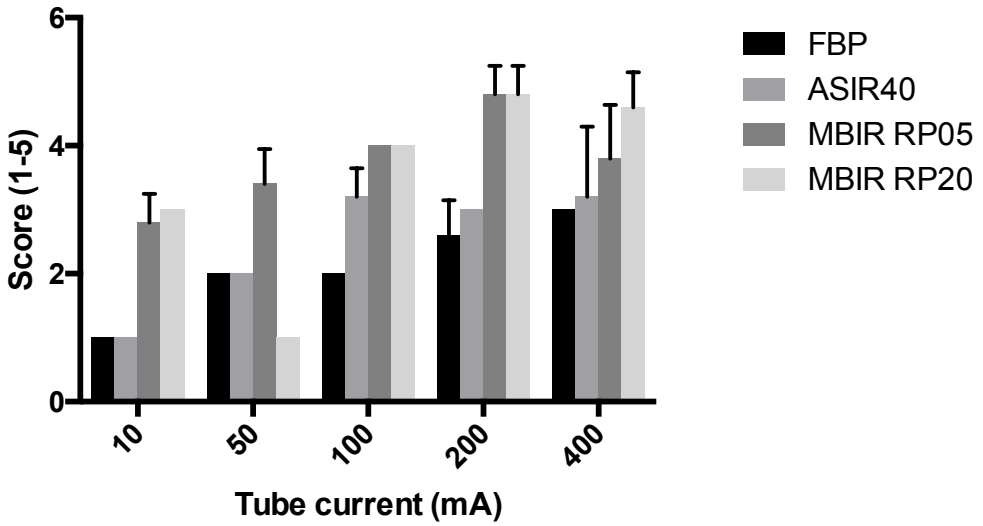

Figure 2.10 Variation in subjective noise scores with choice of reconstruction algorithm at different dose levels for the CT abdomen data sets. Data are plotted as mean and standard deviation.

Subjective image quality scores were significantly higher for both MBIR RP05 and MBIR NR05 reconstructions compared to FBP and ASIR40 reconstructions at the 200, 100, 50, and 10mA levels with the greatest mean difference observed for

both at the 10mA level (p<0.0001)(Figure 2.11). No significant difference was observed between the two MBIR reconstruction methods at all levels.

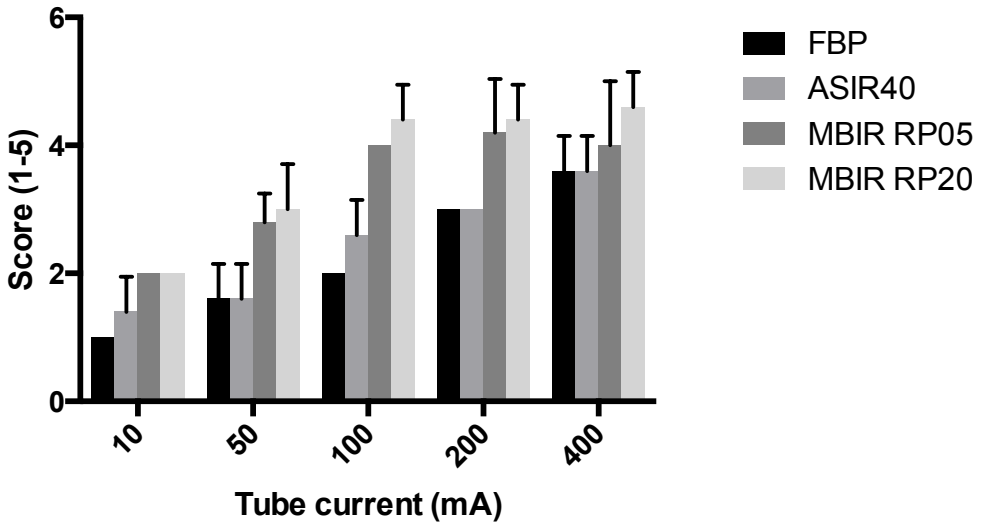

Figure 2.11 Variation in image quality scores with choice of reconstruction algorithm at different dose levels for the CT abdomen data sets. Data are plotted as mean and standard deviation.

Cadaveric abdominal CT

Quantitative analysis of image noise

Objective image noise was significantly different at each dose level (p<0.0001) and between each reconstruction algorithm at every dose level (p<0.0001 for all comparisons) with the greatest levels of image noise at LD1 (Figure 2.12). MBIR reconstructions had significantly lower measures of objective image noise compared to both FBP and ASIR40 reconstructions at all dose levels (p<0.0001

for all comparisons) with the greatest mean difference observed for both at the LD1 level; mean differences of 34.26HU (CI, 30.19 to 38.35) and 20.56HU (CI, 16.47 to 24.64) compared FBP and ASIR40, respectively.

MBIR facilitated percentage noise reductions of 68.1%, 69.2%, 61.02%, and 65% compared to FBP and 56.2%, 57.9%, 52.6%, and 56.6% compared to ASIR40 at the LD1, LD2, LD3, and CD levels, respectively.

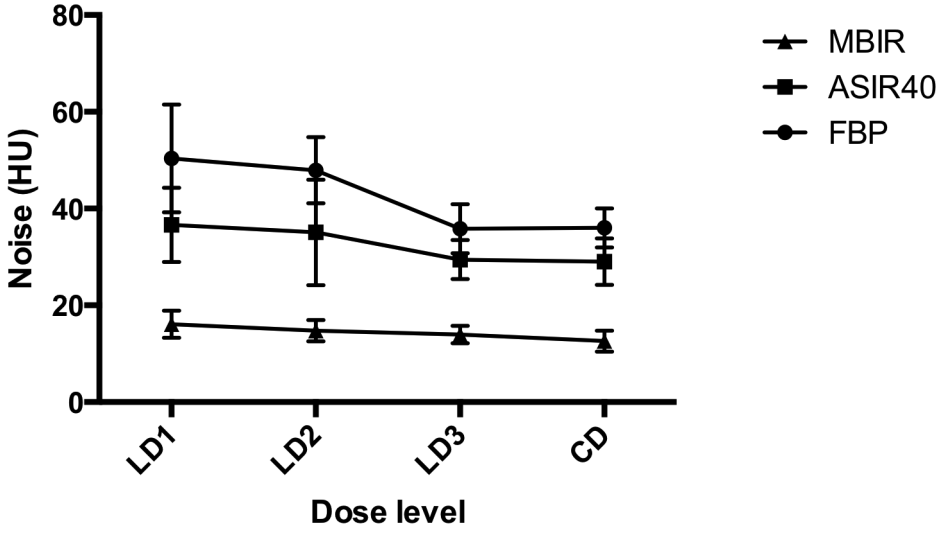

Figure 2.12 Variation in objective image noise (standard deviation of Hounsfield units (HU)) with choice of reconstruction algorithm at each low-dose (LD) and conventional dose (CD) protocol. Data are plotted as mean and standard deviation.

SNR for MBIR data sets was significantly higher than both FBP and ASIR40 data sets at each dose level ($p<0.0001$) with the greatest mean difference compared to FBP at LD2 (2.62 (CI, 1.67 to 3.56)) and compared to ASIR40 at CD (2.26 (CI,

1.3 to 3.2)) (Figure 2.13). No significant difference was observed in SNR between FBP and ASIR40 data sets at all dose levels.

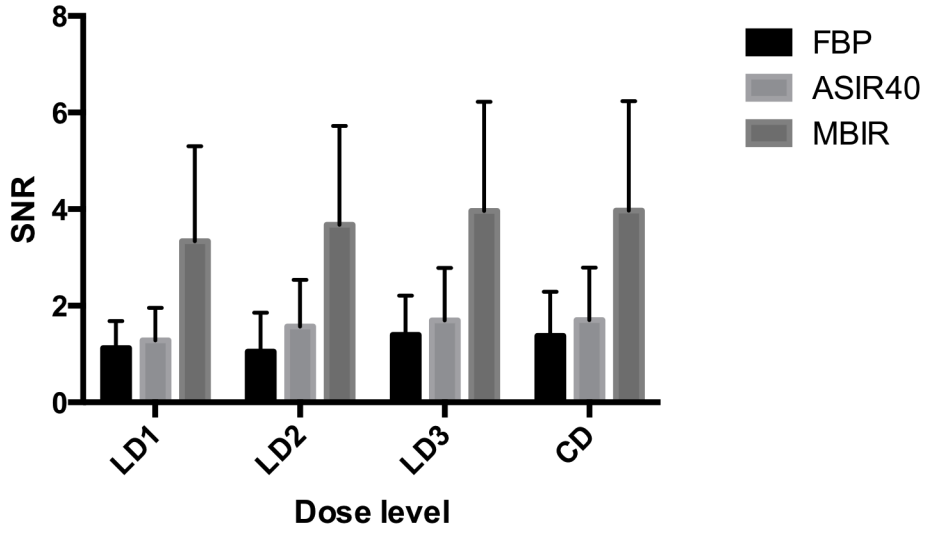

Figure 2.13 Variation in signal-to-noise ratio (SNR) with choice of reconstruction algorithm at low-dose (LD) and conventional dose (CD) protocol. Data are plotted as mean and standard deviation.

Qualitative analysis

There was excellent agreement between the two raters for the assessment of diagnostic acceptability and presence of streak artifact (k, 0.824 and 0.868, $p<0.001$) with moderate agreement for the assessment of subjective image noise and contrast resolution (k, 0.795 and 0.623, $p<0.001$). Mean scores were used for further analysis. Subjective image noise, diagnostic acceptability, and contrast resolution scores were significantly different between each reconstruction algorithm at each dose level ($p<0.0001$ for all comparisons).

MBIR reconstructions had significantly higher qualitative scores compared to both FBP and ASIR40 reconstructions at all dose levels ($p<0.0001$ for all comparisons) with the greatest mean differences observed for all qualitative measures at the LD1 level (Figures 2.14, 2.15 and 2.16).

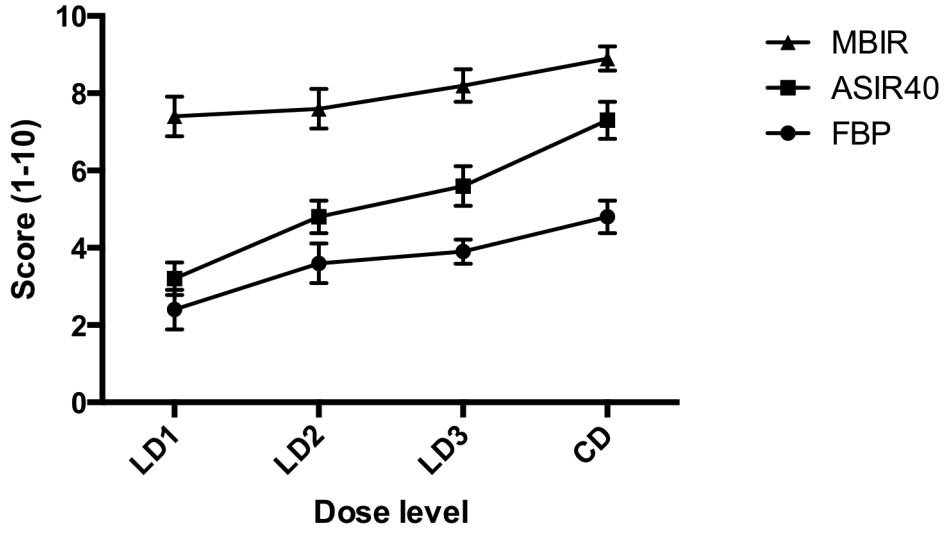

Figure 2.14 Variation in subjective noise scores with choice of reconstruction algorithm at each low-dose (LD) and conventional dose (CD) protocol. Data are plotted as mean and standard deviation.

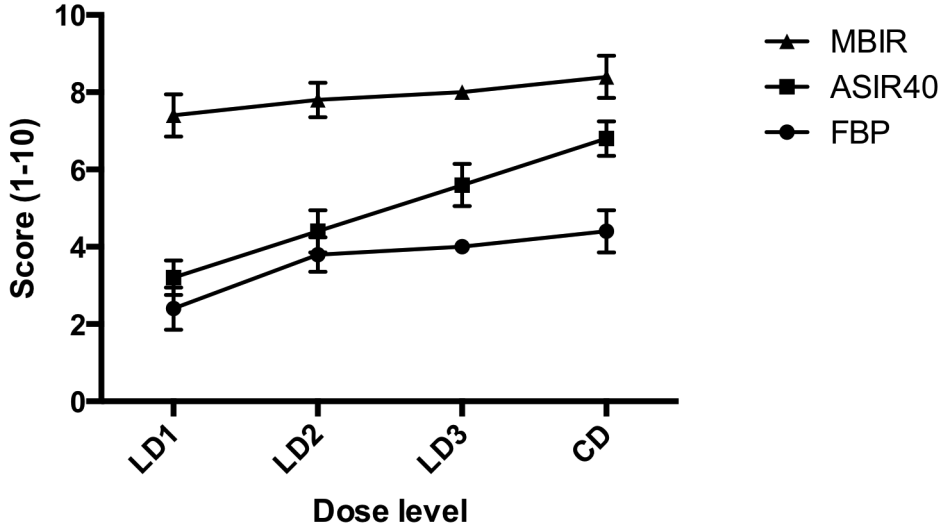

Figure 2.15 Variation in diagnostic acceptability scores with choice of reconstruction algorithm at each low-dose (LD) and conventional dose (CD) protocol. Data are plotted as mean and standard deviation.

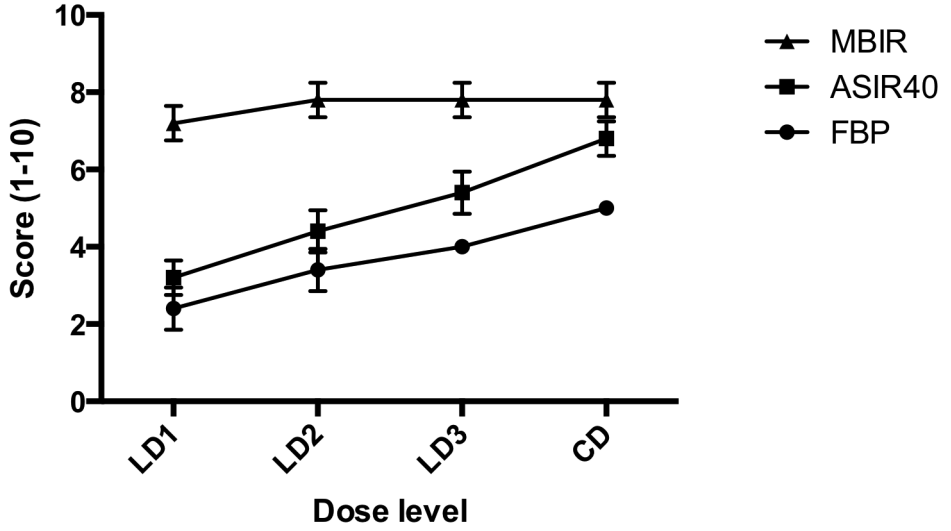

Figure 2.16 Variation in contrast resolution scores with choice of reconstruction algorithm at each low-dose (LD) and conventional dose (CD) protocol. Data are plotted as mean and standard deviation.

MBIR reconstructions had significantly lower levels of streak artifact compared to FBP ($p<0.001$) and ASIR40 ($p<0.01$) at the lowest dose level only (LD1). All other comparisons were non-significant (Figure 2.17).

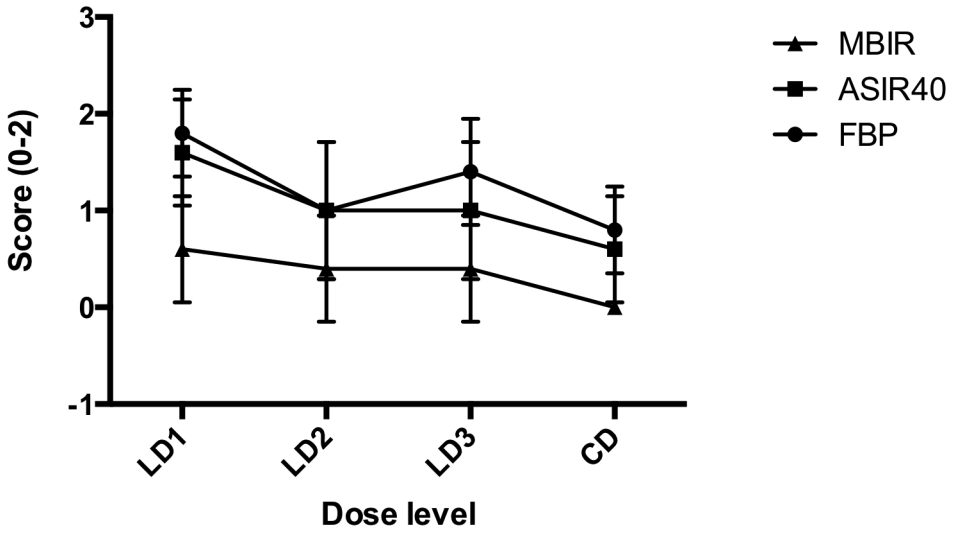

Figure 2.17 Variation in streak with choice of reconstruction algorithm at each low-dose (LD) and conventional dose (CD) protocol. Data are plotted as mean and standard deviation.

Comparison of low-dose MBIR with conventional dose ASIR40

LD MBIR series were acquired with a mean dose reduction compared to CD ASIR40 of 62.17%, 50%, and 29.12% for LD1 MBIR, LD2 MBIR, and LD3 MBIR series, respectively. All LD MBIR reconstructions had significantly lower levels of objective image noise compared to the CD ASIR40 protocol ($p<0.0001$ for all comparisons)(Figure 2.18).

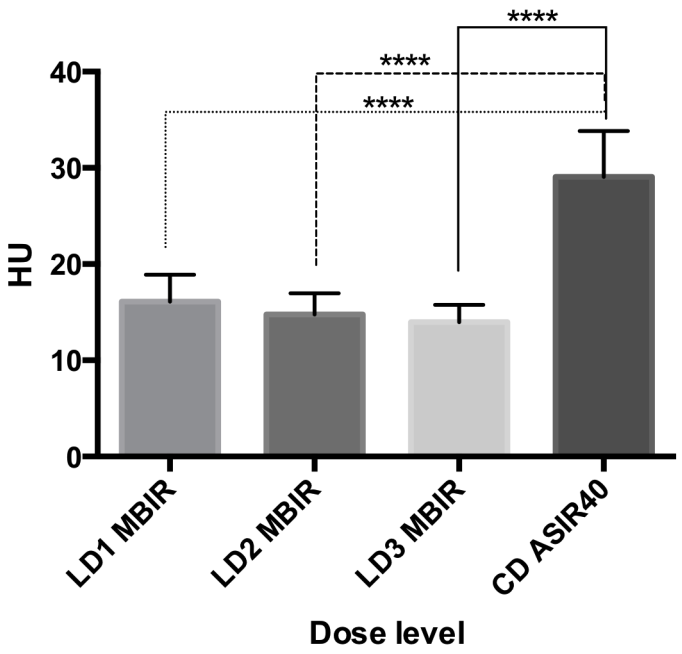

Figure 2.18 Comparison of objective image noise between low-dose protocols reconstructed with MBIR and a conventional dose protocol reconstructed with 40% ASIR. Data are plotted as mean and standard deviation. **** denotes significance at the $p<0.0001$ level.

All low-dose MBIR series and conventional dose ASIR40 series were reported to have above average to excellent subjective image noise, diagnostic acceptability, and contrast resolution scores (Figure 2.19). Diagnostic acceptability and contrast resolution scores were significantly superior for all LD MBIR series

compared to CD ASIR40 ($p<0.0001$ for all comparisons). LD2 MBIR and LD3 MBIR had significantly superior subjective image noise scores compared to CD ASIR40 ($p<0.0001$ for both comparisons) with no significant difference in subjective image noise between LD1 MBIR and CD ASIR40 reconstructions. No significant difference was observed in streak artifact between any of the LD MBIR series and CD ASIR40.

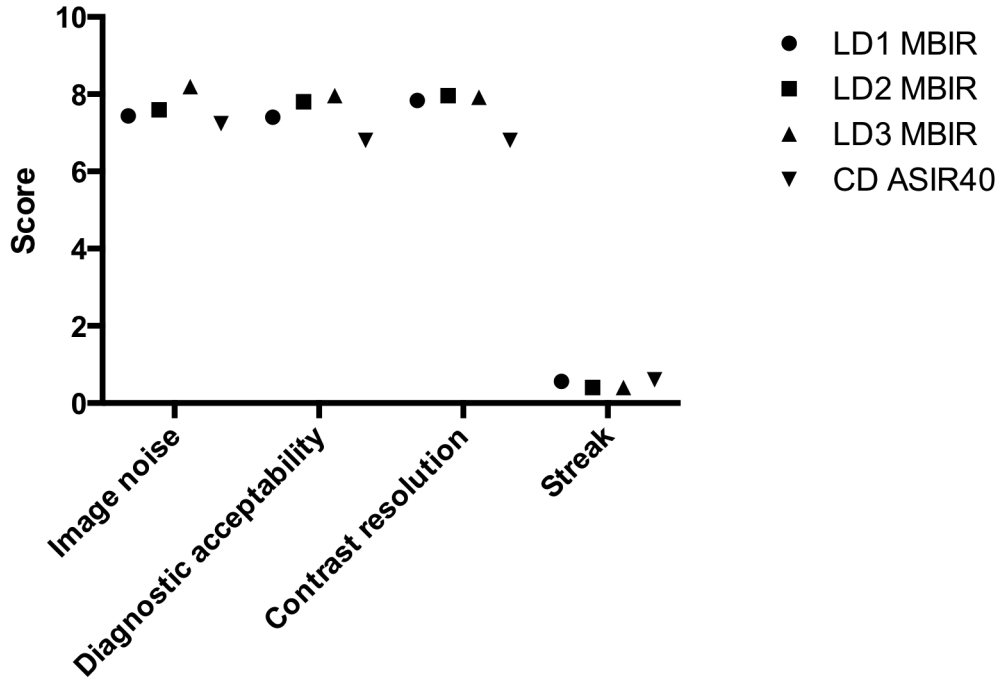

Figure 2.19 Comparison of qualitative measures between low-dose protocols reconstructed with MBIR and conventional dose protocol reconstructed with 40% ASIR. Data are plotted as mean and standard deviation.

Catphan

Spatial resolution tended to be greater for MBIR RP05 and MBIR RP20 data sets compared to FBP and ASIR40 data sets at all tube current levels (Table 2.3). However, when compared by reconstruction algorithm, no significant difference was observed (p=0.139). There was also a tendency, although not significant, towards higher low contrast detectability and CNR values for both MBIR data sets (Tables 2.4 and 2.5).

	400mA	200mA	100mA	50mA	10mA
FBP	8	8	8	7	7
ASIR40	8	8	8	7	7
MBIR RP05	9	9	8	8	7
MBIR RP20	9	9	8	7	7

Table 2.3 Comparison of spatial resolution between each reconstruction algorithm at each dose level.

	400mA	200mA	100mA	50mA	10mA
FBP	3	2	1	.5	0
ASIR40	4	3	1.5	1	0
MBIR RP05	5	4.5	2.5	1.5	0
MBIR RP20	5	4.5	2.5	1.5	0

Table 2.4 Comparison of low contrast detectability between each reconstruction algorithm at each dose level.

	400mA	200mA	100mA	50mA	10mA
FBP	.89	.75	.29	.37	0
ASIR40	1.34	.9	.65	.68	0
MBIR RP05	1.6	1	1.29	.78	0
MBIR RP20	1.7	1.2	.73	1.2	0

Table 2.5 Comparison of contrast-to-noise ratios between each reconstruction algorithm at each dose level.

Discussion

There has been a significant drive in industry in recent years to address concerns regarding the risk of radiation-induced carcinogenesis by way of development of dose reduction applications including IR algorithms. These IR techniques may be statistical or model-based and are replacing traditional analytical algorithms such as FBP that use simple mathematical assumptions of a CT system.

MBIR has been shown to reduce image noise and artifacts and improve image quality compared to FBP and hybrid IR in several conventional dose CT studies.[91,92] Furthermore, MBIR has been used to facilitate significant dose reductions while preserving diagnostic image quality in low-dose clinical studies.[93] Its use in chest CT appears to have the greatest dose reduction potential with reported dose reductions of between 79% and 98% compared to FBP.[94,95]

Although MBIR reduces image noise at both low and conventional radiation doses, few studies have assessed the dose level at which MBIR has the greatest efficacy for noise reduction. In line with previous studies, we found MBIR to have significantly lower levels of objective image noise at all dose levels in CT abdominal data sets and almost all CT thorax data sets compared to FBP in the torso phantom. The greatest noise reduction was seen at the ultra-low-dose level with noise reductions of 74% and 86.9% for thorax and abdominal data sets

respectively. In addition, MBIR significantly outperformed ASIR40 in terms of noise reduction at all dose levels in the abdomen and at the two lowest dose levels in the thorax. A similar finding was observed for subjective image noise and quality assessment with the greatest mean difference compared to FBP and ASIR40 also being observed for both thorax and abdominal data sets at the lowest radiation dose level. With regard to the MBIR data sets, there was a tendency towards greater noise reduction with MBIR RP05 in the thorax and MBIR NR05 in the abdomen at all dose levels but all comparisons were non significant. This is to be expected as the NR05 MBIR algorithm is designed to maximize noise reduction.

With regard to the cadaveric abdominal CT scans, MBIR datasets had significantly lower levels of objective image noise compared to both FBP and ASIR40 at both conventional and low-dose levels with the greatest noise reduction observed at the lowest radiation dose level. A similar finding was observed for the qualitative indices with the greatest improvement in image quality also observed at the lowest dose level. In addition, MBIR significantly reduced streak artifact but at the lowest dose level only.

Compared to conventional dose images reconstructed with ASIR40, MBIR facilitated the acquisition of images with lower levels of image noise, higher diagnostic quality and contrast resolution scores, and comparable subjective image noise and streak artifact scores, while enabling a 62% dose reduction. Given these findings, it would appear that the greatest use of MBIR is in the performance of ultra-low-dose CT, as at this level its noise reducing capabilities can be maximized.

A major limitation to the widespread introduction of MBIR into clinical practice is the prolonged reconstruction time of approximately 45 minutes required. MBIR incorporates modeling of certain parameters previously omitted from the IR process in order to reduce computational time. These include a system model that addresses the nonlinear, polychromatic nature of x-ray tubes by modeling the photons in the data set, a statistical noise model that considers the focal spot and detector size, and a prior model that corrects unrealistic situations in the reconstruction process to decrease the computational time.[96] The incorporation of system optic information enables reductions in image noise and artifacts with improvements in spatial resolution. Although the lengthy reconstruction time required may limit its application in selected clinical settings, such as emergency imaging, this delay will not pose problems for most routine CT examinations. Furthermore, it is likely that future technological advances will shorten the processing time required for reconstruction thus expanding its clinical applications even into the emergency setting.

MBIR-reconstructed images have unique features. Similar to previous studies[68], we found MBIR-reconstructed images to have a somewhat pixilated and 'waxy' appearance that distinguished them from FBP- and ASIR-reconstructed images. A similar 'blotchy, plastic texture' of images reconstructed with pure IR algorithms available from other vendors has also been reported.[97] Initial studies of ASIR also reported a similar phenomenon[98], but partial blending with FBP and further technological advancements in the algorithm seem to have minimized this effect. Other studies have reported new artifacts in MBIR-reconstructed images such as a 'staircase effect' at bone interfaces and a 'bordering blacked-out artifact' on skin surfaces.[85] Although these artifacts had a significant effect on

image quality in all planes, predominantly on axial reformations, the overall effect on image quality was deemed to be minor.

In our study, the readers were familiar with MBIR-reconstructed images and felt that the pixilated phenomenon did not interfere with diagnostic acceptability and was minimized in the coronal plane.

We recognize the limitations of our study. We assessed the image quality characteristics of chest and abdominopelvic CT scans reconstructed with three different reconstruction algorithms. An assessment of the ability of MBIR-reconstructed images to detect lesions and characterize pathological findings was not made and further clinical studies to validate its diagnostic ability are required. Furthermore, the utility of MBIR in angiography and 3D volume rendering was not assessed and further study is warranted.

An anthropomorphic torso phantom may not accurately simulate the behavior of human tissue. However, this study method facilitates repeated scanning with a controlled alteration in radiation dose without the requirement for a separate reference standard. Future in-vivo studies in patients controlling for confounding variables are still required to confirm our results.

Cadaveric imaging precludes the administration of intravenous and oral contrast media. This is particularly relevant to the assessment of streak artifact. Previous clinical studies using intravenous and oral contrast have reported a reduction in streak artifact with the use of MBIR.[85] However, we only observed a reduction in streak artifact in MBIR-reconstructed images at the lowest dose level only, indicating a possible under evaluation of the ability of MBIR to reduce streak artifact in this study. Furthermore, due to the inherent difference in the appearance of MBIR-reconstructed images described above, readers may have

not been completely blinded to the reconstruction algorithm during subjective analysis. However, blinding to the imaging protocol was satisfactory. Finally, the results of our study may not be completely applicable to pure iterative reconstruction algorithms available from other venders and independent validation of these techniques may be required.

In conclusion, our phantom study demonstrates that chest and abdominopelvic CT images reconstructed with MBIR have significantly lower levels of image noise and greater image quality compared to FBP and ASIR40 images at most radiation dose levels, with the greatest improvements being observed at the ultra-low-dose level. MBIR facilities the acquisition of cadaveric abdominopelvic CT scans with lower levels of image noise and greater image quality compared to conventional dose images reconstructed with FBP or ASIR40, while enabling a 62% dose reduction. The results from this study can be used to form the basis for the development of modified low-dose CT protocols using MBIR in patients.

Chapter III

Low-dose carotid CT angiography using pure iterative reconstruction

Introduction

In the past, digital subtraction angiography was considered the gold standard for evaluating carotid artery disease.[99] However, due to the low but identifiable 1.2% procedure-related risk of stroke[100], patient discomfort, cost, limited views, and the variability of calculated percentage stenosis, CT angiography (CTA) has superseded digital subtraction angiography as the imaging modality of choice to evaluate carotid artery disease after screening with Doppler sonography.[101,102] Modern multidetector CT scanners combined with 3D reformatting software offer high spatial and temporal resolution enabling direct quantification of carotid artery stenosis.[103] Consequently, the number of examinations performed both for diagnosis as well as surveillance[104] is increasing, with subsequently increased cumulative radiation exposure in patients from diagnostic imaging, particularly CT. Worldwide, CT accounts for 11% of diagnostic imaging modalities performed, yet it contributes to 67% of effective dose.[105] CTA of the carotid arteries, performed using a standard imaging protocol has an effective dose of approximately 4.9 mSv, a dose one third higher than DSA.[106] Furthermore, the thyroid gland and lens of the eye are within the region of

interest scanned and exposure to ionizing radiation has been associated with an increased risk of developing thyroid malignancy and cataract induction.[107] [108]Thus, it is essential to perform carotid CTA at the lowest dose possible while still maintaining acceptable diagnostic image quality.

The literature is deficient in the area of dose reduction in CTA of the carotid arteries. One study reported a significant dose reduction of 69% and higher attenuation values within the carotid arteries with the use of a tube voltage reduction technique.[109] However, the low-dose studies were limited in image quality at the level of the common carotid artery. Furthermore, the study recommended the exclusion of obese patients from the low-dose protocol. Another study reported a dose reduction of over 30% in carotid CTA with the use of an attenuation-based, kilovolt selection algorithm while still maintaining subjective image quality.[110] A weakness of both studies is a lack of subject controls with patients being randomly assigned to either a low or conventional dose protocol. Our study is unique as it incorporates a control group with the study participants acting as their own controls thereby reducing the likelihood of confounding variables. Furthermore, we use a model based iterative reconstruction technique, which to the best of our knowledge, has not been previously investigated in CTA of the carotid arteries.

The aim of this study is to assess whether the use of a low-dose carotid CTA protocol performed with MBIR is comparable in image quality and diagnostic accuracy to a conventional dose carotid CTA protocol.

Materials and Methods

Institutional ethical board approval was granted for this prospective study. The study population consisted of twenty consecutive patients who underwent CTA of the carotid arteries over a 1-year period. These were patients with known or suspected carotid artery disease, which were referred for clinically indicated CTA of the carotid arteries. Written consent was obtained from each subject. The inclusion criteria consisted of adults that were referred from the vascular, geriatric or neurology services, that required a carotid CTA as part of their carotid artery disease work-up and management, that were scanned during normal daytime working hours and that were able to consent to be included in the study. Exclusion criteria included known allergy to iodinated contrast medium, pregnancy, age < 18 years, and renal insufficiency.

Image Acquisition

All studies were performed on the same 64-slice Lightspeed VCT. All participants consented to have two contemporaneously acquired studies. The protocol for the two carotid CTA examinations was designed so that the combined radiation exposure from both scans did not exceed that of a single conventional carotid CTA. This was achieved by dividing the radiation dose of the carotid CTA into two quotients. The first (conventional dose) CT acquisition used a radiation dose of approximately 70% of the dose of a standard carotid CTA. The second (low-dose) CT acquisition used 30% of the dose of a standard carotid CTA. Patients were scanned supine, cranio-caudally with their arms by their sides. Each subject received 100mls of non-ionic intravenous contrast media (iohexol, Omnipaque

350, GE Healthcare, Mississauga, ON, Canada) at a rate of 5ml per second through a large gauge intravenous cannula placed in the right antecubital fossa followed by a 20ml saline bolus injected via a power injector (Stellant; Medrad, Warrendale, PA). Automatic bolus-tracking software (SmartPrep; GE Healthcare) was used to monitor and identify peak arterial (150 HU) and acquisition commencement. There was a 3-second delay between completion of the conventional dose protocol and the start of the low-dose scan.

The conventional dose protocol used the following parameters: tube voltage, 100 kV; gantry rotation time, 0.4 seconds; tolerated noise index, 38%; and automatic tube current modulation threshold range of 60mA -230mA. The following scanning parameters were utilised for the low-dose study: tube voltage, 100 kV; gantry rotation time 0.4 seconds; tolerated noise index 70%; and automatic tube current modulation threshold range of 30mA -150mA.

CT image reconstruction

Images were reconstructed from an acquisition thickness of 0.625 mm to a final slice thickness of 2 mm. The conventional dose data was reconstructed using the standard department protocol employing hybrid IR, (60% FBP and 40% ASIR), labeled CD ASIR. The low-dose data was reconstructed with MBIR, labeled LD-MBIR in addition to 40% ASIR, named LD ASIR.

CT Dose Measurement

DLP and $CTDI_{vol}$ values were recorded from each CT dose report. $CTDI_{vol}$ and DLP tolerances were verified using a standard 32cm perspex phantom and a 10cm ionization chamber with a Victoreen NERO mAx unit as previously described.

Calibration of the CT unit was performed once per week in accordance with the manufacturer's instructions. The Imaging performance and assessment in CT patient dosimetry calculator (ImPACT version 0.99x, London, England) was used to calculate ED. The radiation exposure resultant from the CT topograms was excluded from analysis.

Objective Image Quality Analysis

Objective image quality measurements were performed by 1 radiologist on a dedicated workstation (Advantage Workstation VolumeShare 2, Version 4.4, GE Medical Systems, Milwaukee, WI). 3mm spherical ROIs (10.6mm^3 volume) were placed in 49 individual anatomical regions on each dataset. Intravascular measurements were taken bilaterally at the following levels: common carotid origin (CCA), CCA bifurcation, superior extracranial internal carotid artery (ICA), terminal intracranial ICA, vertebral artery origin (V1), mid V2 vertebral artery segment and V4 vertebral artery division. Measurements were recorded bilaterally by placing the ROI in the adjacent sternocleidomastoid muscles at the 7 vascular levels. If the sternocleidomastoid was not on the image at the relevant level, the pectoralis major or temporalis muscles were utilised. Background noise was recorded by placing the ROI 5mm from the skin on 3 occasions at each of the 7 levels. ROIs were placed in as homogenous an area as possible. The mean attenuation in HU and standard deviation of the mean attenuation was recorded for each ROI. The standard deviation of the mean attenuation was used as the objective measure of noise. These measurements were used to calculate the CNR and SNR ratios using previously validated methods. CNR was calculated for each of the 7 arterial segments bilaterally using the following equation: CNR = (mean

intravascular HU – mean HU of adjacent sternocleidomastoid muscle) / mean background ROI standard deviation. Signal to noise ratio (SNR) was calculated at the same levels using the following: SNR = mean intravascular HU / mean background ROI standard deviation.[100]

Subjective Image Analysis

Subjective image quality parameters and grading system were adapted from the European Guidelines on Quality Criteria for CT document and were selected on the basis of findings of previous studies[111],[112],[113]. Subjective quality assessment was performed in consensus by 2 experienced readers. One of the observers was familiar with these methods of assessment, having successfully used them previously and trained the other reader prior to analysis using a training set of five standard CT scans.

Subjective image noise, contrast resolution and spatial resolution were scored using a ten-point scale at 7 anatomical levels: right common CCA, right CCA bifurcation, superior extracranial ICA, terminal ICA, right vertebral artery origin (V1), mid V2 vertebral artery segment and V4 vertebral artery division. Subjective image noise was graded according to the extent of "graininess" or "mottle" present on CT images and was graded as acceptable (score of 5) if average graininess was seen with satisfactory depiction of small anatomic structures such as the blood vessels and interface between structures of variable attenuation, unacceptable (score of 1) if graininess interfered with depiction of these structures, and excellent (score of 10) where there was minimal or no appreciable mottle. Contrast resolution and spatial resolution were scored at the same 7 anatomical levels. With regard to contrast resolution, a score of 10

represented superior contrast depiction between different soft tissues, a score of 1 indicated the poorest contrast and 5 indicated acceptable contrast. In terms of spatial resolution, a score of 10 represented excellent edge detail, a score of 1 indicated poor spatial resolution and a score of 5 designated acceptable spatial resolution. The presence and impact of streak artefact was scored at each of the 7 anatomical levels using a 3-point scheme: (0 - no streak artefact; 1 - streak artefact present but not interfering with image interpretation; 2 - streak artefact present and interfering with image interpretation). Diagnostic acceptability was graded as acceptable (score of 5), unacceptable (score of 1) or excellent (score of 10) respectively, if depiction of soft-tissue structures for diagnostic interpretation and degree of image degradation by beam-hardening artifacts was satisfactory, unsatisfactory, or considerably superior. This was assessed for the aortic arch, carotid system, vertebrobasilar system, venous system, thyroid gland and non-thyroid soft tissues individually.

Diagnostic performance

The degree of ICA stenosis was calculated with the use of a semi-automated vessel analysis tool on a dedicated workstation (Advantage Workstation VolumeShare 2, Version 4.4) in a blinded fashion by 2 experienced radiologists in consensus. This was performed as per NASCET (North American Symptomatic Carotid Endarterectomy Trial) criteria, whereby the minimum diameter of the proximal ICA stenosis was compared to the diameter of the parallel-walled superior cervical ICA.[114,115,116] The automated calculation tool was utilised but manual methods were substituted if the readers deemed the tracking to be inaccurate. The stenoses were graded into insignificant (<50%), moderate (50-

69%), severe (70-90%) and critical (>90%). The gradings were compared for each reconstruction. Using the CD ASIR images as the 'gold standard', the mean deviation for the absolute ICA stenosis value for each patient was compared for LD ASIR and LD MBIR reconstructions.

Statistical Analysis

All statistical tests were performed with a commercially available medical statistical package Statistical Package for Social Scientists (SPSS) version 20.0 (IBM, Armonk, NY). Wilcoxon signed rank test was used for statistical analysis to compare non-parametric qualitative parameters. Normally distributed parametric quantitative indices were compared using a paired t-test. Agreement between stenosis grading was compared using Cohen's κ test of agreement. Deviation from the 'gold standard' ICA stenosis value was calculated via a mean-difference / Bland Altman calculation. A difference with a p value of <0.05 was considered statistically significant. All data are presented as mean ± standard deviation or median ± interquartile range unless otherwise stated.

Results

20 patients with a mean age of 66.74±6.74 years were enrolled. Patient demographics are outlined in Table 3.1.

Demographics	Percentage % (number)
Gender	
Male	60% (n=12)
Female	40% (n=8)
Smoking Status	
Smoker	65% (n=13)
Non Smoker	30% (n=6)
Ex Smoker	5% (n=1)
Past medical history of cardiovascular disease/stroke	
No	50%(n=10)
Yes	50% (n=10)
Dyslipidaemia	
Yes	55%(n=11)
No	45% (n=9)
Family history of angina /MI in relative <60yrs	
No	90% (n=18)
Yes	10% (n=2)
Diabetes Mellitus	
No	85% (n=17)
Yes	15% (n=3)
Hypertension	
Yes	75% (n=15)
No	25% (n=5)
Alcohol	
Yes	45% (n=9)
No	40% (n=8)
Abstinent due to alcohol dependency	15% (n=3)

Table 3.1 Patient demographics.

Radiation Exposure

Mean DLP and ED for the low-dose studies were 341.33mGy.cm (range 278.88-411.36mGy.cm) and 1.84mSv (range 1.51-2.22mSv) respectively. Mean dose indices for the conventional dose studies were 687.96mGy.cm (DLP range

563.51-1169.24mGy.cm) and 3.71mSv (ED range 3.04-6.31mSv). The low-dose studies were significantly lower ($p<0.001$), with a mean reduction of 49.6%. There was no significant association between the degree of stenosis and radiation dose incurred for either protocol.

Objective Image Quality Evaluation

CNR and SNR measurements on the low-dose ASIR images were significantly inferior to both the LD MBIR and CD ASIR images at all levels ($p<0.01$ for all comparisons)(Figures 3.1 and 3.2, Table 3.2). There was no significant difference in terms of SNR or CNR between LD MBIR and CD ASIR assessments at most levels. LD MBIR SNR and CNR were significantly superior ($p<0.05$) to CD ASIR at the CCA origin and LD MBIR CNR was significantly superior at V1 ($p=0.004$). Summating all measurements, LD MBIR were insignificantly superior when compared to CD ASIR images in terms of CNR (82.93±80.74 Vs. 77.67±43.91)($p=0.284$) and SNR (99.06±88.97 Vs. 89.78±46.79)($p=0.085$).

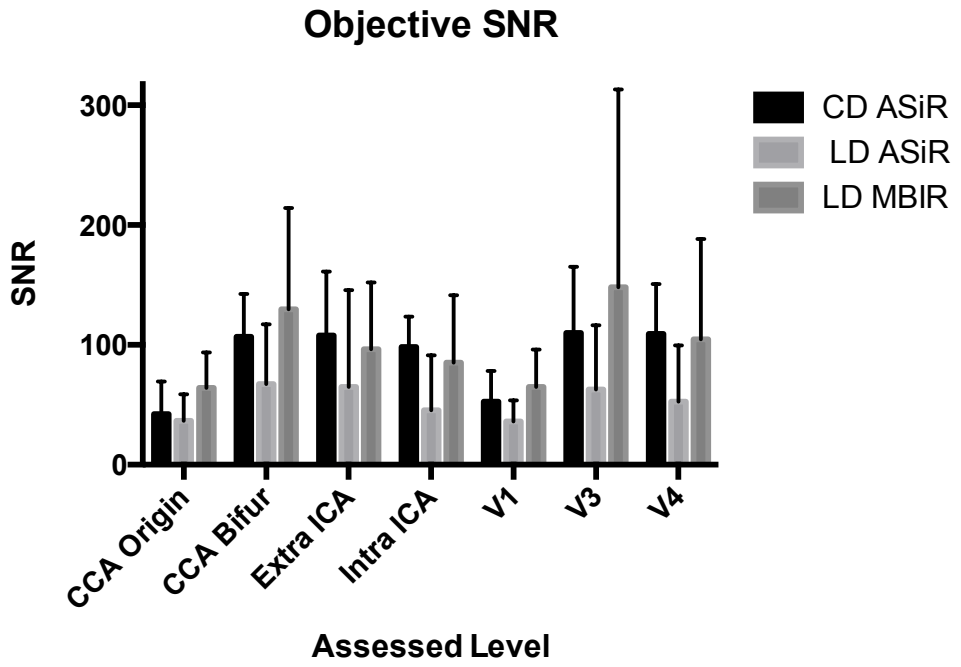

Figure 3.1 Objective signal to noise ratio (SNR) at the 7 assessed levels (CCA origin, CCA bifurcation, extracranial superior cervical ICA, intracranial terminal ICA, V1 vertebral artery segment, mid V3 vertebral artery segment, V4 vertebral artery division).

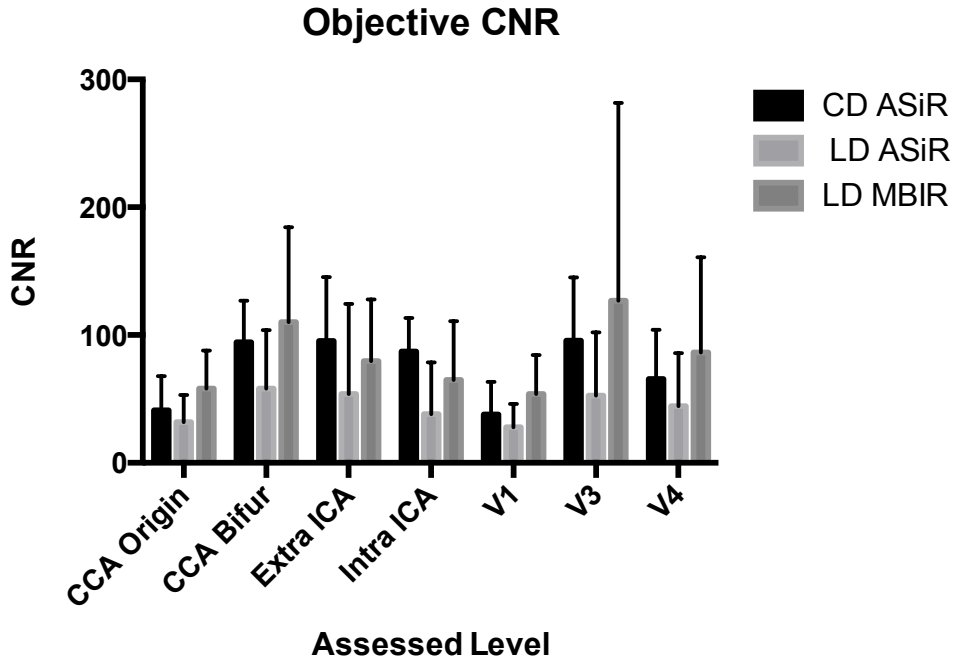

Figure 3.2 Objective signal to noise ratio (SNR) at the 7 assessed levels (CCA origin, CCA bifurcation, extracranial superior cervical ICA, intracranial terminal ICA, V1 vertebral artery segment, mid V3 vertebral artery segment, V4 vertebral artery division).

Level	Parameter	CD ASIR	LD ASIR	LD MBIR
CCA Origin	SNR	47.28±27.15	36.56±22.11	64.07±29.78*
	CNR	41.24±26.62	31.90±21.29	58.07±29.92*
CCA Bifurcation	SNR	106.92±35.72	67.30±49.94	129.76±84.40
	CNR	94.45±32.30	58.05±45.72	110.04±74.26
Extracranial ICA	SNR	107.81±53.50	64.99±80.77	96.47±55.55
	CNR	95.28±50.04	53.80±70.49	79.52±48.30
Intracranial ICA	SNR	98.27±25.42	45.46±45.77	85.14±56.35
	CNR	87.08±26.17	38.12±40.46	64.87±45.93
V1	SNR	52.55±25.65	36.04±17.80	64.82±31.40
	CNR	37.95±25.44	27.78±18.34	53.98±30.31*
V3	SNR	109.96±55.11	62.67±53.78	148.05±165.14
	CNR	95.56±49.50	52.62±49.44	126.99±154.62
V4	SNR	109.22±41.48	52.66±46.97	104.78±83.69
	CNR	95.66±38.49	44.28±41.68	86.33±74.56
All levels	SNR	89.78±46.79	51.95±49.39	99.06±88.97*
	CNR	77.67±43.91	43.56±44.28	82.93±80.74

Table 3.2 Objective signal to noise ratio (SNR) and contrast to noise ratio (CNR) at the 7 assessed levels (CCA origin, CCA bifurcation, extracranial superior cervical ICA, intracranial terminal ICA, V1 vertebral artery segment, mid V3 vertebral artery segment, V4 vertebral artery division). LD ASIR measurements were significantly inferior ($p<0.01$) for all levels when compared with LD MBIR.

Subjective Image Quality Analysis

Results from subjective image quality assessment are shown in figure 3.3. CD ASIR images were significantly superior in terms of subjective noise when compared with LD ASIR (median ± IQR, 7.5±1 vs. 7±2, $p<0.001$) and LD MBIR (7.5±1 vs. 7±1, $p<0.001$). LD MBIR subjective image noise was significantly superior to LD ASIR image assessment in addition ($p=0.036$). In terms of spatial resolution, LD MBIR was deemed superior to CD ASIR (8±0 vs. 7±1, p=004) and LD ASIR images (8±0 vs. 7±1, $p<0.001$). LD MBIR contrast resolution was also superior to CD ASIR (8±1 vs. 7±1, $p=0.002$) and LD ASIR images (8±1 vs. 7±1, $p<0.001$). LD MBIR was superior to the other datasets with regard to diagnostic acceptability (LD MBIR: 9±1, CD ASIR: 8±1, LD ASIR: 7±1; $p<0.001$ for all comparisons). In addition, CD ASIR was superior to LD ASIR with regard to same ($p<0.001$). Non-vascular soft tissue diagnostic acceptability was also superior for LD MBIR (8±0) when compared to CD ASIR (7±0, $p<0.001$) and LD ASIR (6±1, $p<0.001$). Streak artefact reduction was also superior on the LD MBIR reconstructions (1±1) when compared to the CD ASIR (2±0, $p<0.001$) and LD ASIR (1±0, $p<0.001$) reconstructions.

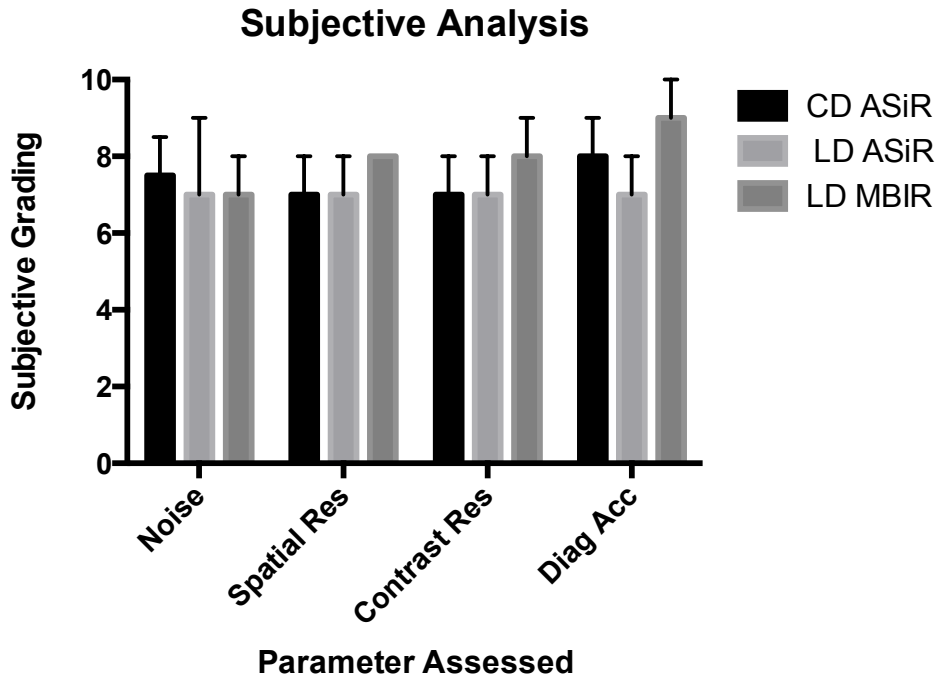

Figure 3.3 Subjective analysis of image noise, spatial resolution, contrast resolution and diagnostic acceptability for each protocol.

Diagnostic Performance

Of the 40 (20 patients) internal carotid arteries assessed, 6 were occluded. All of these were correctly identified on both low-dose reconstructions. Of the remaining 34 patent ICAs, 24 had stenoses of <50%, 3 had moderate stenoses of 50-69%, 5 had severe stenoses of 70-90% and 2 had critical stenoses >90%. For the non-occluded ICAs, there was excellent agreement for stenosis grading accuracy when the LD ASIR (Cohen's $\kappa = 0.806$) and LD MBIR (Cohen's $\kappa = 0.806$) were compared to the CD ASIR assessment (Figure 3.4). Both the LD MBIR and LD ASIR underestimated a single stenosis grading from '50-69%' to '<50%' in one patient. With regard to Bland-Altman / mean-difference performance of the low-dose reconstructions, both the LD MBIR and LD ASIR studies underestimated the stenosis (LD MBIR: -3.23±5.81%; LD ASIR: -3.65±8.46%)

when the absolute per cent stenoses values were compared with the CD ASIR images. LD MBIR was insignificantly superior (p=0.811). When the calculated diameters of the superior cervical ICA were examined, there was no significant difference between mean LD ASIR (5.43±0.94mm) and CD ASIR (5.22±0.78mm) calculations (p=0.130). Mean diameters calculated on the LD MBIR images (4.89±0.94mm) were less than CD ASIR (p<0.007) and LD ASIR (p<0.001) measurements.

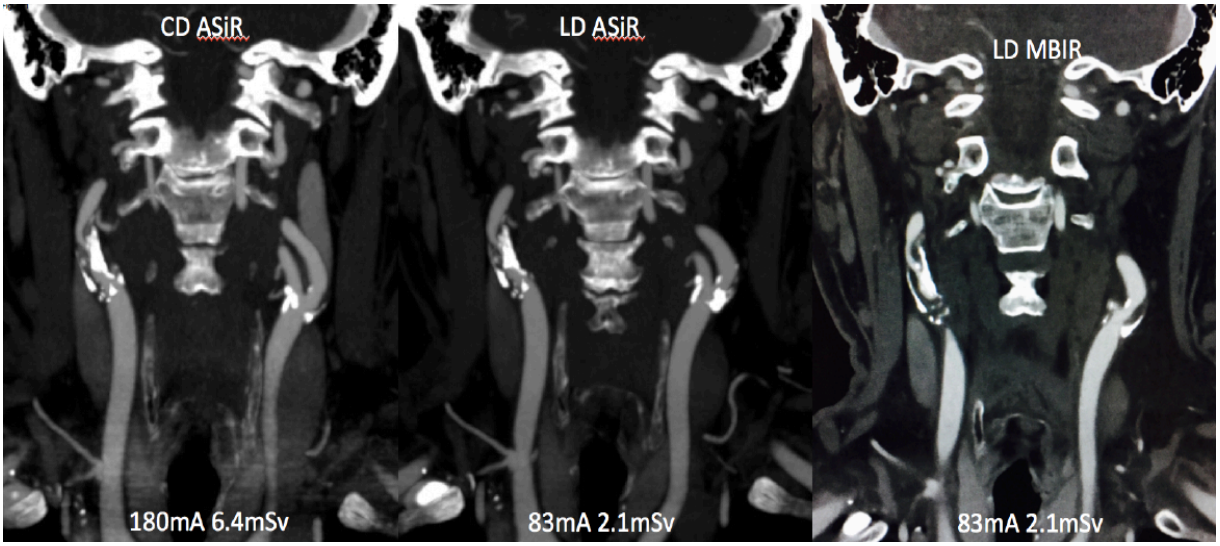

Figure 3.4 Coronal reconstructions of a CT carotid angiogram performed in a 62 year-old male patient with 85% stenosis of the proximal right internal carotid artery. The low-dose images reconstructed with MBIR and 40% ASIR have a similar diagnostic image quality to the conventional dose image (CD ASIR). The tube current (mA) and effective dose of each study are also shown.

Discussion

CTA is the most accurate technique for evaluating carotid artery stenosis with a better performance than magnetic resonance angiography (MRA) (97% vs. 95% for steady-state MRA and 92% for first-pass MRA) and a greater accuracy than carotid Doppler ultrasound (97% vs. 76%).[117] Furthermore, CTA of the carotid arteries has been found to have a pooled sensitivity of 95% and a specificity of 98% for the detection of stenosis greater than 70%.[118]

We found a low-dose carotid CTA protocol performed with MBIR and a conventional dose protocol to be comparable in terms of image quality and diagnostic interpretation, despite a significant reduction in mean effective dose from 3.7mSv (range 3.04-6.31mSv) to 1.8mSv (range 1.51-2.22mSv). This represents a mean effective dose reduction of 50%, which is comparable to other low-dose carotid CTA studies in the literature performed using different dose reduction techniques.[100, 101]

Beitzke et al reported poor image quality at the level of the common carotid artery in a significant percentage of the low-dose cohort compared to the conventional dose studies (9 of the 42 common carotid arteries in the low-dose group). [100] They attributed this to an increase in streak artefact from venous contamination in addition to the increased arterial enhancement obtained in the low-dose cohort. In our study, both objective and subjective image quality were significantly superior at the level of the common carotid artery in the low-dose MBIR studies compared to the conventional dose studies. Furthermore, streak artefact reduction was also superior at the level of the common carotid artery on

the low-dose MBIR reconstructions and we do not report any diagnostic limitation at this level.

With regard to diagnostic performance, both low-dose studies correctly identified all 6 occluded internal carotid arteries with excellent agreement with the conventional dose studies for stenosis grading accuracy in the non-occluded internal carotid arteries. Both the LD MBIR and LD ASIR underestimated a single stenosis grading from '50-69%' to '<50%' in one patient. On review, this was a patient with a 51% degree of stenosis. In cases of a borderline stenosis grading between insignificant (<50%), moderate (50-69%), severe (70-90%) and critical (>90%) grades, assessed with the low-dose protocol, we recommend consideration of performance of the conventional dose protocol if patient management would be altered.

In CTA, image quality is primarily determined by the contrast between the contrast-enhanced arterial lumen and the surrounding soft tissue. For our study protocol, the low-dose CTA scan was acquired three seconds after the conventional dose CTA, thus resulting in a slight reduction in the volume of contrast medium within the arterial lumen on the low-dose scan. However, despite this potential limitation, it did not have a significant impact on objective image quality with the subjective image quality of the low-dose MBIR scans being significantly better than the conventional dose scans.

Although subjective image noise was significantly greater for the low-dose MBIR scans, this is usually of limited importance in CTA as contrast between the arterial lumen and soft tissue is usually high. However, we recognise this as a potential limitation of our study and a recommendation would be to conduct

another study with the low-dose scan being performed first to optimise image quality.

Another limitation of our study was that body mass index was not recorded. Previous studies have recommended the exclusion of obese patients from low-dose CTA protocols due to high levels of image noise and streak artefact at the level of the shoulder girdle.[100] However, other studies report a limited influence of BMI in carotid imaging and attribute a greater importance to factors such as a short neck or elevated muscular shoulders which do not correlate well with BMI.[101] As we did not investigate this, we are currently unable to support or refute the finding that obesity has an impact on CTA image quality at low radiation doses. Furthermore, no assessment of plaque composition was made and the potential effects of calcified versus soft plaque on image quality and radiation dose in this study are unknown.

Our study is unique as it incorporates a control group with the study participants acting as their own controls thereby reducing the likelihood of confounding variables. Furthermore, we use a model based iterative reconstruction technique and assessed diagnostic performance, which to the best of our knowledge, have not been previously investigated in CTA of the carotid arteries.

The use of MRA of the carotid arteries should also be considered as a radiation-free alternative. Although the performance of MRA for the accurate characterization of moderate disease is limited compared to CT[119], MR has the ability to visualize plaque composition and specific plaque components such as lipid-rich necrotic core, intraplaque haemorrhage, calcification and surface defects including erosion, disruption and ulceration, which have been linked to a higher risk of subsequent embolic events.[120]

CTA is commonly performed in the setting of acute stroke, often in conjunction with CT brain perfusion (CTP), which imparts a significant radiation dose. There is a paucity of studies assessing the use of IR with CTP but preliminary phantom and clinical studies are promising indicating that substantial dose reductions may be achievable without significantly compromising image quality.[121], [122] It remains unclear if we can extrapolate our results to the smaller intracranial vessels. Studies combing CTA with pure IR for the imaging of cerebral vessels report improved delineation of smaller vessels in the posterior fossa at conventional doses, [123] but further investigation of MBIR as a dose reduction tool in this setting is needed.

In conclusion, the use a low-dose carotid CTA protocol performed with a model based iterative reconstruction algorithm is comparable to a conventional dose protocol in terms of image quality and diagnostic accuracy, while enabling a dose reduction of almost 50%.

Chapter IV

Low-dose CT imaging of the acute abdomen using model based iterative reconstruction: a prospective study

Introduction

Since its introduction in the 1970s, CT has revolutionized diagnostic decision-making.[124] It has had a major impact on the field of surgery where it has decreased the need for emergency surgery from 13% to 5% and has eliminated the need for many exploratory surgical procedures.[37] Furthermore, in the setting of acute abdominal pain, the increased use of CT in clinical practice has been shown to decrease the proportion of patients requiring inpatient admission from the emergency department.[38]

This increase in the use of CT has raised concerns regarding associated radiation exposure incurred during diagnostic imaging[27]. It is prudent to ensure radiation exposure is optimized to levels, which are as low as reasonably possible without compromising diagnostic yield. This is especially true for abdominopelvic CT, which currently accounts for approximately 50% of the CT collective dose. Therefore, dose reduction strategies targeting this area could potentially result

in a significant decrease in the overall population dose from CT imaging.[64] Dose reduction techniques that have been employed to date in abdominopelvic CT include tube voltage reduction[125], noise reduction filters[126], and automated tube current modulation.[127] These strategies however, are often limited in their ability to reduce radiation dose due to the high levels of image noise and subsequently degraded image quality that are experienced when these low-dose images are reconstructed with the traditional reconstruction algorithm, FBP installed on most CT systems.

IR algorithms that reduce image noise by incorporating statistical information of the CT system including photon statistics and electronic acquisition noise to reduce image noise at substantially reduced radiation doses, thus preserving image quality, have been the focus of much research in recent years. Hybrid IR techniques, such as ASIR, are one such algorithm that may be applied at varying blends with FBP to reduce image noise. This technique has previously been combined with modified low-dose abdominopelvic CT protocols to obtain diagnostic quality images, while achieving dose reductions in the order of 25% to 74%.[54, 69]

Recently, a more computationally intense pure IR algorithm, MBIR, which uses a more complex system of prediction models, has become commercially available. MBIR has been shown to successfully reduce image noise and improve image quality in several conventional dose CT studies[85,128], as well as facilitating dose reductions of up to 80% in a variety of phantom[129], in vivo adult[88, 130], and in vivo paediatric studies.[131] At our institution, we previously developed and reported a modified low-dose CT enterography protocol using MBIR that enabled us to

achieve dose reductions in the order of 75% compared to conventional dose protocols, without compromising image quality and diagnostic accuracy.[73]

Other studies assessing the diagnostic accuracy of low-dose images reconstructed with MBIR have reported a comparable diagnostic accuracy with conventional dose images reconstructed with FBP and hybrid IR for the detection of organ-based focal lesions.[132,133,134] To date, few studies have assessed the utility MBIR in abdominopelvic CT in patients presenting with acute abdominal symptoms.[135,136]

The aim of this prospective feasibility study was to assess the utility of a modified low-dose abdominopelvic CT protocol using pure iterative reconstruction for the assessment of patients presenting to the emergency department with acute abdominal symptoms.

Materials and Methods

Study subjects

Institutional review board approval was granted for the study. All patients presenting to the emergency department of a tertiary referral centre with 'acute abdominal symptoms' as assessed by an attending abdominal surgeon, specialised in abdominal surgery, over a 3-month period were included. We defined 'acute abdominal symptoms' as sudden, severe abdominal pain of undetermined aetiology and of less than 24 hours in duration.

Exclusion criteria included patients who were less than sixteen years of age, history of malignancy, pregnancy, and any patients presenting following

abdominal trauma. Patients with symptoms suggestive of renal colic were also excluded from the study. Written informed consent was obtained from all patients prior to CT. Each patient had his or her weight and height measured using a digital device (Seca electronic measuring station Model 763, Seca Medical, Hamburg, Germany) and his or her BMI was subsequently recorded.

CT technique

All CT studies were acquired using a 64-slice GE Discovery CT 750 CT scanner. All patients consented to have two contrast-enhanced CT scans of the abdomen and pelvis contemporaneously. Both CT scans covered an identical anatomic area extending from the lung bases to the inguinal region. 1.5 litres of oral contrast medium (Gastrografin, Bracco Diagnostic Inc., Princeton, USA) with 2% Gastrografin was ingested 90 minutes prior to CT scanning, in keeping with local practice. A single 100ml bolus of intravenous contrast (Iohexol, Omnipaque 300, GE Healthcare, Mississauga, ON) was delivered via a power injector (Stellant, medrad, Warrendale, PA) at a flow rate of 2.5 ml/sec as per standard departmental practice. The volume of injected intravenous contrast was not adjusted for patient size in order to standardise the technique. Automatic bolus-tracking software (SmartPrep, GE Healthcare, Waukesha, WI, USA) triggered CT data acquisition in the portal venous phase 45 seconds after a threshold of 100 HU was reached within a ROI placed in the abdominal aorta. A low-dose abdominopelvic CT (LD CT) was performed first. The second, conventional dose CT (CD CT) commenced approximately 6 seconds later. Single medio-lateral and antero-posterior scanned projection radiographs were obtained prior to the helical acquisitions. The LD CT was designed to impart a radiation exposure of

approximately 10-20% of a routine abdominopelvic CT scan performed at our institution and the second CD CT to impart an effective dose of 80-90% of a routine CT scan. The LD CT protocol employed a tube voltage of 100kV, rotation time of 0.5s, z-axis ATCM with minimum and maximum tube current thresholds of 20 and 350mA, and a noise index of 70 HU.

The CD CT protocol utilised a tube voltage of 100kV, rotation time of 0.8s, ATCM with minimum and maximum tube current thresholds of 50 and 350mA, and a noise index of 38 HU. Tube voltage was not varied in order to standardise the protocol.

CT image reconstruction

Images were acquired at a slice thickness of 0.625 mm and subsequently reconstructed at a final slice thickness of 3 mm. LD CT data were reconstructed using MBIR, labelled LD MBIR. CD CT images were reconstructed using the standard departmental protocol employing hybrid iterative reconstruction (40% ASIR and 60% FBP, labelled CD ASIR.

CT calibration and radiation dose measurement

DLP and CTDIvol values were recorded from each CT dose report. CTDIvol and DLP tolerances were verified using the technique previously described in chapter 2. The Imaging performance and assessment in CT patient dosimetry calculator was used to effective doses. SSDE was recorded using an automated dose-tracking program (DoseWatch, General Electric Healthcare, Waukesha, WI, USA). The software automatically calculates SSDE by multiplying CTDIvol by a conversion factor (fSSDE), which is determined by patient effective diameter.

The software determines patient effective diameter by measuring the maximum lateral and anteroposterior diameters at the median image of the localizer radiograph of the scanned range. The radiation exposure resultant from the CT topograms was excluded from analysis.

Quantitative analysis of image noise

Objective image quality analysis was performed independently on the GE Advantage Workstation by the author and a second operator with 8 years experience. Attenuation values HU were measured at five levels using spherical histograms of equal size (diameter, 10mm; volume, 519 mm^3). The ROIs were placed in the following anatomical structures: liver parenchyma at the level of the right hemi-diaphragm (level 1); liver parenchyma at the level of the porta hepatis (level 2); erector spinae at the right renal hilum (level 3); psoas muscle at the iliac crest (level 4); and gluteus maximus muscle at the roof of the acetabulum (level 5) (Figure 4.1). The ROIs were placed in as homogenous an area as possible, taking care to avoid fat planes and blood vessels. Objective image noise and SNR were then calculated as described in chapter 2. Each operator took measurements independently and the mean measurement was used for analysis. The operators were blinded to the scanning protocol and reconstruction technique used and the order of the series was randomized.

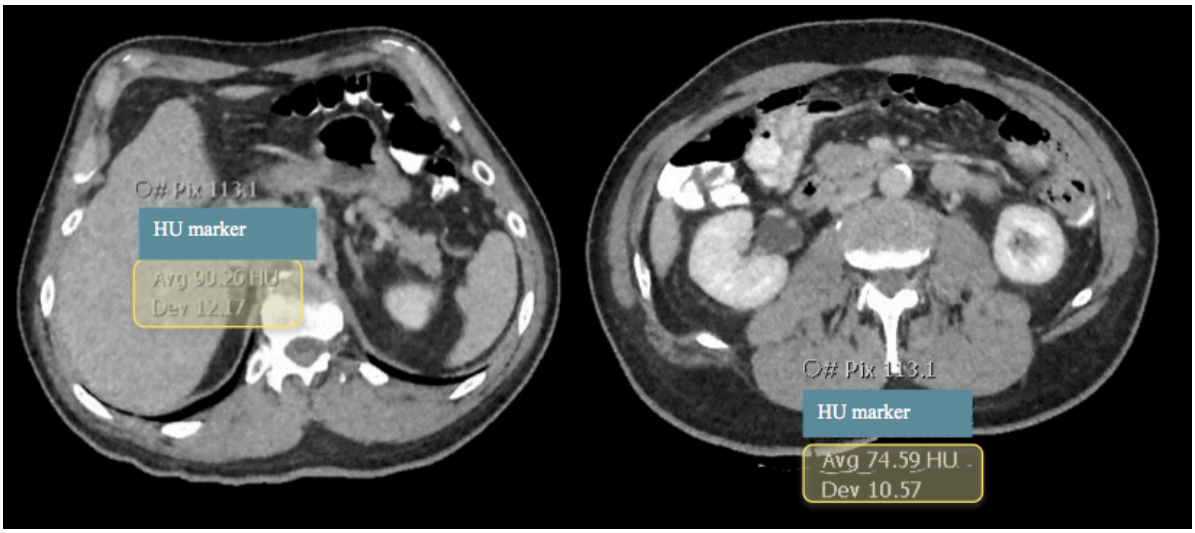

Figure 4.1 Low-dose axial CT images reconstructed with model based iterative reconstruction at the level of the porta hepatis (left image), demonstrating placement of the ROIs. The ROIs were placed in as homogenous an area as possible, taking care to avoid fat planes and blood vessels. The standard deviation of the mean attenuation in the ROI served as an objective measure of image noise. The signal-to-noise ratio of each ROI was calculated by dividing the average HU by its standard deviation.

Qualitative analysis

Subjective image quality assessment was performed independently on the GE Advantage Workstation by two fellowship trained abdominal radiologists with 14 and 15 years experience, respectively. Subjective image noise, diagnostic acceptability, and contrast resolution were graded on a 10-point scale at the same 5 anatomical levels as quantitative assessment was performed. Image noise was graded as acceptable (score of 5) if average graininess was seen with satisfactory depiction of small anatomical structures such as blood vessels and tissue interfaces, unacceptable (score of 1) if graininess interfered with structure

depiction, and excellent (score of 10) if there was no appreciable mottle (Figure 4.2). Diagnostic acceptability was graded as acceptable (score of 5), unacceptable (score of 1), or excellent (score of 10) if depiction of solid organs, large bowel, small bowel, peri-colonic fat, and peri-enteric fat for diagnostic interpretation and degree of image degradation by beam hardening artifacts was satisfactory, unsatisfactory or considerably superior, respectively. Contrast resolution was also graded at the liver, spleen and buttock musculature using a 10-point scale in which a score of 10 represented superior contrast between different abdominal soft tissues, a score of 1 indicated the poorest contrast, and a score of 5 indicated acceptable contrast. Streak artefact was also graded at each level using a 3-point scale: 0, no streak artefact present; 1, streak artefact present but not interfering with image interpretation; and 2, streak artefact present and interfering with image interpretation. The parameters of image quality were selected on the basis of previous studies and the European Guidelines on Quality criteria for Computed Tomography.[80, 81, 82] The readers were familiar with these methods having used them previously.[54] The order of the data sets was randomized and the readers were blinded to the scanning protocol and reconstruction technique. The readers used a combination of axial and coronal reformats for interpretation and altered the CT level and window width at their discretion.

Figure 4.2 CD ASIR and LD MBIR axial CT images acquired at the level of the porta hepatis (level 2) with subjective scores of noise and diagnostic acceptability.

Diagnostic accuracy

The CD ASIR studies were immediately available for review and reporting by the staff radiologist on duty. The final report issued to the referring clinician at the time of scanning was based solely on the CD ASIR study. The LD MBIR images were reviewed at a later time by the study readers only. For the purpose of the study, LD MBIR and CD ASIR images were reviewed independently by two fellowship-trained abdominal radiologists. To minimise the effects of recall bias, all datasets were anonymised and reviewed in a random patient order. In addition, a six-week delay was instituted between the review of LD MBIR and CD

ASIR images. Reviewers were blinded to the original report issued by the staff radiologist on duty at the time of scanning as well as the clinical information provided by the referring clinician.

Images were reviewed on a picture archiving and communication system (Impax 6.5.3; Agfa healthcare, Morstel, Belgium) in a Digital Imaging and Communications in Medicine format on a monitor with a resolution of 3 megapixels using a combination of axial and coronal reformats on soft-tissue window settings (window width, 400 HU; window level, 40 HU). Lung window settings (window width, 1500HU; window level: -500HU) were utilised to assess for the presence of pneumoperitoneum and pneumotosis intestinalis. Any finding to which the patient's acute abdominal pain could be attributable to was recorded as the primary diagnosis. Incidental findings not thought to contribute to the patient's acute abdominal pain were also recorded.

Following review of both datasets, the findings were compared to the original report issued by the staff radiologist on duty at the time of scanning to identify any discrepancies. Any discrepancies were resolved in consensus by the staff radiologist and two study readers with an addendum to the report being issued as necessary.

Statistical analysis

Data was analysed using GraphPad Prism version 7.0 (GraphPad Software Incorporated, San Diago, USA) and Statistical Package for the Social Sciences (SPSS) version 22 (IBM, Chicago, Illinois, USA). Distribution of variables was assessed using D'Agostino-Pearson omnibus normality test. Paired t-test and Wilcoxon matched-paired signed rank tests were used to compare parametric

and non-parametric distributions of two groups of continuous variables. Mann-Whitney test was used to compare non-parametric distributions of two groups of continuous variables.

Inter-rater reliability of subjective measures of image quality was assessed with intraclass correlations. Cohen's kappa analysis was performed to quantify the level of agreement between the two protocols for each reader and to quantify the level of agreement between the two readers for each protocol. P values less than 0.05 were considered to be statistically significant. Data are expressed as means with standard deviation of the mean unless otherwise stated.

Results

57 patients (29% (n=17) male, 71% (n=40) female) with a mean age of 56.5±8 years (range 19-77 years) were enrolled in the study. Mean patient BMI was 27.08±6.76kg/m^2 (range 15-44kg/m^2).

Radiation Exposure

Mean DLP of the LD MBIR studies was 158.5±118.6mGy.cm (median 114.7, range 22.8-505.3mGy.cm) resulting in a mean ED of 2.38±1.78mSv (median 1.72, range 0.34-7.58mSv)(Table 4.1). Patients with a BMI of <25 kg/m^2 (n=25) had mean doses of 1.16±0.76mSv (ED), 77.82±50.78mGy.cm (DLP) and 2.4±1.16mGy (SSDE).

Mean DLP of the CD ASIR studies was 469.1±325.8mGy.cm (median 348.3, range 76.29-1295mGy.cm) resulting in a mean ED of 7.04±4.89mSv (median 5.23,

range 1.14-19.42mSv). The mean ED reduction from total dose using the low-dose protocol was 74.7%. Mean ED dose reduction was 87.6% for patients with a BMI of <25 kg/m^2. There was a statistically significant difference between conventional dose and low-dose studies for all methods of dose measurement (p-value <0.0001 in all cases).

Patients with a BMI ≥25 kg/m^2 received significantly higher radiation doses than patients with a BMI of <25 kg/m^2 for both conventional and low-dose studies for all methods of radiation dose measurement (p<0.0001 for all comparisons).

A statistically significant difference increase in DLP was observed with increasing BMI for both low-dose (r=0.843, p<0.001) and conventional dose studies (r=0.888, P<0.001).

The mean radiation dose of the low-dose studies was significantly lower than the conventional dose studies for all methods of dose measurement when analysed by BMI subgroup (p<0.0001 for all comparisons).

	LD MBIR			CD ASIR		
	All	BMI<25 kg/m^2	BMI≥25 kg/m^2	All	BMI<25 kg/m^2	BMI≥25 kg/m^2
DLP (mGy.cm)	158.5 (118.6)	77.82 (50.78)	221.6 (118.5)	469.1 (325.8)	230.6 (142.9)	655.4 (307)
ED (mSv)	2.38 (1.78)	1.16 (0.76)	3.32 (1.78)	7.04 (4.89)	3.46 (2.14)	9.83 (4.61)
CTDIvol (mGy)	3.4	1.66	4.76	9.57	4.92	13.2

	(2.74)	(1.08)	(2.87)	(6.26)	(3.0)	(5.71)
SSDE (mGy)	3.77	2.4	4.83	10.74	6.32	14.2
	(1.97)	(1.16)	(1.81)	(5.5)	(2.28)	(4.85)

Table 4.1 Summary of dose length product (DLP), effective dose (ED); volume CT dose index (CTDIvol), and size specific dose estimate (SSDE) using convention dose (CD ASIR) and low-dose (LD MBIR) protocols in all patients and also in subgroups with BMI<25 kg/m^2 (n=25) and ≥25 kg/m^2 (n=32). Data represented as means with standard deviation of the mean within parentheses.

Quantitative analysis of image noise

LD MBIR and CD ASIR scans were compared at each of the six anatomical levels described in the materials and methods section. Mean noise and standard deviation of the noise at each level are shown in Figure 4.3. Comparisons between LD MBIR and CD ASIR scans at all levels were found to be statistically significant ($p<0.0001$ at all levels) with LD MBIR images having significantly lower levels of image noise. The greatest mean difference was observed at the level of the roof of the acetabulum in the gluteus maximus muscle (level 5).

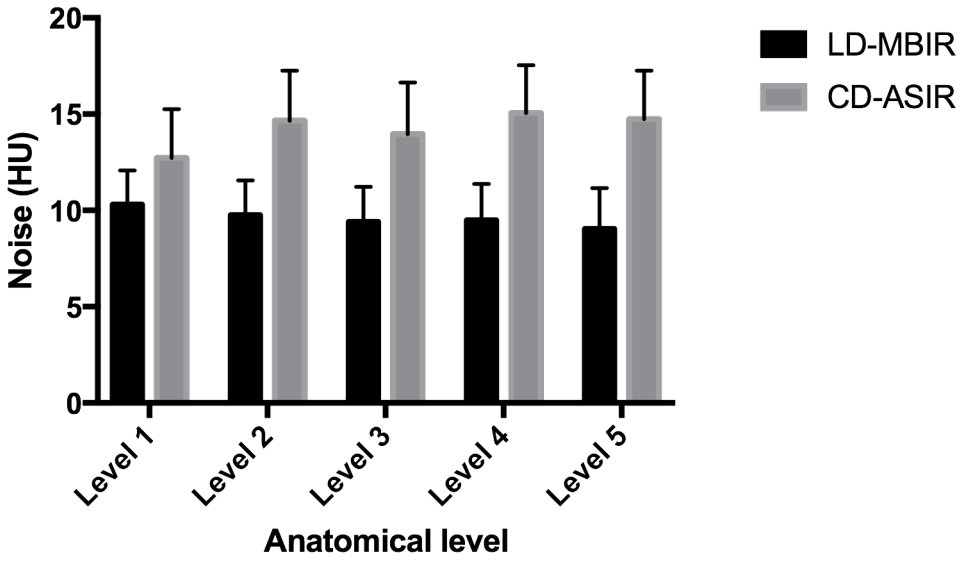

Figure 4.3 Variation in standard deviation of HU (objective image noise) between LD MBIR and CD ASIR images at 5 levels. Data are plotted as mean and standard deviation of the mean as indicated by whiskers. LD MBIR images had significantly lower levels of image noise at all levels ($p<0.0001$ for all comparisons). Level 1 = superior liver at diaphragm, level 2 = liver at porta hepatis, level 3 = erector spinae at the right renal hilum, level 4 = psoas muscle at the iliac crest, level 5 = gluteus maximus muscle at the level of the acetabular roof.

LD MBIR studies had significantly lower levels of image noise than CD ASIR studies in patients with a BMI of <25 kg/m^2 and in patients with a BMI of ≥25 kg/m^2 (Figure 4.2). Objective image noise was significantly higher in patients with a BMI of <25 kg/m^2 compared with a BMI of ≥25 kg/m^2 for the CD ASIR studies (14.73±2.7HU vs. 13.84±2.6HU, p=0.0002)(Figure 4.4). No significant difference in objective image noise was observed between the BMI subgroups for the LD MBIR studies (9.37±1.8HU vs. 9.78±1.9HU, p=0.07).

The magnitude of noise reduction for the LD MBIR studies (derived by subtracting the objective noise on LD MBIR images from CD ASIR images) was significantly greater for patients with a BMI of <25 kg/m^2 compared to patients with a BMI of ≥25 kg/m^2 (5.36±3.2HU vs. 4.05±3.1HU, p<0.0001).

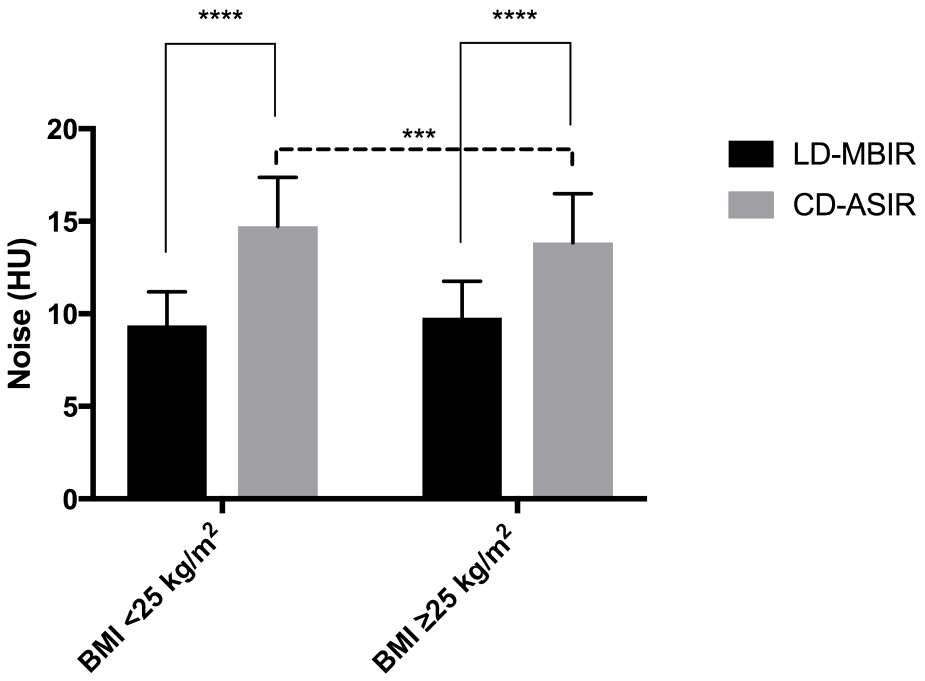

Figure 4.4 Variation in standard deviation of HU (objective image noise) between LD MBIR and CD ASIR images by BMI subgrouping. Data are plotted as mean and standard deviation of the mean as indicated by whiskers. * denotes the significance level.

Mean SNR was also compared between LD MBIR and CD ASIR images at each level (Figure 4.5). Comparisons between each protocol at all levels were found to be statistically significant (p<0.0001 at all levels) with LD MBIR images having higher SNRs at all levels. The greatest mean difference was observed at the level of the porta hepatis (level 2).

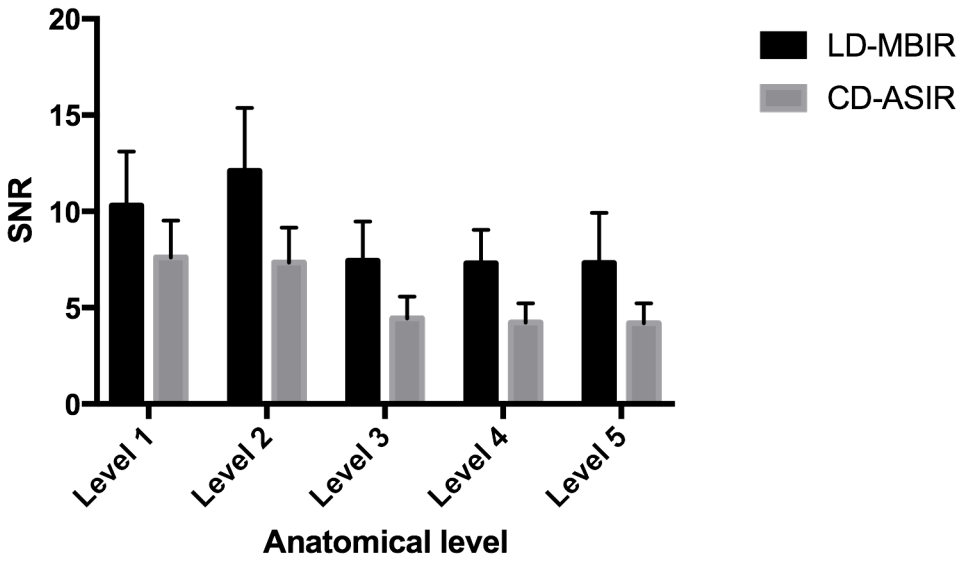

Figure 4.5 Variation in SNR (signal-to-noise) between LD MBIR and CD ASIR images. Data are plotted as mean and standard deviation of the mean as indicated by whiskers. LD MBIR images had significantly higher SNRs at all levels ($p<0.0001$ for all comparison). Level 1 = superior liver at diaphragm, level 2 = liver at porta hepatis, level 3 = erector spinae at the right renal hilum, level 4 = psoas muscle at the iliac crest, level 5 = level 5 = gluteus maximus muscle at the level of the acetabular roof.

Subjective analysis of image quality

Inter-rater variability measures were found to be good to very good for both protocols for all subjective parameters assessed with intraclass correlations of 0.844 (CI, 0.803 to 0.876, $p<0.001$), 0.839 (CI, 0.797 to 0.873, $p<0.001$), and 0.77 (CI, 0.69 to 0.83, $p<0.001$), and 0.808 (CI, 0.75 to 0.851, $p<0.001$), 0.759 (CI, 0.691 to 0.811, $p<0.001$) and 0.835 (CI, 0.778 to 0.878, $p<0.001$) for noise,

diagnostic performance, and contrast resolution for the LD MBIR and CD ASIR studies, respectively; hence, both readers scores were combined for comparison of LD MBIR and CD ASIR protocols.

Both LD MBIR and CD ASIR studies had average to above average subjective noise, contrast resolution, and diagnostic acceptability scores with CD ASIR studies having significantly higher scores for all parameters assessed (Figure 4.6). Qualitative assessment scores were significantly higher in patients with a BMI of ≥25 kg/m^2 compared with a BMI of <25 kg/m^2 for both the LD-MBIR and CD-ASIR studies (p=0.02-0.0001).

Mean subjective noise and diagnostic acceptability scores at each anatomical level assessed are depicted in Figure 4.7. Subjective scores for both noise and diagnostic acceptability were lowest at the level of the porta hepatis for both protocols.

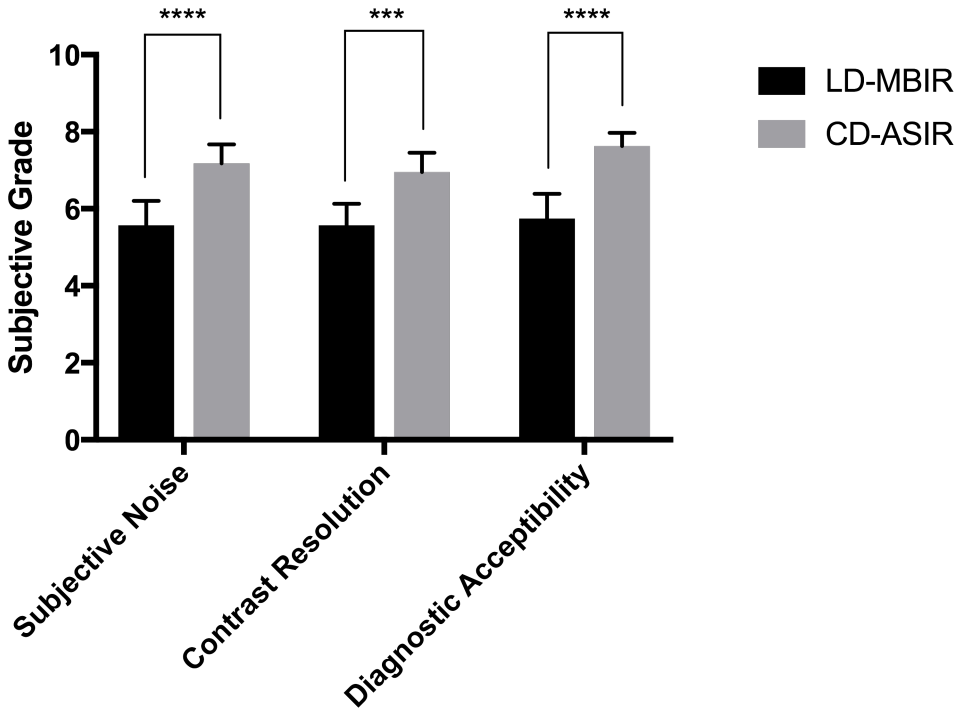

Figure 4.6 Comparison of subjective image quality parameters between LD MBIR and CD ASIR studies. Data are plotted as median and range indicated by whiskers. * denotes the significance level.

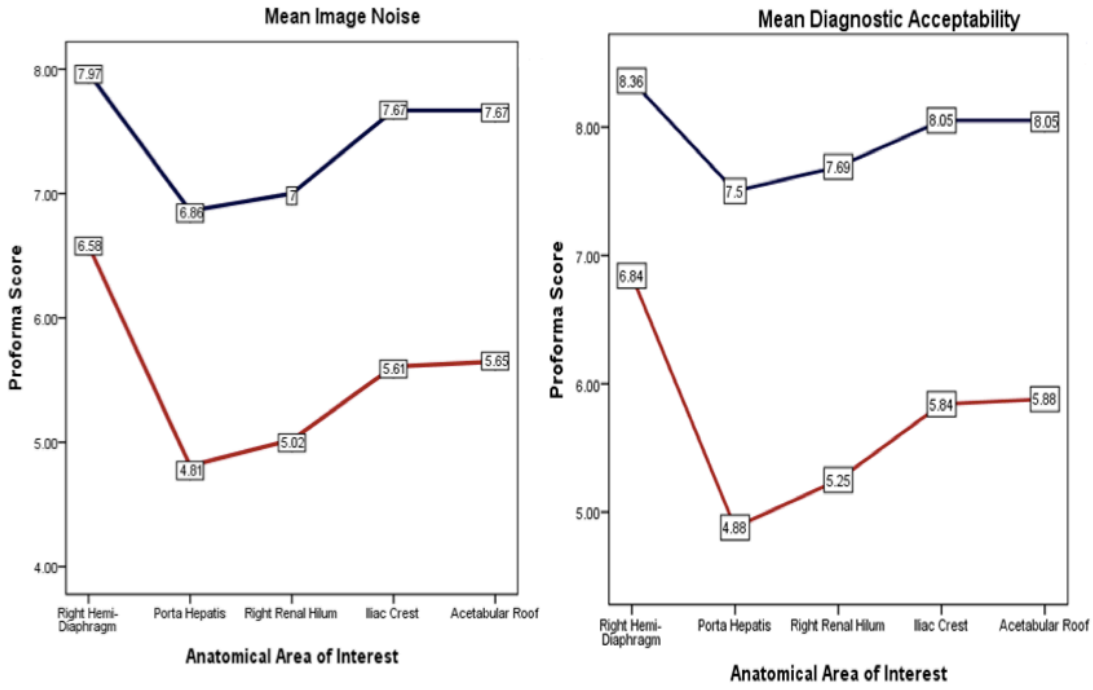

Figure 4.7 Mean subjective noise and diagnostic acceptability scores at each anatomical level assessed for the LD MBIR (red line) and CD ASIR studies (blue line).

No LD MBIR or CD ASIR study was found to have streak artefact interfering with image interpretation. LD MBIR studies had significantly lower streak artefact scores compared to CD ASIR studies at all levels ($p<0.0001$ for all comparison), with the greatest mean difference observed at level 1 (liver parenchyma at the level of the right hemi-diaphragm)(0.03 ± 0.20 vs. 0.7 ± 0.47, $p<0.0001$)(Figure 4.8). The LD MBIR studies had the greatest level of streak artefact present at

level 4 (psoas muscle at the iliac crest)(0.2±0.4) and level 5 (gluteus maximus muscle at the roof of the acetabulum)(0.2±0.46). No significant difference was observed in streak artefact scores between patients with a BMI of <25 kg/m^2 and those with a BMI of ≥25 kg/m^2 for either the LD MBIR or CD ASIR studies ($p>0.06$ for all comparisons).

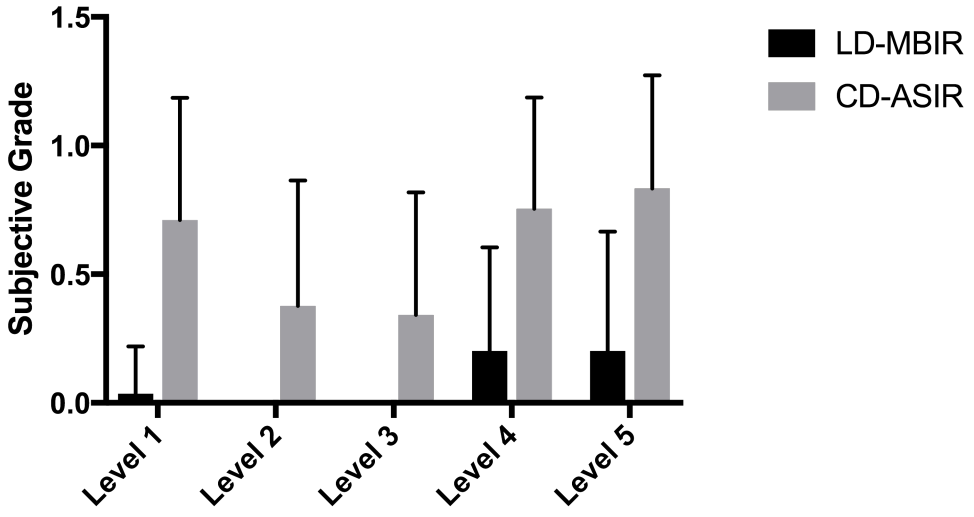

Figure 4.8 Variation in streak artefact scores between LD MBIR and CD ASIR images. Data are plotted as mean and standard deviation of the mean as indicated by whiskers. LD MBIR images had significantly lower streak artefact scores at all levels ($p<0.0001$ for all comparisons). Level 1 = superior liver at diaphragm, level 2 = liver at porta hepatis, level 3 = erector spinae at the right renal hilum, level 4 = psoas muscle at the iliac crest, level 5 = gluteus maximus muscle at the level of the acetabular roof.

Diagnostic Performance

28 patients had a primary diagnosis on conventional dose CT to which their presentation with acute abdominal pain could be attributed. Acute appendicitis (n=6) was the most commonly encountered primary diagnosis, followed by acute diverticulitis (n=4), and focal colitis/diverticulitis (n=4)(Table 4.2). A diagnosis of focal colitis/diverticulitis/tumour (n=3) was offered in patients with a short segment of colonic wall thickening with inflammation (<5cm) in which it was not possible to clearly differentiate between acute colitis and diverticulitis, or an underlying colonic carcinoma was suspected (Figure 4.9). No potential cause of acute abdominal pain was identified in 29 patients (Figure 4.10).

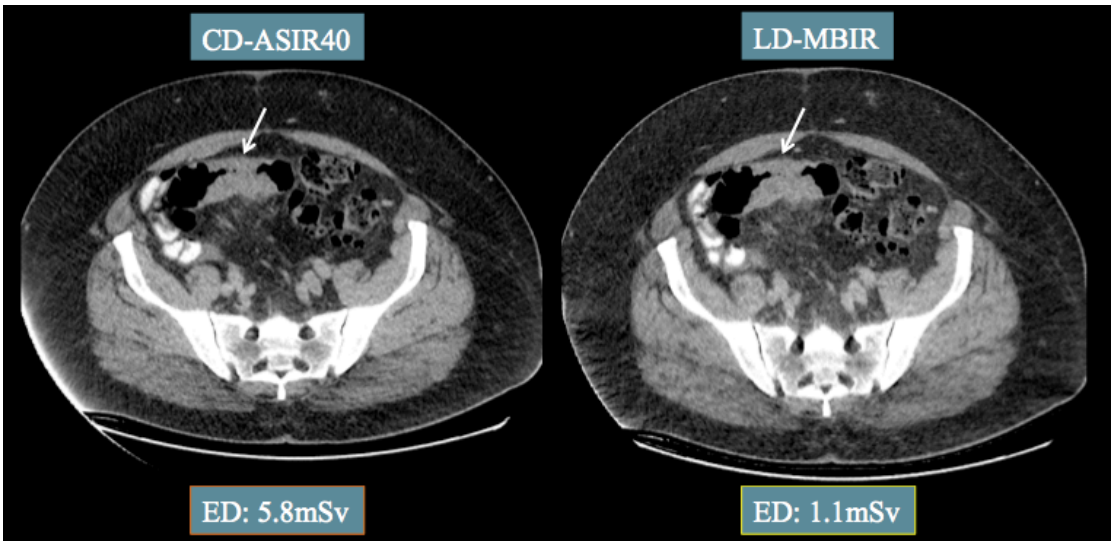

Figure 4.9 CD-ASIR and LD-MBIR axial CT images in a 56 year-old female patient presenting with acute abdominal pain demonstrate a short segment of sigmoid colonic wall thickening with adjacent inflammatory changes.

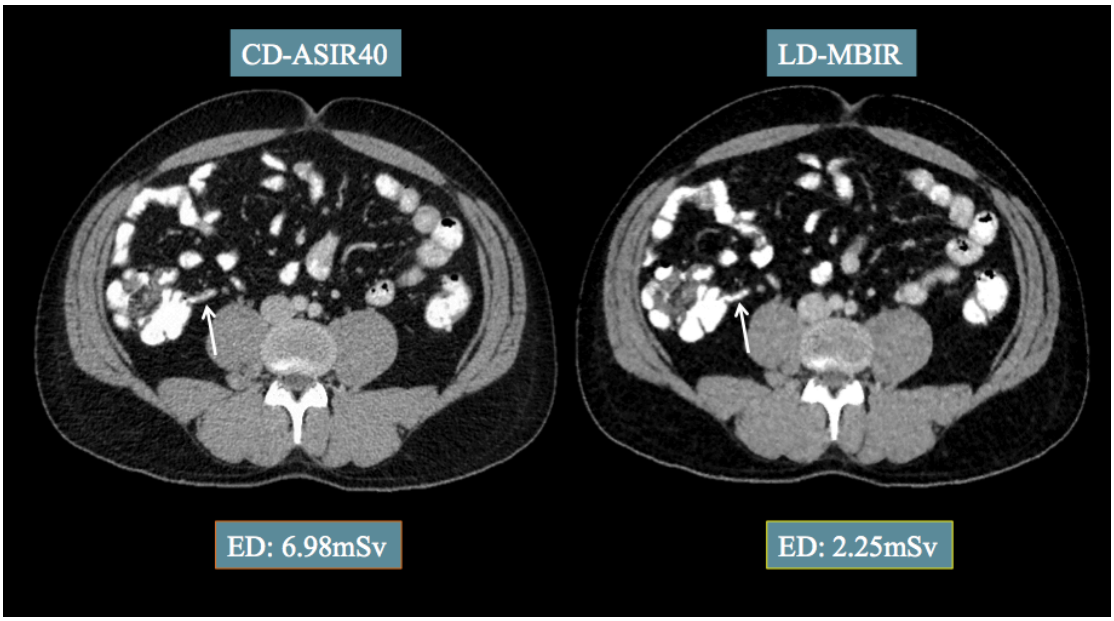

Figure 4.10 CD ASIR and LD MBIR axial CT images in a 29 year-old male patient presenting with acute abdominal pain with a suspected diagnosis of acute appendicitis. The LD MBIR image acquired at a significantly lower dose than the CD ASIR image show a normal appendix filled with oral contrast.

There was perfect intra-observer agreement for both readers and perfect inter-observer agreement for both protocols for nearly all primary findings with the exception of enteritis, which had good intra-observer agreement for both readers (Table 4.2). A short segment of terminal ileitis was not detected on the LD MBIR studies by both readers.

8 patients presented with an acute visceral perforation secondary to acute appendicitis (n=3), focal colitis/diverticulitis/tumour (n=2), acute diverticulitis (n=1), colitis (n=1), and gastric ulcer (identified at surgery)(n=1), for which there was perfect intra- and inter-observer agreement. There was perfect intra- and inter-observer agreement for the diagnosis of adnexal lesions (n=2),

obstructing renal calculi (n=1), small bowel obstruction (n=1), and epiploic appendagitis (n=1)(Figure 4.11).

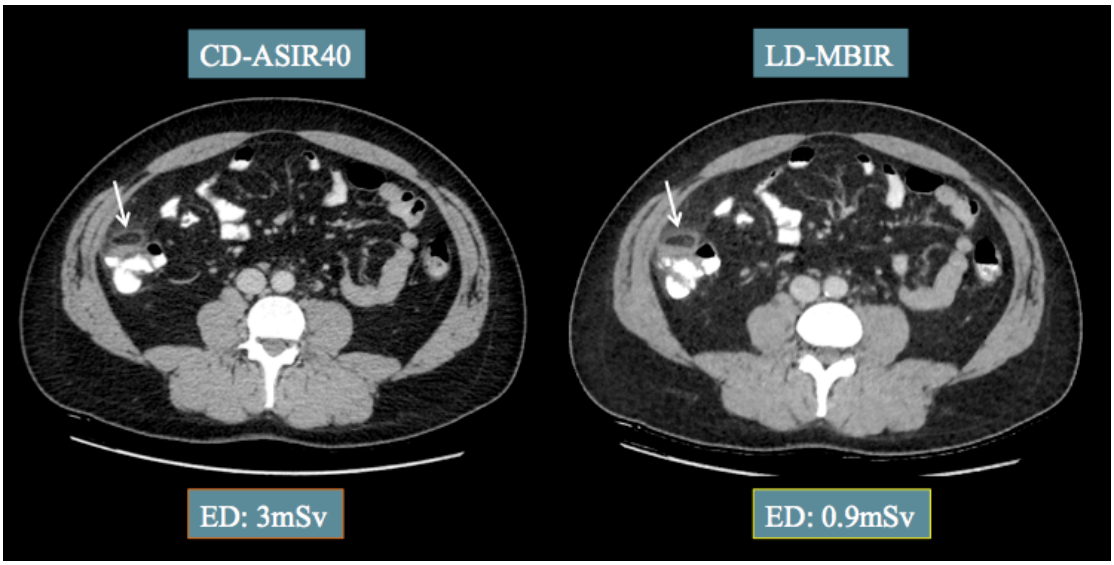

Figure 4.11 CD-ASIR and LD-MBIR coronal CT images in a 28 year-old male patient presenting with acute abdominal pain show a torted epiploic appendage of the ascending colon. The LD-MBIR image was acquired at a significantly lower dose than the CD-ASIR image.

Discrepancies between both readers were assessed by both readers in consensus with the use of the American College of Radiology RADPEER scoring system.[137,138]

A score of 3b (discrepancy in interpretation that should be made most of the time, likely to be clinically significant) was recorded by reader 1 when an occluded aortic graft was not detected on both protocols. A score of 2b (understandable miss, likely to be of clinical significance) was recorded by reader 1 for a 1.5 cm abscess secondary to acute appendicitis not recognised on the LD-MBIR study. A score of 2a (understandable miss, unlikely to be of clinical

significance) was recorded by reader 1 when a 4 mm appendicolith was not detected on both the LD-MBIR and CD-ASIR studies (Figure 4.12).

9 patients underwent surgery following CT including laparoscopic appendectomy for acute appendicitis (n=6), laparotomy for perforated diverticulitis (n=1), laparotomy for perforated gastric ulcer (n=1), and subtotal colectomy for Crohn's colitis (n=1). The findings at surgery were consistent with the primary diagnosis offered on CT in 8 cases with a perforated gastric ulcer being found at the time of surgery in a patient with a pneumoperitoneum of unclear origin.

5 patients underwent colonoscopy with a sigmoid colonic carcinoma being found in 1 of the 3 patients with focal diverticulitis/colitis/tumour. One patient had a second abdominopelvic CT during admission, which showed a post-appendectomy pelvic collection. Acute cholecystitis was diagnosed in a single patient on a subsequent ultrasound. On retrospective review by the study readers, there was mild gallbladder distension evident on CT. In all other cases, the diagnosis at discharge was in keeping with the CT findings or a diagnosis of 'abdominal pain of uncertain origin' was made in patients with no cause for abdominal pain on CT.

2 patients with re-admitted with acute abdominal pain during the follow-up period: a patient with a diagnosis of possible gastroenteritis was re-admitted at 3 months with a final diagnosis of abdominal pain of uncertain origin on the second admission; and a patient with a haemorrhagic ovarian cyst was re-admitted at 1 month with the same diagnosis on discharge.

Data regarding the detection of incidental abdominopelvic findings for the LD-MBIR and CD-ASIR studies are summarized in table 3. Reviewer 1 missed a case

of mild biliary dilation on the LD-MBIR studies (RADPEER score of 2b). Lung consolidation was not detected by reviewer 1 in one of four cases on the LD-MBIR studies (score of 2b). A subcutaneous nodule of indeterminate significance was not detected by reviewer 1 on the LD-MBIR images (Figure 4.13). All other discrepancies were scored as 2a.

Finding	Reviewer 1		Intra-observer Kappa	Reviewer 2		Intra-observer Kappa	Inter-Observer Kappa LD-MBIR	Inter-Observer Kappa CD-ASIR
	LD-MBIR	CD-ASIR		LD-MBIR	CD-ASIR			
Acute appendicitis	6	6	1.00*	6	6	1.00*	1.00*	1.00*
-perforation	3	3		3	3			
-collection	0	1		1	1			
-appendicolith	0	0		1	1			
-inflamed TI	1	1		0	0			
Diverticulitis	5	5	1.00*	5	5	1.00*	1.00*	1.00*
-perforation	1	1		1	1			
Focal colitis/tumor	3	3	1.00*	3	3	1.00*	1.00*	1.00*
-perforation	2	2		2	2			
Colitis	3	3	1.00*	3	3	1.00*	1.00*	1.00*
-perforation	1	1		1	1			
Enteritis	1	2	0.659*	1	1	1.00*	1.00*	0.659*
Pneumoperitoneum	1	1	1.00*	1	1	1.00*	1.00*	1.00*

-cause unclear								
Small bowel obstruction	1	1	1.00*	1	1	1.00*	1.00*	1.00*
Adnexal mass -ovarian torsion -complex ovarian cyst	2 1 1	2 1 1	1.00*	2 1 1	2 1 1	1.00*	1.00*	1.00*
Epiploic appendagitis	1	1	1.00*	1	1	1.00*	1.00*	1.00*
Post partum uterine hemorrhage	1	1	1.00*	1	1	1.00*	1.00*	1.00*
Obstructing VUJ calculus	1	1	1.00*	1	1	1.00*	1.00*	1.00*
Occluded aortic graft	0	0		1	1	1.00*		
Incarcerated abdominal wall hernia	1	1	1.00*	1	1	1.00*	1.00*	1.00*

Table 4.2 Primary findings on LD MBIR and CD ASIR studies for both readers in patients presenting with acute abdominal pain with intra-observer and inter-observer Cohen's kappa agreement. * denotes p value<0.001.

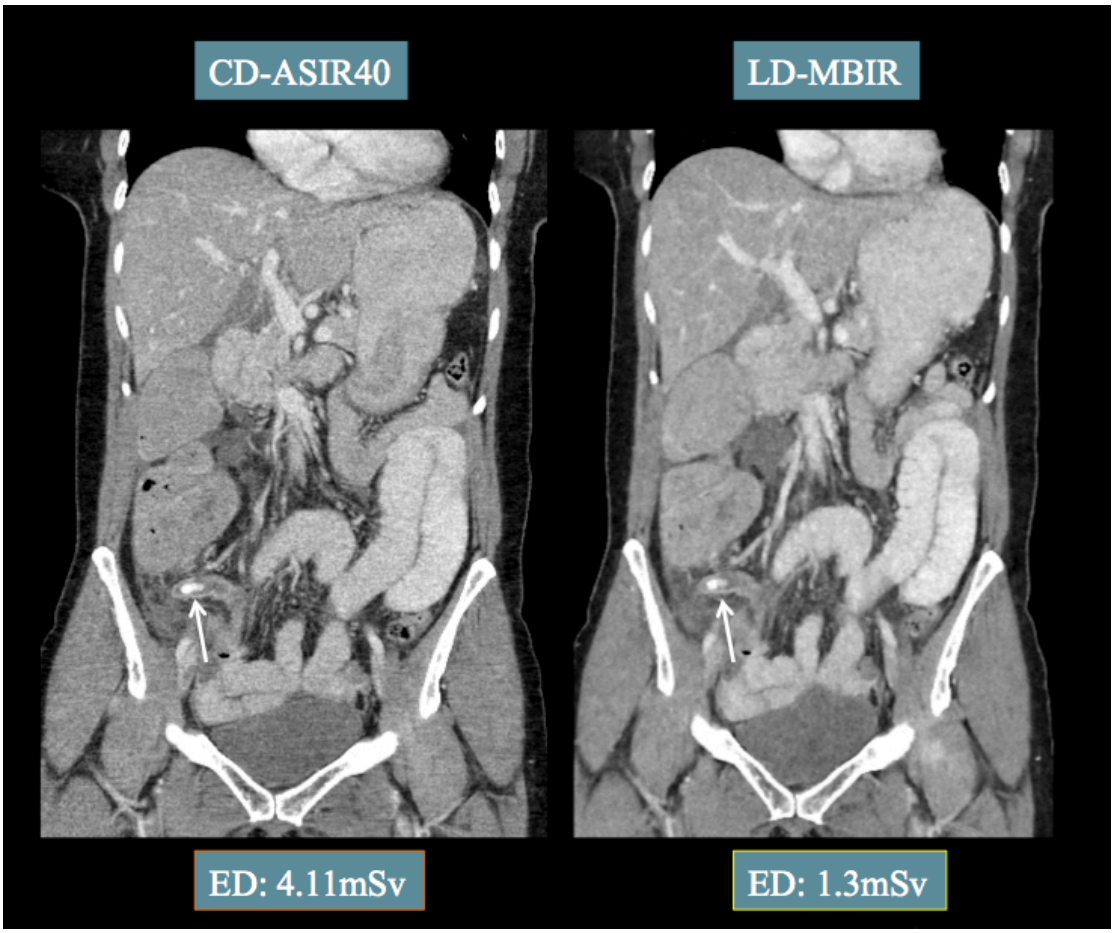

Figure 4.12 CD ASIR and LD MBIR coronal CT images in a 36 year-old male patient presenting with acute abdominal pain with a suspected diagnosis of acute appendicitis. Both images show an inflamed appendix with a 4 mm appendicolith. The LD MBIR image was acquired at a significantly lower dose than the CD ASIR image.

Finding	Reviewer 1		Reviewer 2	
	LD-MBIR	CD-ASIR	LD-MBIR	CD-ASIR
Focal hepatic steatosis	6	6	7	6
Ovarian cysts	5	5	4	5
Diffuse hepatic steatosis	4	3	6	8
Biliary dilatation	1	2	2	2
Lung consolidation	3	4	4	4
Liver lesion	2	2	2	2
Spondylolysis	1	1	1	1
Spina bifida	1	1	1	1
Inguinal hernia	0	1	2	1
Constipation	1	1	1	0
Renal calculus	1	1	0	0
Mesenteric panniculitis	1	1	1	1
Duplex kidney	1	1	0	0
Uterine fibroid	1	1	1	2
Renal scarring	1	1	1	1
Pancreas divisum	1	1	0	0
Pleural effusion	1	1	3	3
Adrenal lesion	1	2	3	3
Transplant kidney	1	1	1	1
Subcutaneous nodule	0	1	1	1
Gallbladder adenomyomatosis	1	2	0	0
Ventriculoperitoneal shunt	1	1	1	1

Table 4.3 Incidental abdominopelvic findings detected by both reviewers on the LD MBIR and CD ASIR studies.

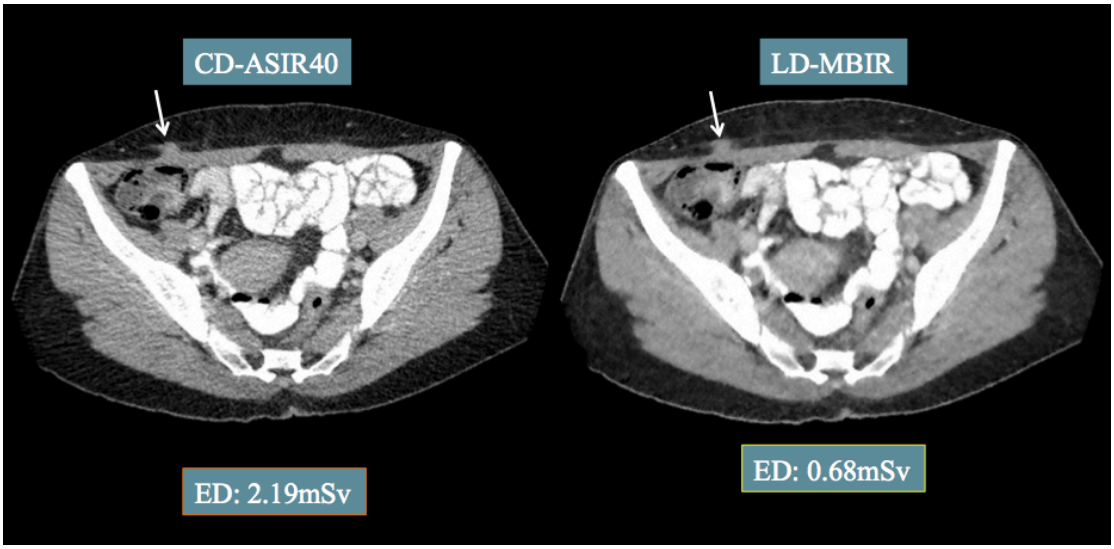

Figure 4.13 CD ASIR and LD MBIR axial CT images in a 42 year-old female patient presenting with acute abdominal pain. Both images show a subcutaneous nodule of indeterminate significance superficial to the lateral margin of the right rectus abdominis muscle. The LD MBIR image was acquired at a significantly lower dose than the CD ASIR image. The nodule was not detected by reviewer 1 on the LD MBIR images.

Discussion

Acute abdominal pain is a common condition amongst patients presenting to the emergency department, accounting for 4-5% of all emergency department attendances.[139] The spectrum of disease that may present with acute abdominal pain ranges from life-threatening conditions requiring immediate surgery to

more benign self-limiting conditions. In a review of approximately 30,000 patients presenting with acute abdominal pain, 28% of patients had appendicitis, 9.7% had acute cholecystitis, 4.1% had small bowel obstruction, 4% had acute gynaecologic disease, 2.9% had acute pancreatitis, 2.9% had acute renal colic, 2.5% had a perforated peptic ulcer, and 1.5% had diverticulitis. No cause could be identified in one third of patients.[140] Given the wide spectrum of pathologies that may present with acute abdominal pain, the first step in assessment is to obtain a careful history and perform a physical examination, followed by appropriate imaging if indicated.

CT is well suited to the assessment of the acute abdomen: it provides rapid, accurate, and minimally invasive diagnostic information that can be invaluable in guiding management decisions. It has been shown to have a superior diagnostic accuracy to ultrasound[141] and conventional radiography[142], to increase physician's level of certainty regarding diagnosis, to reduce hospital admission rates by 24%, and to lead to timelier surgical intervention.[37]

Consequently, the American College of Radiology appropriateness criteria currently recommend contrast-enhanced abdominopelvic CT as the most appropriate first-line imaging examination for left lower, right lower, and non-localized acute abdominal pain in non-pregnant, adult patients.[143]

CT has reported sensitivities of 96%, 94% and 94% and specificities of 99%, 99%, and 96% for the diagnosis of acute appendicitis[144], diverticulitis[145], and small bowel obstruction[146], respectively. CT is the setting of suspected acute appendicitis has been shown to reduce the negative-finding appendectomy rate from 24% to 3%, with a simultaneous increase in CT use, from 20% to 85%, over a period of 10 years.[147]

There has been an exponential increase in the use of CT in the emergency department in recent years. Between 1995 and 2007, the number of attendances that included a CT examination increased from 2.7 million to 16.2 million, constituting a 5.9-fold increase and a compound annual growth rate of 16%.[148] CT remains a relatively high dose procedure in comparison with other conventional radiology examinations contributing a disproportionately large amount towards the collective effective dose from diagnostic imaging.[4] The dramatic increase in the use of CT has raised concerns in the literature regarding the risk of cancer induction associated with CT imaging, particularly in younger patients.[149] Acute abdominal pain, especially due to acute appendicitis, is a common presentation necessitating CT imaging amongst younger patients.[150] The typical effective radiation dose imparted by an abdominopelvic CT is approximately 10mSv. Although controversial, some experts have suggested that a 10mSv CT examination performed in a 25-year-old patient carries an estimated risk of induced cancer of one in 900 individuals and a risk of fatal cancer induction of one in 1800 individuals.[151] These estimated risks however, are generally outweighed by the direct diagnostic benefit of undergoing CT examination and most CT examinations are associated with a favourable ratio of benefit to risk. Nevertheless, CT protocols should be optimized to ensure patient dose is kept as low as reasonably achievable without compromising image quality.

Previous studies of low-dose abdominopelvic CT report the acquisition of diagnostically acceptable images using strategies such as low tube current techniques[152,153] and automated exposure control.[47] Iterative reconstruction algorithms, namely hybrid IR and pure IR are the most promising dose

optimization techniques that have been studied to date.[54, 73] Many studies investigating the potential role of MBIR in abdominopelvic CT have focused on its utility in the setting of renal colic.[154, 155] Vardhanabhuti et al reported superior noise reduction and image quality of conventional dose CT kidney/ureter/bladder images reconstructed MBIR compared to FBP and hydrid IR.[138] Fontarensky et al achieved a dose reduction of 84% with the use of a low-dose abdominopelvic protocol using MBIR without a conspicuous deterioration in image quality.[139] However, dose reductions in the setting of renal colic are largely facilitated by the inherent high contrast difference of renal calculi against the relatively low-density soft tissues surrounding the urinary tract and the performance of MBIR in pathological conditions with lesser contrast differences compared to anatomic structures requires further evaluation.

Two previous studies have assessed the utility of MBIR in low-dose abdominopelvic CT in patients with acute abdominal pain.[121, 122] Poletti et al employed a fixed tube-time-current product technique, which ensures a more predictable final radiation exposure, regardless of body habitus.[121] However, this can result in reduced image quality with increasing BMI, with Poletti et al concluding that low-dose CT with MBIR cannot safely assess acute abdominal pain in obese patients. The use of ATCM in our study, which balances radiation dose against image quality, ensured preservation of image quality in the face of increasing BMI, with no significant difference in image noise being observed between the BMI subgroups for the LD-MBIR studies. Furthermore, we found patients with a BMI of ≥25 kg/m^2 to have superior image quality to patients with a BMI of <25 kg/m^2 for both the LD-MBIR and CD-ASIR studies. . This is partially explained by the fact that a generous quantity of intra-abdominal fat is

considered the abdominal radiologist's friend in detecting abdominal pathology in the acute setting.

The use of ATCM also resulted in higher radiation exposures with increasing BMI. As a large proportion (56%) of our patients had a BMI of ≥25 kg/m^2, the overall mean radiation exposure exceeded the peri-millisievert range. However, in patients with a BMI of <25 kg/m^2, diagnostically acceptable low-dose images were acquired in the peri-millisievert range (1.16±0.76mSv), representing a mean ED dose reduction of 87.6%. This dose reduction is substantially greater than another study assessing low-dose CT with MBIR in acute abdominal pain; Othman et al employed a lower kV technique but only reported a dose reduction in the order of 26.1% (effective dose, 5.72±2.23mSv vs. 2.38±1.78mSv in our study).[122]

There was perfect intra-observer agreement for both readers and perfect inter-observer agreement for both protocols for nearly all the 'key' findings with the exception of enteritis, which had good intra-observer agreement for both readers. All causes of acute abdominal pain requiring surgery were identified including all cases of visceral perforation, and no patient underwent surgery for pathology not identified on low-dose MBIR studies. An occluded aortic graft was not detected on both protocols by one reader (discrepancy score 3b), and a 1.5 cm abscess related to acute appendicitis was not recognised by both readers on the LD MBIR studies (discrepancy score 2b). However, on review of the LD MBIR images by the study authors following the study, it was felt that these discrepancies were due to under-reading rather than suboptimal image quality.

We recognise the limitations of our study. Our reference 'gold standard' conventional dose protocol was acquired at a dose slightly below that of our

standard departmental protocol. However, the authors feel that exposing patients to additional, unnecessary radiation as result of recruitment into the study was ethically prohibited. Furthermore, the radiation dose imparted by our conventional dose protocol is likely to be comparable to that of the standard departmental protocol of other institutions. Our chosen gold standard therefore represents a compromise made in the interests of the safety of study participants. Radiation dose was slightly underestimated in the study as the dose incurred during topogram acquisition was excluded from analysis. The use of a contemporaneous but not simultaneous acquisition process with a 6 second delay between the acquisition of the low-dose and conventional dose scans, may have resulted in slightly different contrast enhancement intensity at the time of scanning and detracted form direct comparisons. Similar to previous authors assessing MBIR-reconstructed images[68], we found MBIR images to have a somewhat pixelated and 'waxy' appearance. Due to this unique appearance, it was not possible to satisfactorily blind the readers to the acquisition protocol. To compensate for this and to minimise the effects of recall bias, a six-week delay was instituted between reviews of both protocols, with the LD MBIR studies being read first. Correlation with surgical findings was not performed. However, as this applied equally to the low- and conventional dose CT studies, there is no risk for bias.

Patients with a history of malignancy were excluded from the study as detection of metastatic disease and cancer staging were beyond the scope of this study. Low-dose abdominopelvic CT with MBIR has previously been assessed for the detection of colorectal hepatic metastatic disease[118] and surveillance of patients with testicular cancer[156], but extrapolation of our results to patients with a

history of malignancy should be made with care. Subjective scores of noise and diagnostic acceptability were also lowest in the liver at the level of the porta hepatis suggesting that our protocol may not be suitable for the detection of hepatic lesions and hepatic metastatic disease. Further study of the role of low-dose abdominopelvic CT with MBIR in cancer staging is required. Finally, the results of our study may not be entirely applicable to pure iterative reconstruction algorithms manufactured by other venders and independent validation of these techniques may be required. The capital cost of the MBIR technology is also another consideration.

The strengths of our study include a large sample size and the contemporaneous acquisition of a gold standard comparison study. This split-dose technique ensures that no patient incurs additional radiation exposure as a result of recruitment into the study, as well as enabling participants to act as their own controls thereby reducing the likelihood of confounding variables. A major strength of our study is the inclusion of a wide range of pathologies that may present with acute abdominal pain, and thereby suggests that the LD MBIR protocol may be applicable to a wide range of abdominopelvic conditions. It should also be noted that our reference 'gold standard' conventional dose protocol for image quality assessment was reconstructed with hydrid IR and not the traditional algorithm, FBP, used in many studies. Given the superior performance of hybrid IR over FBP in noise reduction[54], the noise reducing capability of MBIR compared to FBP is likely to have been underestimated in our study.

The major limitation to the widespread introduction of MBIR into clinical practice is the lengthy reconstruction time required (approximately 35 minutes

in our study), compared to FBP and hybrid IR algorithms, which are computationally time efficient. This is particularly relevant in the acute setting where a delayed diagnosis imposed by a prolonged reconstruction time may result in adverse patient outcomes. In certain clinical scenarios, if the referring clinician feels that the increased time from scan acquisition to issuance of the final report would not have a significant impact on patient management or outcome, use of the LD MBIR protocol may be appropriate given the substantial radiation dose reduction that can be achieved.

However, the delay may not be justified in selected clinical scenarios, such as patients in whom bowel perforation or mesenteric ischemia is suspected. Patients presenting following abdominal trauma were excluded from our study, as the need for a rapid diagnosis, particularly in the context of suspected active haemorrhage, would generally preclude the use of the LD MBIR protocol. Additional strategies that may be employed in conjunction with the LD MBIR protocol could include special triaging of patients to ensure that other potential causes of delay prior to scanning are minimized. Eliminating oral contrast[157] or administration of oral contrast over a shorter time period would also expedite scanning but the impact of this strategy on the diagnostic accuracy of low-dose abdominopelvic CT reconstructed with MBIR has yet to be investigated. It is possible that future technological advances will increase the computational efficiency of the MBIR algorithm and shorten the processing time required expanding its applicability to all acute abdominal presentations, including the trauma setting. We currently are planning to conduct a prospective feasibility study using the LD MBIR protocol alone in selected patients presenting to the emergency department with acute abdominal symptoms.

In conclusion, low-dose abdominopelvic CT performed with pure IR facilitated a mean dose reduction of 74.7% in all patients, and 87.6% in patients with a BMI of <25 kg/m^2, compared to a conventional dose protocol using hybrid IR, without compromising diagnostic accuracy. Low-dose abdominopelvic CT performed with pure IR is a feasible radiation dose reduction strategy for selected patients presenting with acute abdominal pain.

Chapter V

Low-dose chest CT using pure iterative reconstruction at chest radiography dose levels: a prospective study in patients with cystic fibrosis undergoing treatment with Ivacaftor (Kalydeco)

Introduction

Pulmonary disease is the primary cause of morbidity and mortality in patients with cystic fibrosis (CF).[158] Early detection of the onset of lung disease and complications is essential to facilitate appropriate treatment adaptation expeditiously with the ultimate aim of limiting disease progression.[159]

The current annual rate of lung function decline in patients with CF is approximately 0.7% making it difficult to detect subtle changes with standard monitoring methods such as chest radiography and pulmonary function tests (PFTs).[160] Several studies have shown CT to be more sensitive than chest radiography and PFTs for the detection and surveillance of lung disease[161,162,163], making it the most appropriate technique for monitoring pulmonary disease in the current CF population.

The major limitation to routine adoption of CT for monitoring CF lung disease is the substantial radiation exposure associated with conventional chest CT compared with plain radiography (3.5 mSv vs 0.02 mSv). High CEDs from diagnostic imaging have been documented in a number of patient groups with

chronic relapsing conditions including CF.[7, 8, 9, 10] Given that patients with CF undergo repeated chest CT from a young age, carry an increased lifetime risk of developing cancer[164], and with a progressively longer life expectancy and more years of life in which to develop a radiation-induced cancer[165], it is essential to keep CED from diagnostic imaging in this patient cohort as low as reasonably possible.

A standard protocol CT thorax imparts an effective dose ranging from approximately 1.7mSv in an infant to 5.4mSv in an adult.[166] Several dose optimization strategies may be employed when performing chest CT in patients with CF including the use of low-dose protocols, automated exposure control[167], and automated patient centering techniques.[168] At our specialized CF center, we routinely use a modified 7-section low-dose protocol that we have previously validated and reported in the literature[77], involving the acquisition of a limited number of thin CT sections to impart a mean effective dose of 0.14mSv, equivalent to the dose of a postero-anterior (PA) and lateral chest radiograph (0.1mSv).[169] We are currently using this low-dose protocol to monitor pulmonary disease in cystic fibrosis patients in a trial assessing the safety, efficacy and tolerability of cystic fibrosis transmembrane conductance regulator modulation with Ivacaftor (Kalydeco).

Ivacaftor has been shown to produce significant increases in forced expiratory volume in one second (FEV_1) (>10% absolute) and BMI, as well as reductions in sweat chloride levels, patient-reported respiratory symptoms and pulmonary exacerbation rate in patients with the G551D-CFTR mutation.[170,171,172]

The prevalence of this mutation at our CF center is the highest in the world at 23%, compared to 4% in the United States[173], making it uniquely placed to provide a single center insight into CFTR potentiation.

The efficacy of many dose reduction strategies to reduce radiation dose while preserving image quality is often limited by the innate limitations of the traditional FBP reconstruction algorithm installed on most CT systems. IR algorithms have been the focus of much dose optimization research in recent years. Hybrid IR algorithms such as ASIR, are the most studied methods to date in chest CT facilitating dose reductions in the order of 57% while preserving image quality.[174,175]

To date, there is a paucity of studies assessing the use of pure IR in chest CT.[176,177] The purpose of this prospective feasibility study was to assess the utility of a modified low-dose CT thorax protocol reconstructed with pure IR for the surveillance of pulmonary disease in patients with CF.

Methods

Study population

This current study forms part of a prospective trial currently being conducted at our institution, a designated tertiary CF center, assessing the impact of cystic fibrosis transmembrane conductance regulator modulation with Ivacaftor on the CF lung.

As part of this study, 15 clinically stable, Ivacaftor-naive adult patients with CF and at least one copy of the G551D allele gave written informed consent to

undergo a low-dose CT thorax prior to initiation of Ivacaftor therapy followed by routine quarterly radiological follow-up with a low-dose CT thorax for 12 months (CT thorax at 3, 6, 9 and 12 months) with a final low-dose CT thorax at 24 months.

BMI of each patient was calculated at the time of each CT scan using height and weight measurements recorded with a digital device (Seca electronic measuring station Model 763, Seca Medical, Hamburg, Germany). Pulmonary function tests including FEV_1 and forced vital capacity (FVC) were also recorded at the time of each CT scan in a dedicated pulmonary function laboratory using a Jaeger Masterscreen Pneumo spirometer (Jaegar/HP/Dell; San Diago, CA, USA).

Institutional review board approval was granted for the study.

CT technique and image reconstruction

All studies were acquired using a 64-slice multidetector CT scanner (General Electric Discovery CT 750 HD; GE Healthcare, GE Medical Systems, Milwaukee, WI, USA) without intravenous contrast material.

7-section low-dose protocol

A modified 7-section, low-dose axial CT protocol previously validated at our institution was used for the pre-treatment and first 12-month quarterly studies.[77]

Single anteroposterior and mediolateral localizer radiographs were used to identify 5 levels, evenly spaced, at which images were acquired (Figure 5.1). Images were obtained with the patient at end-inspiration through the lung apices, aortopulmonary window, carina, and at the widest cardiac and thoracic

diameters. Two further images were obtained with the patient in full expiration at the level of the aortopulmonary window and at the widest cardiac diameter (Figure 5.2). The following parameters were used: tube voltage of 120 kV; gantry rotation time of 0.4 seconds; FOV of 32cm; and z-axis automatic tube current modulation with minimum and maximum tube current thresholds set at 10 and 100 mA with a tolerated noise index of 29HU. Images were acquired at each of the 7 levels at a slice thickness of 0.625mm and reconstructed to a slice thickness of 3mm with the standard departmental protocol employing hybrid IR: 70% FBP and 30% ASIR, labeled low-dose LD ASIR.

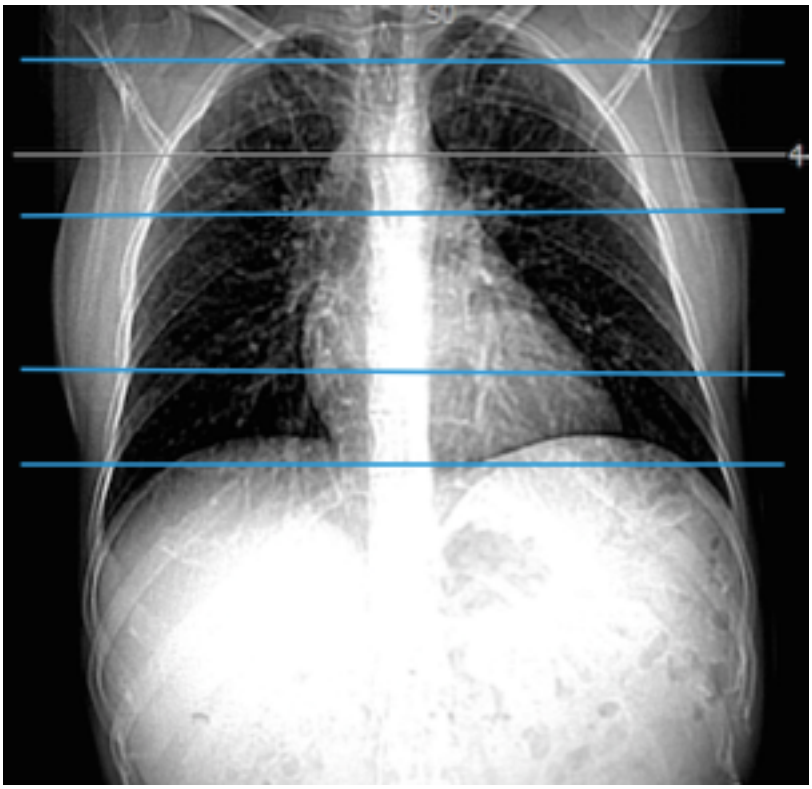

Figure 5.1 Anteroposterior scanned projection radiograph used to identify 5 levels at which images were acquired for the 7-section low-dose protocol. Images were obtained at the level of the lung apices, aortopulmonary window, carina, and at the widest cardiac and thoracic diameters.

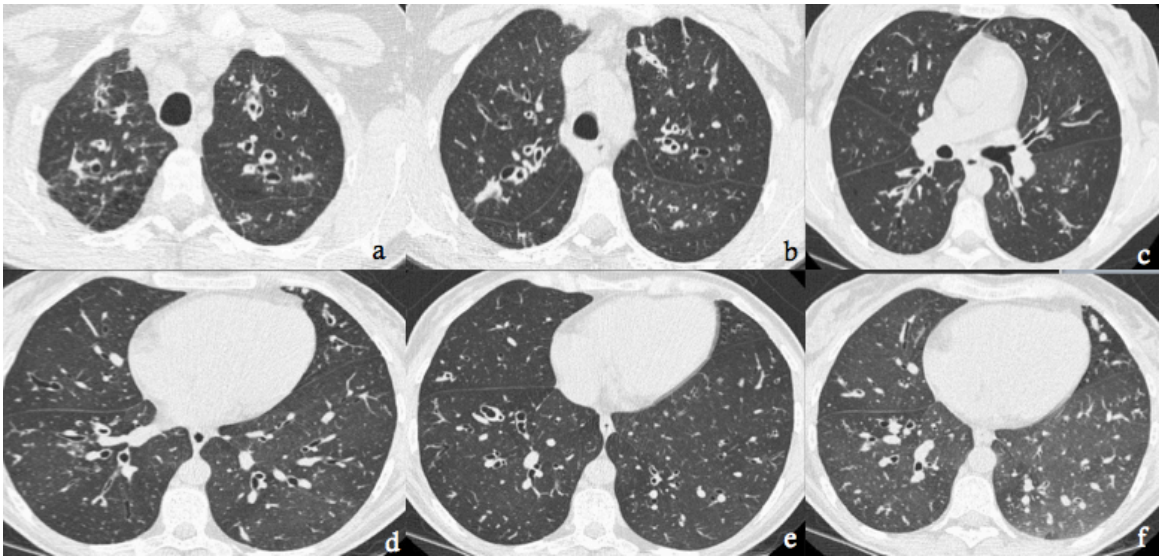

Figure 5.2 Low-dose axial CT images acquired in a 21-year-old male patient with cystic fibrosis at 12-months of treatment with Ivacaftor using the 7-section LD ASIR protocol (effective dose 0.1mSv). Images were obtained at the level of the lung apices (a), aortopulmonary window (b), carina (c), and at the widest cardiac (d) and thoracic (e) diameters. Expiration phase images were obtained at the level of the aortopulmonary window (not shown) and at the widest cardiac diameter (f).

Volumetric low-dose protocol

A novel low-dose volumetric protocol was designed for the 24-month surveillance CT. Preliminary anthropomorphic torso phantom (CT Torso Phantom CTU41, Kyoto Kagaku, Fushimi-ku, Kyoto, Japan) and technical phantom (Catphan 600, The Phantom Laboratory, Greenwich, NY, USA) studies were conducted to determine the optimal protocol settings. Technical

parameters were altered to assess the effect on radiation dose and diagnostic quality with the following parameters indicating that studies could potentially be acquired at a dose of approximately 0.08mSv: tube voltage of 80 kV; tube current of 20mA; gantry rotation time of 0.4 seconds; pitch factor of 1.375; and FOV of 32cm. To ensure the radiation exposure remained low for patients of all body habitus, a fixed tube current technique was employed.

Scanning was performed at end-inspiration from the lung apices to the bases, including the costophrenic recesses. No additional expiratory phase imaging was performed. Images were acquired at a slice thickness of 0.625mm and reconstructed at a final slice thickness of 3mm with MBIR in axial, coronal, and sagittal planes, labeled LD-MBIR (Figure 5.3). Images were also reconstructed with hybrid IR (40% ASIR and 60% filtered back projection), labeled LD ASIR. The latest generation of the MBIR software offers two reconstruction algorithms for use with chest CT: 'MBIR RP05' and 'MBIR RP20.' The phantom datasets were reconstructed with both algorithms and analyzed quantitatively (objective image noise, signal-to-noise ratio (SNR), contrast-to-noise ratio, spatial resolution, and low-contrast detectability) and qualitatively (subjective image noise and subjective image quality) by two chest radiologists. Although all comparisons were non-significant, there was a tendency towards higher subjective image quality and spatial resolution scores with the MBIR RP20 algorithm, with a tendency towards lower levels of objective image noise with the MBIR RP05 algorithm. On the basis of these results, the MBIR RP20 algorithm was chosen for the study. Images were also reconstructed at the same 5 levels as the 7-section ASIR inspiratory phase scans to facilitate a direct, blinded comparison between both low-dose techniques.

Figure 5.3 Representative coronal CT image acquired in a 23-year-old male patient with cystic fibrosis at 24 months of treatment with Ivacaftor using the volumetric low-dose MBIR protocol (effective dose 0.08mSv).

Verification of dose measurements

DLP and CTDIvol values were recorded from each CT dose report.

The Imaging performance and assessment in CT patient dosimetry calculator (ImPACT version 0.99x, London, England) was used to calculate effective dose (ED). Size specific dose estimates (SSDE) were recorded from an automated dose-tracking program (DoseWatch, General Electric Healthcare, Waukesha, WI, USA). The radiation exposure resultant from the CT topograms was excluded from analysis. For the 7-section LD-ASIR studies, doses from each image were summated to give a total dose.

Quantitative analysis

Objective image quality analysis was performed independently on a dedicated workstation by the author and a second operator with 7 years experience. The operators were blinded to the scanning protocol used and the order of the datasets was randomized. Attenuation values were measured in HU at three levels: the aortic arch, the carina, and the maximum cardiac diameter. Measurements were recorded by placing circle histograms of equal size (diameter, 10mm) in the descending aorta and paraspinal muscles of the posterior chest wall at each level. Objective image noise and SNR were then calculated as previously described. Measurements were taken three times by each operator to reduce error and the mean recorded. The mean of both operators' measurements was used for analysis.

Qualitative analysis

The subjective image quality parameters and grading system were selected on the basis of the findings of previous studies.[47, 77] Images were reviewed on a picture archiving and communication system (Impax 6.5.3; Agfa healthcare, Morstel, Belgium) in a Digital Imaging and Communications in Medicine format on a monitor with a resolution of 3 megapixels.

Image noise, diagnostic acceptability, depiction of bronchovascular structures within 2cm of the pleural margin, and presence of streak artifact were assessed at 5 levels (lung apices, aortopulmonary window, carina, and at the widest cardiac and thoracic diameters) for all datasets by two fellowship trained chest radiologists in consensus. To facilitate a direct and blinded comparison between

both low-dose techniques, only axial reformations were used for analysis. The readers were blinded to the scanning protocol used and the order of the datasets was randomized.

Image noise was assessed at mediastinal window settings (window width, 350HU; window level, 50HU) on the basis of the amount of image mottle present using a 5-point scale: 1, unacceptable; 2, minimally acceptable; 3, acceptable; 4, highly acceptable; and 5, excellent. If peripheral blood vessels and the interfaces between adjacent tissues were adequately visualized, a score of 3 was assigned. A score of 1 indicated extensive graininess in the image while a score of 5 indicated absent graininess. Diagnostic acceptability was scored at both mediastinal and lung window (window width, 1500HU; window level: -500HU) settings using the same 5-point scale. A score of 3 was allocated if images were considered acceptable for diagnostic purposes. Scores of 1 and 5 indicated unacceptable or excellent diagnostic quality, respectively. The depiction of bronchovascular structures within 2cm of the pleural margin was assessed on lung window settings using the same 5-point scale.

The presence of streak artifact was assessed at mediastinal window settings using a 3-point scale: 1, no streak artifact; 2, streak artifact present but not interfering with image interpretation; and 3, streak artifact present and interfering with image interpretation.

Quantification of lung disease

Disease severity was scored independently by the same two readers using a validated scoring system (Bhalla score) that assesses the severity of cystic fibrosis based on the appearance of pulmonary parenchyma and aiways.[178] Both

readers had significant prior experience assessing the severity of CF using the Bhalla system. To minimize the effects of recall bias, all datasets were anonymized and reviewed in a random order. In addition, a 6-week delay was instituted between the review of the baseline and 1-year 7-section ASIR studies and the 2-year LD MBIR studies. Images were reviewed on lung window settings (window width, 1500HU; window level: -500HU) on the picture archiving and communication system using axial reformations for the 7-section ASIR studies and a combination of axial and coronal reformations for the LD MBIR studies. The presence and severity of 9 morphological changes were evaluated including: severity of bronchiectasis; peribronchial thickening; extent of bronchiectasis (number of bronchopulmonary segments); extent of mucus plugging (number of lung segments); abscesses or sacculations (number of lung segments); generations of the bronchial divisions involved; number of bullae; air trapping (number of lung segments); and collapse/consolidation. A score of 0 to 3 (0: absent; 1: mild; 2: moderate; 3: severe) was assigned to each category to give a total score ranging from 0 to 25. A score of 0 indicated that no abnormality was detected.

Digital ray sum chest radiographs

Digital ray sum chest radiographs were generated for each LD-MBIR study and analyzed independently by the same two raters (MMM and OJOC) using a 3-point scale: 1, unacceptable; 2, acceptable; and 3, highly acceptable. Qualitative parameters selected on the basis of the European Guidelines on Quality criteria for Diagnostic Imaging, included depiction of pulmonary vascular structures,

tracheobronchial tree, cardiac borders, diaphragm and costophrenic recesses, reticular details at the lung periphery, retrocardiac lung, and thoracic spine.[179] Images were also assessed for the presence of consolidation, atelectasis, ground glass opacities, fibrosis, volume loss, bronchiectasis, mucus plugging, cavitation, mediastinal adenopathy, pleural effusion, and pneumothorax. The most recent chest radiograph was also analyzed independently by the study raters for comparison with the ray sum radiographs.

Statistical analysis

Distribution of variables was assessed using D'Agostino-Pearson omnibus normality test. Data are described as mean and standard deviation for parametric distributions or as median and range for non-parametric distributions. Mann-Whitney test was used to compare non-parametric distributions of two groups of continuous variables. Two-way analysis of variance and Tukey's multiple comparisons test were used to compare quantitative measures of noise and SNR. Friedman test was used to compare qualitative measures between datasets. Inter-rater reliability of disease quantification scores was assessed with intraclass correlations. Normally distributed repeated parametric quantitative indices were compared using paired t-tests. Pearson's correlations were used to assess the strength of association between normally distributed continuous variables respectively. Cohen's kappa analysis was used to quantify the level of agreement between the digital ray and chest radiograph scores. P values less than 0.05 were considered to be statistically significant.

Results

Study subjects

15 patients (7 female, 8 male) with a mean age of 26.5±6.1 years of age were included in the study. Table 5.1 demonstrates the change in mean BMI, FEV_1, and FVC over the study period. BMI increased significantly compared to baseline after 1 year of treatment. FEV_1 and FVC increased significantly compared to baseline at 1 and 2 years of treatment. No significant difference was observed for any of the measures between 1 year and 2 years.

	Baseline	*1-year*	*2-years*
BMI (kg/m²)	21.38±3.18	22.94±3.63*	22.37±2.44
FEV_1 (% predicted)	63.4±17.5	74.27±16.33***	72.2±17.54**
FVC (% predicted)	81.13±15.16	89.87±10.7***	86.8±14.07*

Table 5.1 Change in BMI (body mass index), FEV_1 (forced expiratory volume in one second), and FVC (forced vital capacity) over the study period. Data are expressed as mean±SD. * denotes the significance level of the change at 1 year and 2 years compared to the baseline measurement. All other comparisons were non-significant.

Radiation exposure

The volumetric LD-MBIR protocol was performed with a mean DLP of 5.04±0.52mGy.cm resulting in a mean ED of 0.09±0.01mSv. The 7-section ASIR

protocol was performed with a mean DLP of 5.89±1.24mGy.com with a mean ED of 0.10±0.02mSv. LD-MBIR studies were acquired at a significantly lower radiation dose than the 7-section ASIR studies (Table 5.2).

No significant radiation dose difference was observed between BMI subgroups for either protocol due to the use of a fixed tube current technique.

Dose measurement	*LD ASIR*	*Volumetric LD MBIR*	*P value*
DLP (mGy.cm)	5.89±1.24	5.04±0.52	0.01*
ED (mSv)	0.10±0.02	0.09±0.01	0.02*
CTDIvol (mGy)	46.9±9.78	0.017±0.01	<0.0001*
SSDE (mGy)	_	0.25±0.02	_

Table 5.2 Comparison of dose measurements between LD ASIR and LD MBIR protocols. Data are expressed as mean±SD. * denotes significance at the less than 0.05 level.

The mean CTDIvol of the 7-section ASIR studies was significantly higher than the LD-MBIR studies as a much smaller volume of tissue received a similar radiation dose. Mean SSDE for the volumetric LD-MBIR studies was 0.25±0.02mGy.

The LD-MBIR protocol resulting in a mean ED dose reduction of 20% compared to the 7-section ASIR protocol. Effective doses were reduced by 98.5% and 98.1% compared to a conventional dose volumetric CT thorax in an adult patient (5.4mSv) for the LD-MBIR and L7-section ASIR protocols, respectively.

Quantitative analysis

Quantitative measures of image noise at 3 levels from each protocol are shown in Figure 5.4. Both axial and coronal LD MBIR images were significantly superior to LD ASIR images at all levels (23.03±6.4HU vs. 72.53±11.58HU, p<0.0001 and 19.2±5.7HU vs. 72.53±11.58HU, p<0.0001, respectively). 7-section ASIR images had significantly lower levels of image noise at all levels compared to LD-ASIR images (22.15±8.9HU vs. 72.53±11.58HU, p<0.0001). The greatest mean noise difference was observed between coronal LD MBIR and LD ASIR images, with the greatest difference at the level of the maximum cardiac diameter (55.8HU). All other comparisons at all levels were non-significant (p=0.08-0.94).

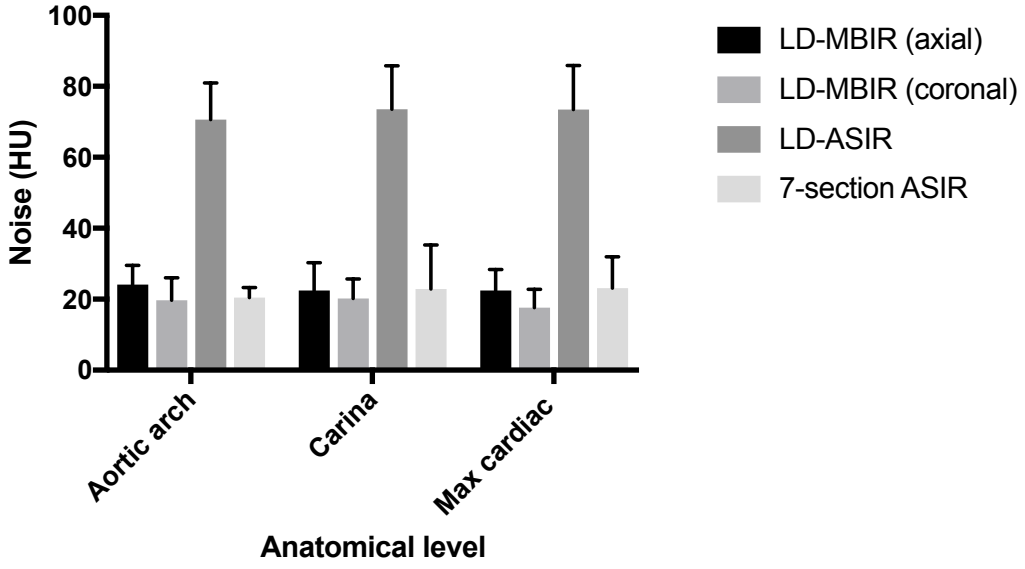

Figure 5.4 Chart depicts mean image noise for LD-MBIR, LD-ASIR, and 7-section ASIR protocols at each of the three levels assessed. Data are plotted as mean and standard deviation as indicated by whiskers. LD-MBIR and 7-section ASIR

images had significantly lower levels of image noise than LD-ASIR images. All other comparisons were non-significant.

Mean SNR was also compared between each protocol at each level (Figure 5.5). Both axial and coronal LD-MBIR images had significantly higher SNRs than LD-ASIR images at all levels ($p<0.001$ for all comparisons). 7-section ASIR images had significantly higher SNRs than LD-ASIR images at all levels ($p<0.0001$). Coronal LD-MBIR images were found to have significantly higher SNRs than axial LD-MBIR images at the level of the maximum cardiac diameter ($p=0.0002$). Axial and coronal LD-MBIR images also had significantly higher SNRs than 7-section ASIR images at the level of the maximum cardiac diameter (p values of 0.017 and 0.001, respectively). All other comparisons were non-significant.

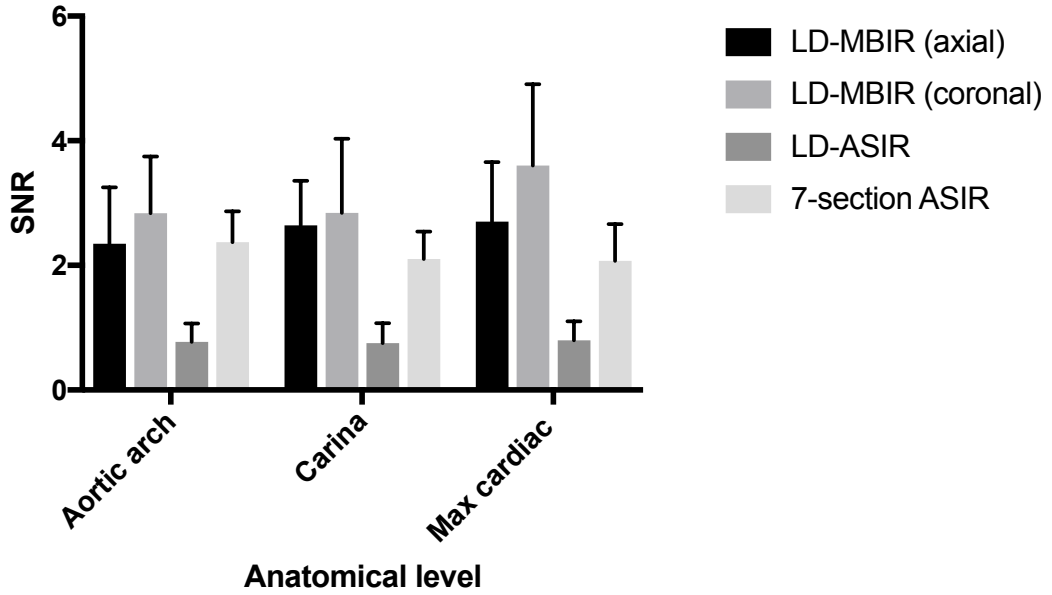

Figure 5.5 Chart depicts mean SNR for each dataset and level assessed with SD (whiskers). Both axial and coronal LD-MBIR images had significantly higher

SNRs than LD-ASIR images at all levels and significantly higher SNRs than 7-section ASIR images at the level of the maximum cardiac diameter.

Qualitative analysis

No significant difference was found across the five anatomical levels within each dataset for each parameter assessed; hence, the multilevel information was summated for comparison between protocols (Figure 5.6).

Axial and coronal LD-MBIR images were significantly superior to LD-ASIR images for all qualitative parameters assessed ($p<0.0001$ for all comparisons). Diagnostic acceptability scores on lung windows and depiction of bronchovascular structures within 2cm of the pleural margin were found to be acceptable for axial LD-MBIR images (median 3, range 1-4; median 3, range 1-5, respectively) and highly acceptable for coronal LD-MBIR images (median 4, range 2-5 for both) with coronal images being significantly superior ($p<0.0001$ for both comparisons). LD-ASIR images were minimally acceptable for both parameters (median 2, range 1-3 for both)(Figure 5.7).

Image noise in the mediastinum was minimally acceptable for both axial and coronal LD-MBIR images (median 2, range 1 to 3 for both) and unacceptable for LD-ASIR images (median 1, range 1-3). Diagnostic acceptability in the mediastinum was also minimally acceptable for both axial and coronal LD-MBIR images (median 2, range 1 to 3 for both) and unacceptable for LD-ASIR images (median 1, range 1-2).

Streak artefact interfering with image interpretation was observed more often in the LD-ASIR images (median 3, range 2-3) than the LD-MBIR images ($p<0.0001$). Streak artefact was present on axial and coronal LD-MBIR images but it did not

interfere with image interpretation (median 2, range 1-3 for both). No significant difference was observed in streak artefact between axial and coronal reformats. Streak artefact was greatest at the level of the lung apices for all reconstructions.

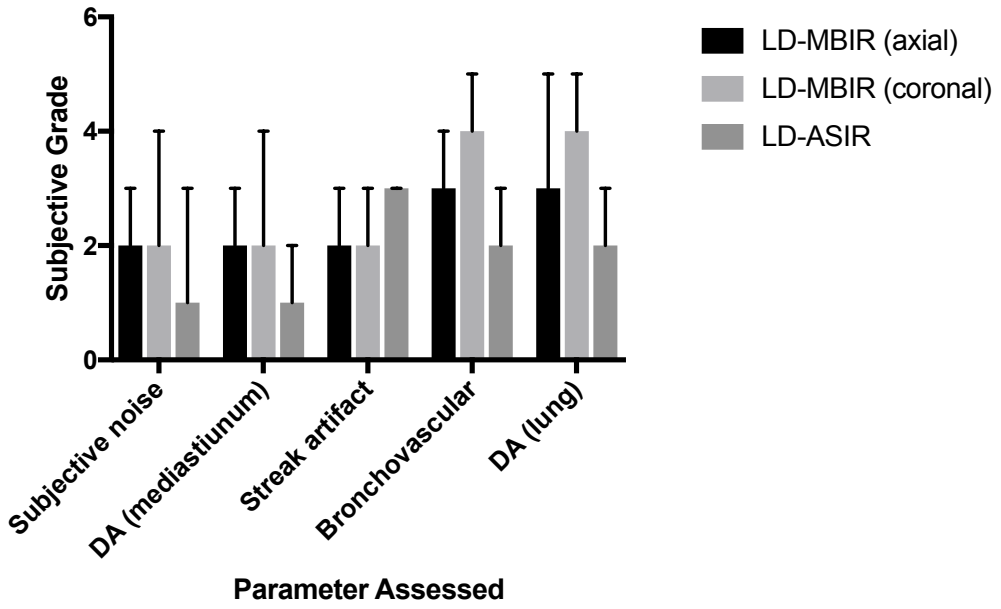

Figure 5.6 Comparison of subjective image quality parameters between axial and coronal LD-MBIR and LD-ASIR datasets. Data are plotted as median and range.

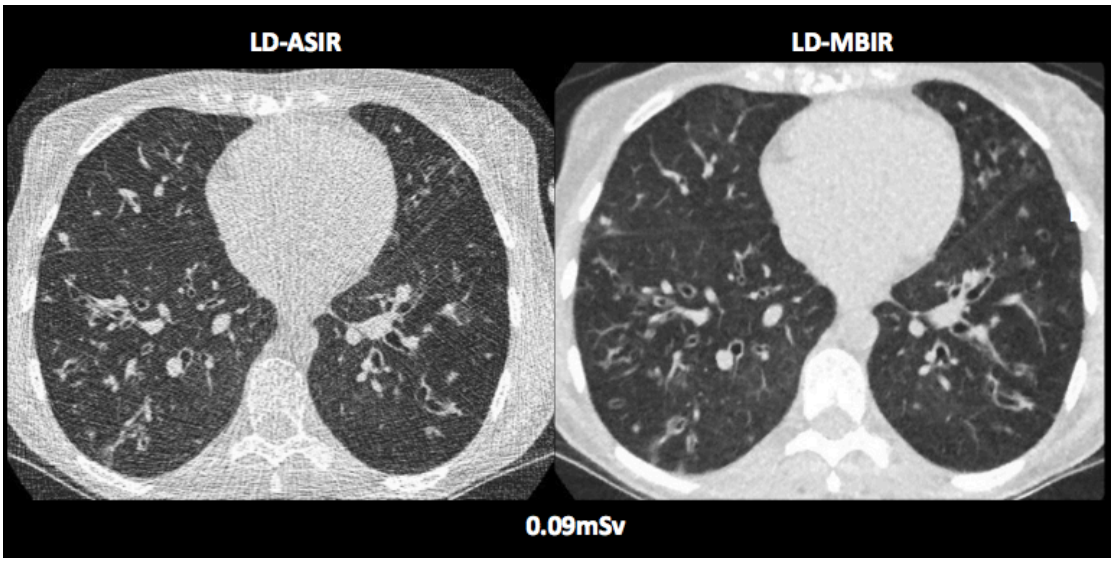

Figure 5.7 Representative LD-ASIR and LD-MBIR axial CT images acquired in a 22-year-old female patient with cystic fibrosis at the level of the maximum cardiac diameter illustrating the noise reducing capabilities of MBIR (effective dose 0.09mSv). Diagnostic acceptability and depiction of bronchovascular structures with 2 cm of the pleural margin were considered acceptable for the LD-MBIR image (score of 3) and minimally acceptable (score of 2) for the LD-ASIR image.

Quantification of lung disease

Disease severity was assessed on the 1-year 7-section ASIR studies and the 2-year LD-MBIR studies. Inter-rater variability measures were very good for total Bhalla score and all 9 morphological changes for both the 7-section ASIR studies and the LD-MBIR studies, with intraclass correlations of 0.881 (CI, 0.69 to 0.973, $p<0.001$) and 0.812 (CI, 0.439 to 0.937, $p<0.001$), for total Bhalla score, respectively; hence, mean reader scores were used to assess disease severity.

No significant change was observed in the mean Bhalla score between the 1-year and 2-year studies (11.03±2.7 vs. 10.9±3.99, p=0.84)(Figure 5.8). There was a moderate strength of association between Bhalla score and FEV_1 at 1-year (r=0.43, p=0.1) and 2-years (r=0.78, p=0.01).

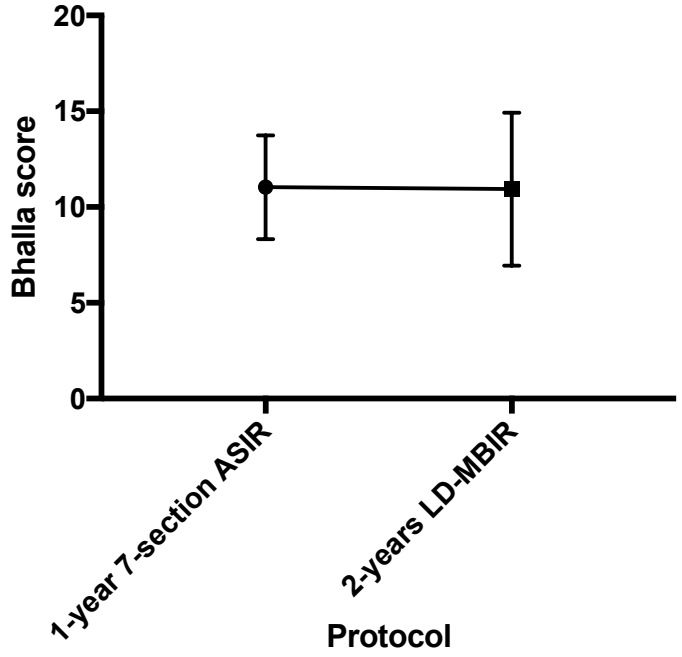

Figure 5.8 Change in mean Bhalla score over time between 1 and 2-years of treatment. Bhalla score was scored using the 7-section ASIR protocol and the 2-year Bhalla score was measured using the LD-MBIR protocol. Data are plotted as mean and standard deviation as indicated by whiskers.

Bronchiectasis was the most severe and consistent lung abnormality identified at low-dose CT (Table 5.3). All patients had bronchiectasis and it was rated as mild, moderate and severe in 22% (n=4), 26% (n=5), and 52% (n=10) at 1-year, and

as mild, moderate and severe in 47.4% (n=9), 10.5% (n=2), and 42.1% (n=8) at 2-years, respectively (Figure 5.9). 47.4% (n=9) of patients had bronchiectasis involving more than 9 bronchopulmonary segments and 42.1% (n=8) had bronchiectasis involving between 6 and 9 bronchopulmonary segments with no significant interval change between studies.

A single patient had between 1 and 5 sacculations at 1-year, with 22% (n=4) having between 1 and 5 sacculations and 26% (n=5) having between 6 and 9 sacculations at 2-years (Figure 5.10). Air trapping was graded as mild in 47.4% (n=9) and moderate in 23% (n=3) of patients at 1-year. No air trapping was identified on any of the 2-year inspiratory-phase only LD-MBIR studies. Subsegmental consolidation or collapse was present in 23% (n=3) of patients at 1-year and 47.4% (n=9) of patients at 2-years. Lobar consolidation was present in 10.5% (n=2) of patients at 1-year and 2-years. There was a significant decrease in the severity of bronchiectasis and peribronchial thickening at 2-years compared to the 1-year studies, with a significant increase in the number of cases with sacculations and subsegmental consolidation or collapse.

Lung abnormality	*1-year*	*2-years*
Bhalla score	11.03±2.7	10.9±3.99
Bronchiectasis	2.3±0.82	1.9±0.97*
Peribronchial thickening	1.3±0.89	0.58±0.90**
Extent of bronchiectasis	2.7±0.58	2.7±0.68
Extent of mucus plugging	1.5±1.17	1.5±0.90

Sacculations or abscesses	0.05±0.23	0.74±0.87**
Generations of bronchial divisions	2.5±0.90	2.3±0.82
Bullae	0.26±0.65	0.11±0.32
Emphysema	0.79±0.71	0
Collapse or consolidation	0.37±0.68	0.68±0.67*

Table 5.3 Change in qualitative scores of disease severity (Bhalla score) between the 1-year and 2-year CT studies. Data are expressed as mean±SD. * denotes the degree of statistical significant change between the studies.

Digital ray sum radiographs

Digital ray sum radiographs were generated for each LD-MBIR study and compared to the most recent chest radiograph (mean time 3.4±2.1 months). Inter-rater variability measures were strong for total qualitative score for both the digital ray sum (ICC 0.817,CI, 0.74 to 0.871, p<0.001) and chest radiographs (ICC 0.81, CI, 0.717 to 0.857, p<0.001); hence, mean rater scores were used for comparison. Both digital ray sum and chest radiograph images had acceptable to highly scores qualitative scores for all parameters assessed. Depiction of pulmonary vascular structures was significantly superior for chest radiographs (median 2, range 2-3 vs. median 3, range 2-3, p<0.0001). All other comparisons were non-significant.

There was moderate agreement between raters on both the ray sum and chest radiographs for the detection of consolidation (k=0.526, p=0.011; k=0.561, p=0.015), ground-glass opacities (k=0.556, p=0.09; k=0.621, p=0.02), atelectasis (k=0.471, p=0.43; k=0.478, p=0.17), volume loss (k=0.53, p=0.814; k=0.457,

p=0.08), and scarring (k=0.723, p=0.002; k=0.482, p=0.15). There was fair to poor agreement for the detection of mucus plugging, bronchiectasis, and cavitation. No patient had a pleural effusion or pneumothorax.

Comparisons between digital ray sum and chest radiograph images for rater 1 showed perfect agreement for ground-glass opacities (k=1, p<0.001) and bronchiectasis (k=1, p<0.001), very good agreement for scarring (k=0.852, p<0.001), and moderate agreement for consolidation (k=0.525, p=0.011), atelectasis (k=0.620, p=0.004), cavitation (k=0.609, p<=0.02), mucus plugging (k=0.491, p=0.16), and volume loss (k=0.471, p=0.43).

Comparisons between digital ray sum and chest radiograph images for rater 2 showed perfect agreement for atelectasis (k=1, p<0.001), very good agreement for volume loss (k=0.852, p<0.001) and scarring (k=0.87, p=0.03), and moderate agreement for ground-glass opacities (k=0.491, p=0.16) and cavitation (k=0.437, p=0.63). There was fair agreement for consolidation (k=0.341, p=0.138), mucus plugging (k=0.367, p=0.099), and bronchiectasis (k=0.217, p=0.63).

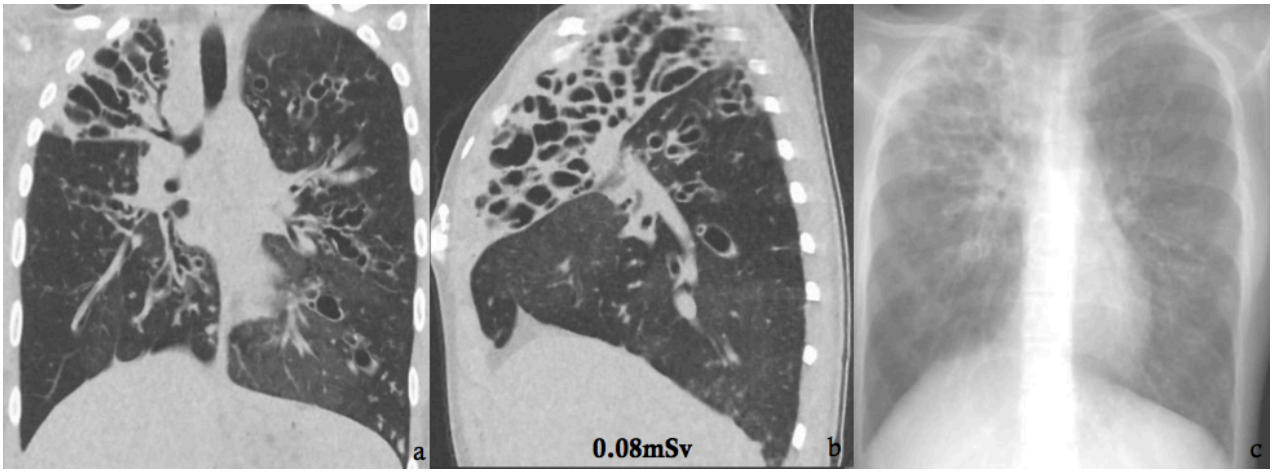

Figure 5.9 Representative coronal (a) and sagittal (b) CT images with a digital ray sum chest radiograph (e) acquired in 20-year-old male patient with cystic fibrosis at 24 months of treatment with Ivacaftor using the volumetric low-dose MBIR protocol (effective dose 0.08mSv). There is severe bronchiectasis affecting more than nine bronchopulmonary segments and sixth-generation bronchial divisions. Bronchial wall thickening was moderate with mucous plugging affected more than nine bronchopulmonary segments. There were fewer than five sacculations, fewer than three bullae, and no lung consolidation or collapse. The Bhalla score was 16.

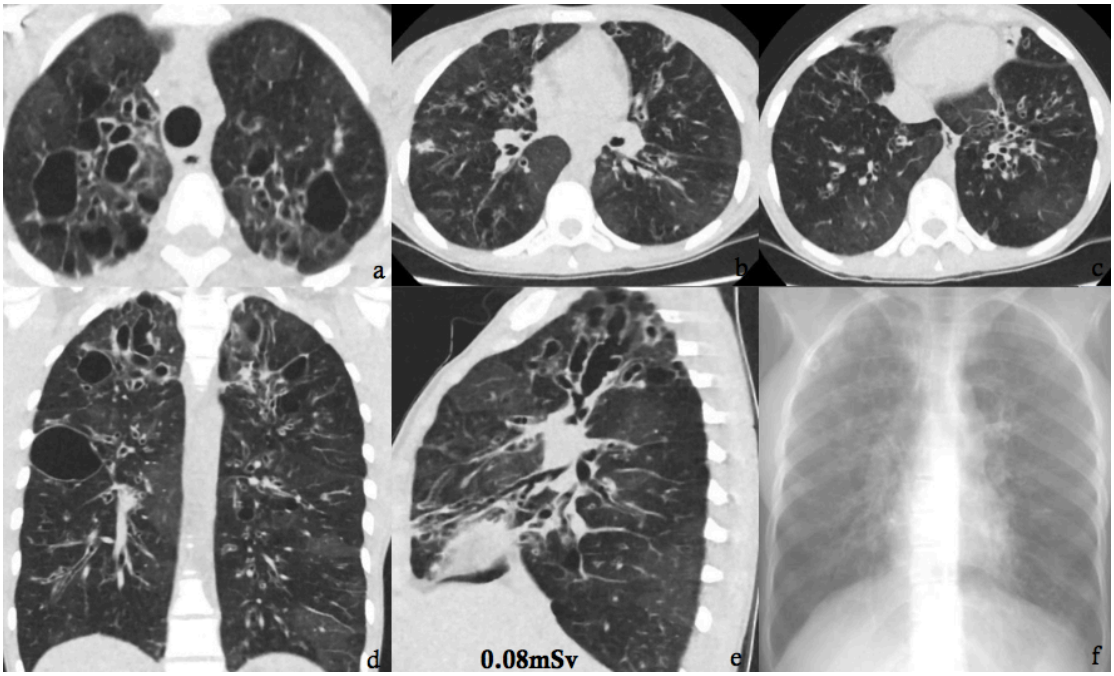

Figure 5.10 Representative multiplanar CT images (a-e) with a digital ray sum radiograph (f) acquired in 26-year-old male patient with cystic fibrosis at 24 months of treatment with Ivacaftor using the volumetric low-dose MBIR protocol (effective dose 0.08mSv). There is moderate bronchiectasis affecting between six

and nine bronchopulmonary segments and sixth-generation bronchial divisions. Bronchial wall thickening was mild with mucous plugging affected between six and nine bronchopulmonary segments. There were between six and nine sacculations, fewer than three bullae, and segmental lung consolidation. The Bhalla score was 15.

Discussion

Respiratory disease accounts for over 80% of deaths in patients with CF.[143] Consequently, there has been a six-fold increase in the use of CT in CF to monitor pulmonary disease progression and complications over the past fifteen years.[7] It is estimated that patients with CF will undergo an average of 3.2 chest CT scans during their lifetime resulting in CEDs far in excess of the general population.[180] The mean age of the first CT scan has also fallen, from 20 years for patients born before 1980 to 1.9 years for patients born after 1997.[164]

Chest CT performed at such a young age can readily detect the earliest radiological manifestation of CF; mucus plugging. Chest CT has also been shown to be more sensitive for the detection of lung function deterioration and superior for the quantification of bronchiectasis compared to both chest radiography and PFTs.[147, 148, 181] CT can thus provide valuable information regarding presence and type of complication, and estimation of disease severity to inform management decisions such as consideration of patients for lung transplantation, as well as predicting future morbidity and guiding prognosis.[163]

The major limitation to the use of sequential chest CT to monitor pulmonary disease progression in patients with CF is the cumulative radiation dose

incurred.[7] Physicians must remain cognizant of the risk of radiation-induced carcinogenesis, and given the improving life expectancy among CF patients,[182] and the increasing use of CT to monitor pulmonary disease, it is imperative to keep radiation exposure from chest CT as low as reasonably possible without compromising diagnostic performance. There is currently major industry drive to develop and implement new dose reduction technologies in CT. Chest CT is well suited to the development of dose optimization protocols with the high inherent contrast and low radiation absorption of the lung.[183]

Many dose reduction strategies utilized to date have resulted in increased levels of image noise and reduced image quality, which has a negative impact on the ability of CT images to detect and characterize pathology. Advanced IR algorithms that serve to improve image quality through noise reduction and spatial resolution improvements, thus facilitating the generation of diagnostic quality images at reduced radiation doses, have been studied in recent years. Hybrid IR systems have been well validated in chest CT achieving dose reductions in the order of 46% to 80% without compromising image quality.[184,185]

MBIR has enabled even greater dose reductions than hybrid IR[186] with one preliminary study reporting the acquisition of diagnostic quality chest CT images at a dose approaching that of a PA and lateral chest radiograph (0.16 ± 0.006mSv).[162] We achieved an even greater dose reduction with our protocol that enabled the acquisition of a diagnostically acceptable, full-volume, low-dose CT thorax at a dose equivalent to a PA and lateral chest radiograph (0.09±0.01mSv). Performance of ASIR at this dose level was suboptimal with LD-

ASIR images having significantly higher levels of image noise and inferior qualitative scores than LD-MBIR images.

We recognize the limitations of our study. A concurrent conventional dose CT scan was not performed as a reference 'gold standard'. However, we believed that an additional conventional dose study was not ethically justifiable as our aim was to develop a low-dose protocol to replace chest radiography for the purpose of routine pulmonary disease assessment, and as all patients were clinically stable, no indication existed to perform a conventional dose study. Comparison of disease severity scores may not be entirely comparable as the limited section protocol may have lead to clinically important disease being missed. In addition, expiratory phase imaging was omitted from the LD MBIR protocol and a comparison could not be made with the expiratory sections of the 7-section ASIR studies. Furthermore, our patient cohort was small which limits the strength of the conclusions drawn.

Imaging of the mediastinum and upper abdomen was suboptimal with both protocols. However, assessment of the mediastinum is of less concern in patients with CF where evaluation of pulmonary disease is the primary intention. This is therefore an acceptable limitation in our opinion, given the substantial reduction in radiation dose achieved.

MBIR currently requires a prolonged processing time of approximately 40 minutes, which has limited its widespread introduction into clinical practice, especially in the emergency setting. However, this is unlikely to be prohibitive to the routine assessment of pulmonary disease in patients with CF, particularly in stable patients in an outpatient setting.

The findings of our study strengthen the case for the use of low-dose CT in patients with CF with some experts suggesting that surveillance CT should be performed biannually.[187] Our low-dose protocol could also potentially have a role in screening for non-CF bronchiectasis. Low-dose CT in this setting may detect mild bronchiectasis and prevent patients with early bronchiectasis and a normal chest radiograph being misdiagnosed as having asthma.[188] Thus in the assessment of non-CF patients presenting with suspected bronchiectasis, consideration should be given to the replacement of chest radiograph with low-dose chest CT reconstructed with MBIR.

In conclusion, the use of MBIR with a volumetric low-dose protocol enabled the acquisition of diagnostic quality chest CT images at a dose equivalent to that of a PA and lateral chest radiograph.

Chapter VI

Conclusion

Quantifying the risk of detrimental effects from radiation exposure through medical imaging is difficult and remains an area of debate. While it is generally accepted that exposure to high doses of ionizing radiation places an individual at an exponentially increased risk of developing cancer in their lifetime, the risk of cancer induction associated with the relatively low levels of radiation exposure incurred during diagnostic imaging remains uncertain.

Many authors have questioned the applicability of the traditional *linear no-threshold model* to low-dose exposures, proposing instead a *threshold-model* of cancer risk with the risk increasing exponentially with cumulative radiation doses in excess of 75 to 100mSv. While this threshold is unlikely to be encountered in the majority of patients undergoing diagnostic imaging, acceptance of the *threshold-model* does not negate a physician's responsibility to keep patient radiation exposures as low as reasonably practicable and to have adequate justification for exposure. This is especially true in at-risk groups such as young patients and patients with chronic medical conditions at risk for high cumulative radiation doses from repeated diagnostic CT imaging. CT is currently the greatest contributor to medical radiation population dose; hence strategies targeting dose reduction in CT are critical in limiting high cumulative radiation doses in patients. The European Society of Radiology and US Summit on Management of Radiation dose in CT have set 1mSv or less as a target effective dose when performing CT imaging of any body part[189, 190]

As outlined in chapter I, there are several dose optimization strategies that may be employed including judicious protocoling to minimize the number of phases acquired, use of clinical decision support tools, limiting the scan range, ensuring correct patient positioning in the gantry, noise reduction filters, and automated tube current and voltage selection techniques. Ultimately, strategies that work to eliminating unnecessary examinations and phases will likely have the greatest effect on lowering overall population CT radiation dose.

IR algorithms are one of the most significant developments in CT dose optimization in recent years. Hybrid IR uses a distinct percentage or 'blend' of both IR and FBP and is not too computationally intense or time-consuming to perform on today's CT computer systems. Pure IR is a newer IR technique that also models system optics to create the final image. The process is mathematically more complex but reportedly more accurate than hybrid IR. MBIR, the focus of this thesis, is one such algorithm. As CT manufacturers adopt different algorithmic approaches to pure IR and the exact methodology is proprietary and generally unknown, careful clinical validation of MBIR as a dose reduction technique is essential prior to its widespread introduction into clinical practice.

We performed a preliminary technical and anthropomorphic phantom and cadaveric study to examine the performance of MBIR compared to FBP and hybrid IR with regard to noise reduction and image quality over a range of radiation dose levels. We found MBIR to have significantly lower levels of objective image noise in all CT abdominal data sets and almost all CT thorax data sets compared to FBP in the torso phantom. The greatest noise reduction was seen at the ultra-low-dose level with noise reductions of 74% and 86.9% for

thorax and abdominal data sets, respectively. In addition, MBIR significantly outperformed hybrid IR in terms of noise reduction at all dose levels in the abdomen and at the two lowest dose levels in the thorax. A similar finding was observed for subjective image noise and quality assessment with the greatest mean difference compared to FBP and hybrid IR also being observed for both thorax and abdominal data sets at the lowest radiation dose level.

With regard to the cadaveric abdominal CT scans, MBIR datasets had significantly lower levels of objective image noise compared to both FBP and hybrid IR at both conventional and low-dose levels with the greatest noise reduction observed at the lowest radiation dose level. A similar finding was observed for the qualitative indices with the greatest improvement in image quality also observed at the lowest dose level.

Compared to conventional dose images reconstructed with hybrid IR, MBIR facilitated the acquisition of images with lower levels of image noise, higher diagnostic quality and contrast resolution scores, and comparable subjective image noise and streak artefact scores, while enabling a 62% dose reduction. Given these findings, we concluded that the greatest utility of MBIR is in the performance of ultra-low-dose CT, as at this level its' noise reducing capabilities can be maximized.

We subsequently performed a clinical study to assess if a low-dose carotid CTA protocol performed with MBIR has comparable diagnostic accuracy to a conventional dose protocol. We found both protocols to be comparable in terms of image quality and diagnostic interpretation, despite a significant reduction in mean effective dose from 3.7mSv (range 3.04-6.31mSv) to 1.8mSv (range 1.51-2.22mSv), representing a mean effective dose reduction of 50%.

The low-dose MBIR protocol correctly identified all 6 occluded internal carotid arteries with excellent agreement with the conventional dose studies for stenosis grading accuracy in the non-occluded internal carotid arteries. A single stenosis grading was underestimated from '50-69%' to '<50%' in one patient. On review, this was a patient with a 51% degree of ICA stenosis and in patients with a borderline stenosis grading as assessed with the low-dose protocol, we recommend consideration of performance of the conventional dose protocol if patient management would be altered. In addition, unlike a prior study assessing low-dose CT carotid angiography that reported poor image quality at the level of the common carotid artery due to streak artefact, we found superior image quality and streak artefact scores at this level and do not report any diagnostic limitation.

Chapter IV outlines a prospective feasibility study assessing the utility of a modified low-dose abdominopelvic CT protocol using MBIR in patients presenting to the emergency department with acute abdominal symptoms.

We acquired the low-dose MBIR studies at a mean ED of 2.38±1.78mSv, which equates to a radiation dose reduction of 74.7% compared to a conventional dose protocol using hybrid IR, without compromising diagnostic accuracy. Previous groups performing low-dose abdominopelvic CT have employed a fixed tube-time-current product technique, which ensures a more predictable radiation exposure, regardless of body habitus.[136, 137]

The use of ATCM in our study, which balances radiation dose against image quality, resulted in higher radiation exposures with increasing BMI. As 56% of our patients had a BMI of ≥25 kg/m^2, the overall mean radiation exposure exceeded the target peri-millisievert range. However, in patients with a BMI of

<25 kg/m^2, diagnostically acceptable low-dose images were acquired in the target peri-millisievert (1.16±0.76mSv) range, a level which is not very different to typical exposures of 0.7mSv associated with plain abdominal radiography. This represents a mean ED dose reduction of 87.6% for patients with a BMI of <25 kg/m^2, compared to conventional dose protocols. A major strength of this study was the inclusion of a wide range of pathologies that may present with acute abdominal pain, which increases the generalizability of our study results. We are currently conducting a prospective feasibility study using the low-dose MBIR protocol alone in selected patients presenting to the emergency department with acute abdominal symptoms targeting the submillisievert range. We subsequently utilized MBIR to acquire diagnostically acceptable, volumetric, low-dose chest CT studies at a dose equivalent to that of a PA and lateral chest radiograph (mean ED 0.09±0.01mSv). Initial efforts at our institution to optimize dose from chest CT in patients with CF involved the development of a non-contiguous thin-section protocol performed at a mean effective dose of 0.14±0.05mSv in pediatric patients.[77] Although excellent correlation was observed between disease severity scores and chest radiography scores in this study, limiting the number of slices to reduce dose may potentially impact accurate assessment of true disease severity. Our volumetric protocol enabled reliable calculation of CT disease severity scores, which was used to monitor disease progression in patients with CF. Early and sustained improvements in CT disease severity scores as assessed with our ultra-low-dose technique have recently been shown to parallel improvements in respiratory symptoms, circulating inflammatory markers, and favourable changes in the lung microbiota.[191] This ultra-low-dose protocol is currently employed at our

institution for the surveillance of pulmonary disease in all patients with CF, as well the detection and monitoring of lung disease in young patients with suspected and known non-CF bronchiectasis in lieu of chest radiography.

The advantages of our novel low-dose protocol over the 7-section low-dose protocol include acquisition of a full volume of data allowing thin contiguous cuts. Thus the airways can be systematically evaluated throughout their course from centrally to peripherally. Another major advantage is the ability to generate high quality multiplanar and 3D reconstructions. In our experience, coronal reconstructions, in particular, are extremely useful in assessing the severity and location of parenchymal and airway complications of CF. We believe that the additional ability to generate a digital ray sum radiographs is also valuable in comparing the location and severity of CF complications with earlier chest radiographs, when prior CT scans are not available for review.

There are a number of limitations to the MBIR technology that must be acknowledged. A significant capital investment of approximately 250,000 to 300,000 euros is required to install the technology. This may not be economically feasible at many centers not employing MBIR as their primary reconstruction algorithm. High computational load with a lengthy reconstruction time of approximately 30 minutes remains one of the greatest challenges for pure IR, potentially prohibiting its use in certain clinical settings. However, this is unlikely to be prohibitive for most patients and it is likely that further advances in the technology will shorten the processing time required expanding its applicability to all settings, including trauma. Other strategies such as eliminating oral contrast or administration of oral contrast over a shorter time period would also expedite scanning but the impact of these strategies on the

diagnostic accuracy of low-dose abdominopelvic CT has yet to be investigated. MBIR-reconstructed images have a unique 'waxy' and 'smooth' appearance compared to FBP and hybrid IR-reconstructed images. However, the readers at our institution found that they quickly become accustomed to the texture difference.

There are other pure IR algorithms commercially available from other venders to which our findings may not be entirely applicable and independent validation of these techniques may be required. Direct comparisons between pure IR algorithms offered by different vendors is generally difficult as image acquisition and reconstruction are fully integrated and vendor specific on most CT systems. Thus data cannot be reconstructed with a different vendors' algorithm. A phantom study comparing MBIR with IMR (Philips Healthcare, Eindhoven, The Netherlands) indicates a marginal superiority of IMR with regard to objective noise reduction.[192] We did not assess the utility of MBIR in cone-beam CT but prior studies report superior noise reduction and improved image quality when MBIR is used in this setting.[193] Its utility in dose reduction has not yet been assessed but it has promising potential.

The split-dose technique adopted in this thesis was a novel method of providing simultaneously low and conventional dose imaging enabling patients to act as their own controls while ensuring patient safety. This technique enabled to us to achieve a dose reduction of 75% in abdominopelvic CT, a dose reduction in keeping with prior studies.[73, 119, 120] There are limited reports of dose reduction with MBIR beyond the 80% range in the abdomen with one study reporting images of insufficient diagnostic quality.[194] Given the average to above average image quality scores and satisfactory comparable diagnostic performance of our

low-dose protocol, further dose reductions without compromising diagnostic performance may be feasible in future studies. Careful consideration needs to be given to the potential detrimental effects of dose reduction beyond the 80% range and further studies are required.

The benefits of pure IR to the staff of diagnostic radiology departments also needs to be considered. While the annual occupational exposure incurred by CT scan workers is relatively less than those working other areas such as fluoroscopy[195], pure IR is likely to further reduce this exposure, particularly for staff involved in the performance of CT-guided procedures.

This thesis examined the potential role of MBIR in the development of low-dose CT carotid angiography, chest and abdominopelvic protocols. MBIR facilitated the acquisition of low-dose CT images at radiation doses approaching the one millisievert target suggested by the ESR and US Summit on Management of Radiation Dose in CT. Chest CT was performed at a radiation dose equivalent to that of a PA and lateral chest radiograph while abdominopelvic CT was performed in the peri- and submillisievert range in patients of normal and low BMI, respectively. Dose reduction to the submillisievert range for patients with an elevated BMI remains a challenge.

The current era is extremely exciting in terms of radiation dose optimization in CT. This thesis is a demonstration of the potential for substantial reductions in radiation exposure, when the benefits of iterative reconstruction are combined with automated tube current modulation and other CT scanner technologies. The combination of all these hardware and software developments is now seeing major benefits for the patient and moving beyond the narrow aim of radiation exposure reduction to a complete change in practice, towards replacement of

conventional radiography with low-dose CT, without any penalty for the patient in terms of radiation exposure.

Bibliography

[1] Mettler FA Jr, Wiest PW, Locken JA, Kelsey CA. CT scanning: patterns of use and

[2] Radiation Doses received by the Irish Population, 2014. Radiological Protection Institute of Ireland.

[3] Friedberg W, Copeland K, Duke FE, O'Brien K 3rd, Darden EB Jr. Radiation exposure during air travel: Guidance provided by the FAA for air carrier crews. *Health Phys* 79(5):591–595; 2000.

[4] Committee to assess health risks from exposure to low levels of ionizing radiation NRC: BEIR VII Phase 2 (2006): Health Risks from Exposure to Low Levels of Ionizing Radiation. Washington DC, National Academies Press, 2006. NCRP Report No. 160, Ionizing Radiation Exposure of the Population of the United States (2009). National Council on Radiation Protection and Measurements.

[5] Smith-Bindman R, Miglioretti DL, Johnson E, et al. Use of Diagnostic Imaging Studies and Associated Radiation Exposure for Patients Enrolled in Large Integrated Health Care Systems, 1996-2010. *JAMA.* 2012;307(22):2400-2409.

[6] Brenner DJ, Hall EJ. Computed Tomography — An Increasing Source of Radiation Exposure. *N Engl J Med* 2007;357(22):2277–84.

[7] IMV 2006 CT Market Summary Report. Des Plains, IL: IMV Medical Information Division, 2006.

[8] Schauer DA, Linton OW. National Council on Radiation Protection and Measurements report shows substantial medical exposure increase. *Radiology* 2009;253(2):293–6.

[9] O'Connell OJ, McWilliams S, McGarrigle A, et al. Radiologic imaging in cystic fibrosis: cumulative effective dose and changing trends over 2 decades.

Chest. 2012 Jun;141(6):1575-83.

[10] Desmond AN, O'Regan K, Curran C, et al. Crohn's disease: factors associated with exposure to high levels of diagnostic radiation. *Gut.* 2008 Nov;57(11):1524-9.

[11] Coyle J, Kinsella S, McCarthy S, et al. Cumulative ionizing radiation exposure in patients with end stage kidney disease: a 6-year retrospective analysis. *Abdom Imaging.* 2012 Aug;37(4):632-8.

[12] Sullivan CJ, Murphy KP, McLaughlin PD, et al. Radiation exposure from diagnostic imaging in young patients with testicular cancer. *Eur Radiol.* 2015 Apr;25(4):1005-13.

[13] Fazel R, Krumholz HM, Wang Y, et al. Exposure to Low-Dose Ionizing Radiation from Medical Imaging Procedures. *N Engl J Med* 2009;361(9):849–57.

[14] Mettler FA Jr, Bhargavan M, Faulkner K, et al. Radiologic and nuclear medicine studies in the United States and worldwide: frequency, radiation dose, and comparison with other radiation sources--1950-2007. Radiology 2009;253(2):520–31.

[15] Rehani MM, Frush DP, Berris T, et al. Patient radiation exposure tracking: worldwide programs and needs - results from the first IAEA survey. *Eur J Radiol* 2012 Oct;81(10):e968-76.

[16] Nakashima M, Kondo H, Miura S, et al. Incidence of multiple primary cancers in Nagasaki atomic bomb survivors: association with radiation exposure. *Cancer Sci* 2008; 99: 87-92.

[17] Pierce DA, Preston DL. Radiation-related cancer risks at low doses among atomic bomb survivors. *Radiat Res* 2000; 154: 178-86.

[18] Cardis E, Vrijheid M, Blettner M, et al. Risk of cancer after low doses of ionizing radiation: retrospective cohort study in 15 countries. *BMJ* 2005; 331: 77.

[19] Berrington de González A, Mahesh M, Kim K-P, et al. Projected cancer risks from computed tomographic scans performed in the United States in 2007. Arch Intern Med 2009;169(22):2071–7.

[20] Andrieu N, Easton DF, Chang-Claude J, et al. Effect of chest X-rays on the risk of breast cancer among BRCA1/2 mutation carriers in the international BRCA1/2 carrier cohort study: a report from the EMBRACE, GENEPSO, GEO-HEBON, and IBCCS Collaborators' Group. *J Clin Oncol.* 2006 Jul 20;24(21):3361-6.

[21] Ronckers CM, Erdmann CA, Land CE. Radiation and breast cancer: a review of current evidence. *Breast Cancer Res.* 2005;7(1):21-32.

[22] Cardis E, Vrijheid M, Blettner M, et al. The 15-Country Collaborative Study of Cancer Risk among Radiation Workers in the Nuclear Industry: estimates of radiation-related cancer risks. *Radiat Res.* 2007 Apr;167(4):396-416.

[23] Hendee WR, O'Connor MK. Radiation risks of medical imaging: separating fact from fantasy. *Radiology* 2012; 264:312–321.

[24] Doss M. Linear No-Threshold Model VS. Radiation Hormesis. *Dose-Response* 2013;11(4):495–512.

[25] Tubiana M, Feinendegen LE, Yang C, Kaminski JM. The linear no-threshold relationship is inconsistent with radiation biologic and experimental data. Radiology 2009; 251:13–22

[26] Preston DL, Ron E, Tokuoka S, et al. Solid cancer incidence in atomic bomb survivors: 1958-1998. *Radiat Res* 2007;168(1):1–64.

[27] Health Physics Society. Position statement of Health Physics Society. Radiation risk in perspective. [Internet]. Available from:http://hps.org/documents/radiationrisk.pdf

[28] Brenner DJ, Elliston CD, Hall EJ, et al. Estimated risks of radiation-induced fatal cancer from pediatric CT. *American Journal of Roentgenology,* 2001; 176: 289–296.

[29] Brenner DJ, Doll R, Goodhead DT, et al. Cancer risks attributable to low doses of ionizing radiation: Assessing what we really know. *Proc Natl Acad Sci* 2003;100(24):13761–6.

[30] Pearse M, Salotti J, Little M, et al. Radiation exposure from CT scans in childhood and subsequent risk of leukaemia and brain tumours: a retrospective cohort study. *The Lancet* 2012;380(9840):499–505.

[31] Mathews JD, Forsythe AV, Brady Z, et al. Cancer risk in 680,000 people exposed to computed tomography scans in childhood or adolescence: data linkage study of 11 million Australians. *BMJ* 2013;346:f2360.

[32] Coren ME, Ng V, Rubens M, Rosenthal M, Bush A. The value of ultrafast computed tomography in the investigation of pediatric chest disease. *Pediatr Pulmonol* 1998;26(6):389–95.

[33] Goldberg-Stein S, Liu B, Hahn PF, Lee SI. Body CT during pregnancy: utilization trends, examination indications, and fetal radiation doses. *AJR Am J Roentgenol.* 2011 Jan;196(1):146-51.

[34] Mayo-Smith WW, Hara AK, Mahesh M, Sahani DV, Pavlicek W. How I do it: managing radiation dose in CT. *Radiology.* 2014 Dec;273(3):657-72.

[35] ICRP Publ. 103: The 2007 Recommendations of the International Commission on Radiological Protection.

[36] Huda W, Magill D, He W. CT effective dose per dose length product using ICRP 103 weighting factors. *Med Phys.* 2011 Mar;38(3):1261–5.

[37] Huda W, Ogden KM, Khorasani MR. Converting dose-length product to effective dose at CT*. Radiology.* 2008 Sep;248(3):995–1003.

[38] Boone J, Strauss K, Cody D et al. Size-specific dose estimates (SSDE) in pediatric and adult body CT examinations. Report of AAPM Task Group 204. College Park: American Association of Physicists in Medicine, 2011.

[39] McCollough CH, Leng S, Yu L, Cody DD, Boone JM, McNitt-Gray MF. CT dose index and patient dose: they are not the same thing. *Radiology* 2011 May;259(2):311-6. doi: 10.1148/radiol.11101800.

[40] Christner JA, Braun NN, Jacobsen MC, Carter RE, Kofler JM, McCollough CH. Size-specific dose estimates for adult patients at CT of the torso. *Radiology* 2012 Dec;265(3):841-7.

[41] Chan VO, McDermott S, Buckley O, et al. The relationship of body mass index and abdominal fat on the radiation dose received during routine computed tomographic imaging of the abdomen and pelvis.Can Assoc Radiol J. 2012 Nov;63(4):260-6.

[42] Rosen MP, Sands DZ, Longmaid HE 3rd, Reynolds KF, Wagner M, Raptopoulos V. Impact of abdominal CT on the management of patients presenting to the emergency department with acute abdominal pain. *AJR Am J Roentgenol* 2000;174(5):1391–6.

[43] Rosen MP, Siewert B, Sands DZ, Bromberg R, Edlow J, Raptopoulos V. Value of abdominal CT in the emergency department for patients with abdominal pain. *Eur Radiol* 2003;13(2):418–24.

[44] McCollough CH. CT dose: how to measure, how to reduce. *Health Phys* 2008;95(5):508–17.

[45] Smith-Bindman R, Lipson J, Marcus R, et al. RAdiation dose associated with common computed tomography examinations and the associated lifetime attributable risk of cancer. *Arch Intern Med* 2009;169(22):2078–86.

[46] Kalra MK, Maher MM, Toth TL, Kamath RS, Halpern EF, Saini S. Radiation from "extra" images acquired with abdominal and/or pelvic CT: effect of automatic tube current modulation. *Radiology.* 2004 Aug;232(2):409–14.

[47] Toth T, Ge Z, Daly MP. The influence of patient centering on CT dose and image noise. *Med Phys.* 2007 Jul;34(7):3093-101.

[48] Habibzadeh MA, Ay MR, Asl ARK, et al. Impact of miscentering on patient dose and image noise in x-ray CT imaging: phantom and clinical studies. *Phys Med.* 2012 Jul;28(3):191–9.

[49] Kaasalainen T, Palmu K, Lampinen A, et al. Effect of vertical positioning on organ dose, image noise and contrast in pediatric chest CT--phantom study. *Pediatr Radiol.* 2013 Jun;43(6):673–84.

[50] Gudjonsdottir J, Svensson JR, Campling S, et al. Efficient use of automatic exposure control systems in computed tomography requires correct patient positioning. *Acta Radiol.* 2009 Nov;50(9):1035-41.

[51] Lifeng Yu, Xin Liu, Shuai Leng, et al. Radiation dose reduction in computed tomography: techniques and future perspective. *Imaging Med.* 2009 Oct; 1(1): 65–84.

[52] Kalra MK, Maher MM, Kamath RS, Horiuchi T, Toth TL, Halpern EF, et al. Sixteen-detector row CT of abdomen and pelvis: study for optimization of Z-axis modulation technique performed in 153 patients. *Radiology.* 2004 Oct;233(1):241–9.

[53] May MS, Kramer MR, Eller A, Wuest W, Scharf M, Brand M, et al. Automated tube voltage adaptation in head and neck computed tomography between 120 and 100 kV: effects on image quality and radiation dose. *Neuroradiology.* 2014 Sep;56(9):797–803.

[54] Yu L, Li H, Fletcher JG, McCollough CH. Automatic selection of tube potential for radiation dose reduction in CT: a general strategy. *Med Phys* 2010;37(1):234–43.

[55] Budoff MJ. Maximizing dose reductions with cardiac CT. *Int J Cardiovasc Imaging.* 2009 Aug; 25(Suppl 2): 279–287.

[56] McCollough CH, Primak AN, Braun N, Kofler J, Yu L, and Christner J. Strategies for Reducing Radiation Dose in CT. *Radiol Clin North Am*. 2009 Jan; 47(1): 27–40.

[57] Mendrik AM, Vonken E-J, Rutten A, Viergever MA, van Ginneken B. Noise reduction in computed tomography scans using 3-d anisotropic hybrid diffusion with continuous switch. *IEEE Trans Med Imaging* 2009;28(10):1585–94.

[58] Euler A, Heye T, Kekelidze M, Bongartz G, Szucs-Farkas Z, Sommer C, et al. Assessment of image quality and low-contrast detectability in abdominal CT of obese patients: comparison of a novel integrated circuit with a conventional

discrete circuit detector at different tube voltages. *Eur Radiol.* 2015 Mar;25(3):687–93.

[59] Hidajat N, Mäurer J, Schröder RJ, Wolf M, Vogl T, Felix R. Radiation exposure in spiral computed tomography. Dose distribution and dose reduction. *Invest Radiol* 1999;34(1):51–7.

[60] Kalra MK, Maher MM, Toth TL, et al. Strategies for CT radiation dose optimization. *Radiology.* 2004 Mar;230(3):619-28.

[61] O'Neill SB, Mc Laughlin PD, Crush L, O'Connor OJ, Mc Williams SR, Craig O, et al. A prospective feasibility study of sub-millisievert abdominopelvic CT using iterative reconstruction in Crohn's disease. *Eur Radiol.* 2013 Sep;23(9):2503–12.

[62] Padole A, Ali Khawaja RD, Kalra MK, Singh S. CT radiation dose and iterative reconstruction techniques. *AJR Am J Roentgenol.* 2015 Apr;204(4):W384-92.

[63] Kondratyev E, Karmazanovsky G. Low radiation dose 256-MDCT angiography of the carotid arteries: effect of hybrid iterative reconstruction technique on noise, artifacts, and image quality. *Eur J Radiol.* 2013 Dec;82(12):2233–9.

[64] Yamada Y, Jinzaki M, Hosokawa T, Tanami Y, Sugiura H, Abe T, et al. Dose reduction in chest CT: comparison of the adaptive iterative dose reduction 3D, adaptive iterative dose reduction, and filtered back projection reconstruction techniques. *Eur J Radiol.* 2012 Dec;81(12):4185–95.

[65] Funama Y, Taguchi K, Utsunomiya D, Oda S, Yanaga Y, Yamashita Y, et al. Combination of a low-tube-voltage technique with hybrid iterative reconstruction (iDose) algorithm at coronary computed tomographic angiography. *J Comput Assist Tomogr.* 2011 Jan;35(4):480–5.

[66] McLaughlin PD, Murphy KP, Hayes SA, Carey K, Sammon J, Crush L, et al. Non-contrast CT at comparable dose to an abdominal radiograph in patients with acute renal colic; impact of iterative reconstruction on image quality and diagnostic performance. *Insights Imaging.* 2014 Apr 7;5(2):217–30.

[67] Scheffel H, Stolzmann P, Schlett CL, et al. Coronary artery plaques: cardiac CT with model-based and adaptive-statistical iterative reconstruction technique. *Eur J Radiol.* 2012 Mar;81(3):e363-9

[68] Khawaja RDA, Singh S, Blake M, Harisinghani M, Choy G, Karosmangulu A, et al. Ultra-low dose abdominal MDCT: Using a knowledge-based Iterative Model Reconstruction technique for substantial dose reduction in a prospective clinical study. *Eur J Radiol.* 2015 Jan;84(1):2–10.

[69] Machida H, Takeuchi H, Tanaka I, Fukui R, Shen Y, Ueno E, et al. Improved delineation of arteries in the posterior fossa of the brain by model-based iterative reconstruction in volume-rendered 3D CT angiography. AJNR Am J *Neuroradiol.* 2013 May;34(5):971–5.

[70] Fuchs TA, Stehli J, Bull S, et al. Coronary computed tomography angiography with model-based iterative reconstruction using a radiation exposure similar to chest X-ray examination. *Eur Heart J.* 2014 May;35(17):1131-6.

[71] Mettler FA Jr, Thomadsen BR, Bhargavan M, et al. Medical radiation exposure in the U.S. in 2006: preliminary results. *Health Phys.* 2008 Nov;95(5):502-7.

[72] Allen BC, Baker ME, Einstein DM et al. Effect of altering automatic exposure control settings and quality reference mAs on radiation dose, image quality, and diagnostic efficacy in MDCT enterography of active inflammatory Crohn's disease. *AJR. American journal of roentgenology.* 2010;195(1):89–100.

[73] Ippolito D, Talei Franzesi C, Fior D, et al. Low kV settings CT angiography (CTA) with low dose contrast medium volume protocol in the assessment of thoracic and abdominal aorta disease: a feasibility study. *Br J Radiol.* 2015 May;88(1049):20140140.

[74] Rampinelli C, Origgi D, Vecchi V, et al. Ultra-low-dose CT with model-based iterative reconstruction (MBIR): detection of ground-glass nodules in an anthropomorphic phantom study. *Radiol Med.* 2015 Jul;120(7):611-7.

[75] Katsura M, Sato J, Akahane M, et al. Comparison of pure and hybrid iterative reconstruction techniques with conventional filtered back projection: image quality assessment in the cervicothoracic region. *Eur J Radiol.* 2013 Feb;82(2):356-60.

[76] Prakash P, Kalra MK, Kambadakone AK, et al. Reducing abdominal CT radiation dose with adaptive statistical iterative reconstruction technique. Invest Radiol. 2010 Apr;45(4):202-10.

[77] Patino M, Fuentes JM, Hayano K, et al. A quantitative comparison of noise reduction across five commercial (hybrid and model-based) iterative reconstruction techniques: an anthropomorphic phantom study. *AJR Am J Roentgenol.* 2015 Feb;204(2):W176-83.

[78] Yamamura J, Tornquist K, Buchert R, et al. Simulated low-dose computed tomography in oncological patients: a feasibility study. *J Comput Assist Tomogr.* 2010 Mar-Apr;34(2):302-8.

[79] Singh S, Kalra MK, Do S, et al. Comparison of hybrid and pure iterative reconstruction techniques with conventional filtered back projection: dose

reduction potential in the abdomen. *J Comput Assist Tomogr.* 2012 May-Jun;36(3):347-53.

[80] Murphy KP, Crush L, Twomey M, et al. Model-based iterative reconstruction in CT enterography. *AJR Am J Roentgenol.* 2015 Dec;205(6):1173-81.

[81] De Crop A, Smeets P, Van Hoof T, et al. Correlation of clinical and physical-technical image quality in chest CT: a human cadaver study applied on iterative reconstruction. *BMC Med Imaging.* 2015 Aug 19;15:32.

[82] Schramek GGR , Stoevesandt D, Reising A, Kielstein JT, Hiss M, Kielstein H. Imaging in anatomy: a comparison of imaging techniques in embalmed human cadavers. *BMC Med Educ*. 2013; 13: 143.

[83] Reed AB, Crafton C, Giglia JS, Hutto JD. Back to basics: use of fresh cadavers in vascular surgery training. *Surgery.* 2009 Oct;146(4):757-62; discussion 762-3.

[84] O'Connor OJ, Vandeleur M, McGarrigle AM, et al. Development of low-dose protocols for thin-section CT assessment of cystic fibrosis in pediatric patients. *Radiology.* 2010 Dec;257(3):820-9.

[85] Marin D, Nelson RC, Schindera ST, et al. Low-tube-voltage, high-tube-current multidetector abdominal CT: improved image quality and decreased radiation dose with adaptive statistical iterative reconstruction algorithm--initial clinical experience. *Radiology.* 2010 Jan;254(1):145-53.

[86] Schindera ST, Odedra D, Raza SA, et al. Iterative reconstruction algorithm for CT: can radiation dose be decreased while low-contrast detectability is preserved? *Radiology.* 2013 Nov;269(2):511-8.

[87] Bongartz G, Golding SJ, Jurik AG, et al (2000). European guidelines on quality criteria for computed tomography, EUR 16262. The European Commission's

Stidy group on development of Quality Criteria for Computed Tomography. Office for Official publications of the European Communities, Luxembourg.

[88] Bongartz G, Golding SJ, Jurik AG et al (2004). 2004 CT quality criteria. Office for Official Publications of the European Communities, Luxembourg.

[89] Singh S, Kalra MK, Hsieh J, et al. Abdominal CT: comparison of adaptive statistical iterative and filtered back projection reconstruction techniques. *Radiology.* 2010 Nov;257(2):373-83.

[90] Verdun FR, Denys A, Valley JF, et al. Detection of low-contrast objects: experimental comparison of single- and multi-detector row CT with a phantom. *Radiology.* 2002 May;223(2):426-31.

[91] Vardhanabhuti V, Ilyas S, Gutteridge C, et al. Comparison of image quality between filtered back-projection and the adaptive statistical and novel model-based iterative reconstruction techniques in abdominal CT for renal calculi. *Insights Imaging.* 2013 Oct; 4(5): 661–669.

[92] Deák Z, Grimm JM, Treitl M, et al. Filtered back projection, adaptive statistical iterative reconstruction, and a model-based iterative reconstruction in abdominal CT: an experimental clinical study. *Radiology.* 2013 Jan;266(1):197-206.

[93] Pickhardt PJ, Lubner MG, Kim DH, et al. Abdominal CT with model-based iterative reconstruction (MBIR): initial results of a prospective trial comparing ultralow-dose with standard-dose imaging. *AJR Am J Roentgenol.* 2012 Dec;199(6):1266-74.

[94] Katsura M, Matsuda I, Akahane M, et al. Model-based iterative reconstruction technique for radiation dose reduction in chest CT: comparison with the adaptive

statistical iterative reconstruction technique. *Eur Radiol.* 2012 Aug;22(8):1613-23.

[95] Neroladaki A, Botsikas D, Boudabbous S, et al. Computed tomography of the chest with model-based iterative reconstruction using a radiation exposure similar to chest X-ray examination: preliminary observations. *Eur Radiol.* 2013 Feb;23(2):360-6.

[96] Yu Z, Thibault JB, Bouman CA, et al. Fast model-based X-ray CT reconstruction using spatially nonhomogeneous ICD optimization. *IEEE Trans Image Process.* 2011 Jan;20(1):161-75.

[97] Yasaka K, Katsura M, Akahane M, Sato J, Matsuda I, Ohtomo K. Model-based iterative reconstruction for reduction of radiation dose in abdominopelvic CT: comparison to adaptive statistical iterative reconstruction. *Springerplus* 2013;2:209.

[98] Prakash P, Kalra MK, Digumarthy SR, et al. Radiation dose reduction with chest computed tomography using adaptive statistical iterative reconstruction technique: initial experience. *J Comput Assist Tomogr.* 2010 Jan;34(1):40-5.

[99] Ferguson GG, Eliasziw M, Barr HW, et al. The North American Symptomatic Carotid Endarterectomy Trial: surgical results in 1415 patients. *Stroke.* 1999;30(9):1751-8.

[100] Endarterectomy for asymptomatic carotid artery stenosis. Executive Committee for the Asymptomatic Carotid Atherosclerosis Study. *JAMA.* 1995;273(18):1421-8.

[101] Brott TG, Halperin JL, Abbara S, et al. ASA/ACCF/AHA/AANN /AANS/ACR/ASNR/CNS/ SAIP/SCAI/SIR/SNIS/SVM/SVS guideline on the

management of patients with extracranial carotid and vertebral artery disease: executive summary. A report of the American College of Cardiology Foundation/American Heart Association Task Force on Practice Guidelines, and the American Stroke Association, American Association of Neuroscience Nurses, American Association of Neurological Surgeons, American College of Radiology, American Society of Neuroradiology, Congress of Neurological Surgeons, Society of Atherosclerosis Imaging and Prevention, Society for Cardiovascular Angiography and Interventions, Society of Interventional Radiology, Society of NeuroInterventional Surgery, Society for Vascular Medicine, and Society for Vascular Surgery. Circulation. 2011 Jul 26;124(4):489-532.

[102] Bartlett ES, Walters TD, Symons SP, et al. Quantification of carotid stenosis on CT angiography. *AJNR Am J Neuroradiol.* 2006;27(1):13-9.

[103] Koelemay MJ, Nederkoorn PJ, Reitsma JB, et al. Systematic review of computed tomographic angiography for assessment of carotid artery disease. *Stroke.* 2004 ;35(10):2306-12.

[104] Van Gils MJ, Vukadinovic D, van Dijk AC, et al. Carotid atherosclerotic plaque progression and change in plaque composition over time: a 5-year follow-up study using serial CT angiography. *AJNR Am J Neuroradiol*. 2012;33(7):1267-73.

[105] International Commission on Radiological Protection. *Managing patient dose in computed tomography.* ICRP publication 87. Pergamon Press, Oxford;2000.

[106] Manninen AL, Isokangas JM, Karttunen A, et al. A comparison of radiation exposure between diagnostic CTA and DSA examinations of cerebral and cervicocerebral vessels. *AJNR Am J Neuroradiol.* 2012;33(11):2038-42.

[107] Mazonakis M, Tzedakis A, Damilakis J, et al. Thyroid dose from common head and neck CT examinations in children: is there an excess risk for thyroid cancer induction? *Eur Radiol.* 2007;17(5):1352-7.

[108] Yamauchi-Kawara C, Fujii K, Aoyama T, Yamauchi M, Koyama S. Radiation dose evaluation in multidetector-row CT imaging for acute stroke with an anthropomorphic phantom. *Br J Radiol.* 2010 Dec; 83(996): 1029–1041.

[109] Beitzke D, Wolf F, Edelhauser G, et al. Computed tomography angiography of the carotid arteries at low kV settings: a prospective randomised trial assessing radiation dose and diagnostic confidence. *Eur Radiol*. 2011;21(11):2434–44.

[110] Eller A, Wuest W, Kramer M, et al. Carotid CTA: radiation exposure and image quality with the use of attenuation-based, automated kilovolt selection. *AJNR Am J Neuroradiol.* 2014;35(2):237-41.

[111] Bongartz G, Geleijns J, Golding S, et al. European guidelines on quality criteria for computed tomography. *European Commission.* 1999.

[112] Siddiki HA, Fidler JL, Fletcher JG, et al. Prospective comparison of state-of-the-art MR enterography and CT enterography in small-bowel Crohn's disease. *AJR Am J Roentgenol.* 2009;193(1):113–21.

[113] Winklehner A, Karlo C, Puippe G, et al. Raw data-based iterative reconstruction in body CTA: evaluation of radiation dose saving potential. *Eur Radiol.* 2011;21(12):2521–6.

[114] Moneta GL, Edwards JM, Chitwood RW, et al. Correlation of North American Symptomatic Carotid Endarterectomy Trial (NASCET) angiographic definition of

70% to 99% internal carotid artery stenosis with duplex scanning. *J Vasc Surg.* 1993;17(1):152–7; discussion 157–9.

[115] Fisher M, Martin A, Cosgrove M, et al. The NASCET-ACAS plaque project. North American Symptomatic Carotid Endarterectomy Trial. Asymptomatic Carotid Atherosclerosis Study. *Stroke.* 1993;24(12 Suppl):I24–5; discussion I31–2.

[116] Gasecki AP, Hachinski VC, Mendel T, et al. Endarterectomy for symptomatic carotid stenosis. Review of the European and North American Symptomatic Carotid Surgery Trials. *Nebr Med J*. 1992;77(6):121–3.

[117] Anzidei M, Napoli A, Zaccagna F, et al. Diagnostic accuracy of colour doppler ultrasonography, CT angiography and blood-pool-enhanced MR angiography in assessing carotid stenosis: a comparative study with DSA in 170 patients. *Radiol Med.* 2012;117(1):54-71.

[118] Prokop M, Waaijer A, Kreuzer S. CT angiography ofthe carotid arteries. *JBR-BTR.* 2004;87(1):23-9.

[119] Nonent M, Ben Salem D, Serfaty JM, et al. Overestimation of moderate carotid stenosis assessed by both Doppler US and contrast enhanced 3D-MR angiography in the CARMEDAS study. *J Neuroradiol*. 2011 Jul;38(3):148-55.

[120] Makris GC, Teng Z, Patterson AJ, Lin JM, Young V, Graves MJ, Gillard JH. Advances in MRI for the evaluation of carotid atherosclerosis. *Br J Radiol.* August 2015; 88(1052): 20140282.

[121] Niesten J, van der Schaaf IC, Riordan AJ, et al. Radiation dose reduction in cerebral CT perfusion imaging using iterative reconstruction. *Eur Radiol*. 2014 Feb;24(2):484-93.

[122] Li B, Lyu Q, Ma J, Wang J. Iterative reconstruction for CT perfusion with a prior-image induced hybrid nonlocal means regularization: Phantom studies. *Med Phys.* 2016 Apr;43(4):1688.

[123] Machida H, Takeuchi H, Tanaka I, et al. Improved delineation of arteries in the posterior fossa of the brain by model-based iterative reconstruction in volume-rendered 3D CT angiography. *AJNR Am J Neuroradiol.* 2013 May;34(5):971-5.

[124] Esses D, Birnbaum A, Bijur P, Shah S, Gleyzer A, Gallagher EJ. Ability of CT to alter decision making in elderly patients with acute abdominal pain. *Am J Emerg Med* 2004;22(4):270–2.

[125] Seyal AR, Arslanoglu A, Abboud SF, Sahin A, Horowitz JM, Yaghmai V. CT of the Abdomen with Reduced Tube Voltage in Adults: A Practical Approach. *Radiographics.* 2015 Nov-Dec;35(7):1922-39.

[126] Kalra MK, Maher MM, Sahani DV, et al. Low-dose CT of the abdomen: evaluation of image improvement with use of noise reduction filters pilot study. *Radiology.* 2003 Jul;228(1):251-6.

[127] Kalra MK, Maher MM, Toth TL, et al. Comparison of Z-axis automatic tube current modulation technique with fixed tube current CT scanning of abdomen and pelvis. *Radiology.* 2004 Aug;232(2):347-53.

[128] Notohamiprodjo S, Deak Z, Meurer F, et al. Image quality of iterative reconstruction in cranial CT imaging: comparison of model-based iterative reconstruction (MBIR) and adaptive statistical iterative reconstruction (ASiR). *Eur Radiol.* 2015 Jan;25(1):140-6.

[129] Hérin E, Gardavaud F, Chiaradia M, et al. Use of Model-Based Iterative Reconstruction (MBIR) in reduced-dose CT for routine follow-up of patients with

malignant lymphoma: dose savings, image quality and phantom study. *Eur Radiol.* 2015 Aug;25(8):2362-70.

[130] Yanagawa M, Gyobu T, Leung AN, et al. Ultra-low-dose CT of the lung: effect of iterative reconstruction techniques on image quality. *Acad Radiol.* 2014 Jun;21(6):695-703.

[131] Miéville FA, Berteloot L, Grandjean A, et al. Model-based iterative reconstruction in pediatric chest CT: assessment of image quality in a prospective study of children with cystic fibrosis. *Pediatr Radiol.* 2013 Mar;43(5):558-67.

[132] Volders D, Bols A, Haspeslagh M, Coenegrachts K. Model-based iterative reconstruction and adaptive statistical iterative reconstruction techniques in abdominal CT: comparison of image quality in the detection of colorectal liver metastases. *Radiology.* 2013 Nov;269(2):469-74.

[133] Pickhardt PJ, Lubner MG, Kim DH, et al. Abdominal CT With Model-Based Iterative Reconstruction (MBIR): Initial Results of a Prospective Trial Comparing Ultralow-Dose With Standard-Dose Imaging. *AJR Am J Roentgenol.* 2012 Dec; 199(6): 1266–1274.

[134] Shuman WP, Chan KT, Busey JM, et al. Standard and reduced radiation dose liver CT images: adaptive statistical iterative reconstruction versus model-based iterative reconstruction-comparison of findings and image quality. *Radiology.* 2014 Dec;273(3):793-800.

[135] Poletti PA, Becker M, Becker CD, et al. Emergency assessment of patients with acute abdominal pain using low-dose CT with iterative reconstruction: a comparative study. *Eur Radiol.* 2017 Aug;27(8):3300-3309.

[136] Othman AE, Bongers MN, Zinsser D, et al. Evaluation of reduced-dose CT for acute non-traumatic abdominal pain: evaluation of diagnostic accuracy in comparison to standard-dose CT. *Acta Radiol.* 2017 Jan 1:284185117703152.

[137] Jackson VP, Cushing T, Abujudeh HH, et al. Rad-Peer scoring white paper. *J Am Coll Radiol* 2009; 6:21–25.

[138] Larson PA, Pyatt RS, Grimes CK, Abudujeh HH, Chin KW, Roth CJ. Getting the most out of Rad-Peer. *J Am Coll Radiol* 2011; 8:543–548

[139] Stoker J, van Randen A, Laméris W, Boermeester MA. Imaging patients with acute abdominal pain. *Radiology.* 2009 Oct;253(1):31-46.

[140] de Dombal FT. *Diagnosis of acute abdominal pain* 2nd ed. New York, NY: Churchill-Livingstone, 1991.

[141] Doria AS, Moineddin R, Kellenberger CJ, et al. US or CT for Diagnosis of Appendicitis in Children and Adults? A Meta-Analysis. *Radiology.* 2006 Oct;241(1):83-94. Epub 2006 Aug 23.

[142] MacKersie AB, Lane MJ, Gerhardt RT, et al. Nontraumatic acute abdominal pain: unenhanced helical CT compared with three-view acute abdominal series. *Radiology.* 2005 Oct;237(1):114-22.

[143]ACR appropriateness criteria, 2006. American College of Radiology Web site. https://acsearch.acr.org/docs/69467/Narrative/. Accessed November 11, 2016.

[144] Lane MJ, Liu DM, Huynh MD, Jeffrey RB Jr, Mindelzun RE, Katz DS. Suspected acute appendicitis: nonenhanced helical CT in 300 consecutive patients. *Radiology.* 1999 Nov;213(2):341-6.

[145] Laméris W, van Randen A, Bipat S, Bossuyt PM, Boermeester MA, Stoker J. Graded compression ultrasonography and computed tomography in acute

colonic diverticulitis: meta-analysis of test accuracy. *Eur Radiol.* 2008 Nov;18(11):2498-511.

[146] Megibow AJ. Bowel obstruction: evaluation with CT. *Radiol Clin North Am* 1994;32:861–870.

[147] Raman SS, Osuagwu FC, Kadell B, Cryer H, Sayre J, Lu DS . Effect of CT on false positive diagnosis of appendicitis and perforation. *N Engl J Med* 2008;358:972–973.

[148] Larson DB, Johnson LW, Schnell BM, Salisbury SR, Forman HP. National trends in CT use in the emergency department: 1995-2007. *Radiology.* 2011 Jan;258(1):164-73.

[149] Preston DL, Ron E, Tokuoka S, et al. Solid cancer incidence in atomic bomb survivors: 1958–1998. *Radiat Res* 2007; 168: 1-64.

[150] Flum DR, Morris A, Koepsell T, Dellinger EP. Has misdiagnosis of appendicitis decreased over time? A population-based analysis. *JAMA.* 2001 Oct 10;286(14):1748-53.

[151] The 2007 recommendations of the International Commission on Radiological Protection. ICRP publication 103. *Ann ICRP* 2007;37:1–332.

[152] Keyzer C, Zalcman M, De Maertelaer V, et al. Acute appendicitis: comparison of low-dose and standard-dose unenhanced multi–detector row CT. *Radiology* 2004;232:164–172.

[153] Tack D, Bohy P, Perlot I, et al. Suspected acute colon diverticulitis: imaging with low-dose unenhanced multi-detector row CT. *Radiology* 2005;237:189–196.

[154] Vardhanabhuti V, Ilyas S, Gutteridge C, Freeman SJ, Roobottom CA. Comparison of image quality between filtered back-projection and the adaptive

statistical and novel model-based iterative reconstruction techniques in abdominal CT for renal calculi. *Insights Imaging.* 2013 Oct;4(5):661-9.

[155] Fontarensky M, Alfidja A, Perignon R, et al. Reduced Radiation Dose with Model-based Iterative Reconstruction versus Standard Dose with Adaptive Statistical Iterative Reconstruction in Abdominal CT for Diagnosis of Acute Renal Colic. *Radiology.* 2015 Jul;276(1):156-66.

[156] Murphy KP, Crush L, O'Neill SB, et al. Feasibility of low-dose CT with model-based iterative image reconstruction in follow-up of patients with testicular cancer. *Eur J Radiol Open*. 2016 Jan 1;3:38-45.

[157] Levenson RB, Camacho MA, Horn E, Saghir A, McGillicuddy D, Sanchez LD.Eliminating routine oral contrast use for CT in the emergency department: impact on patient throughput and diagnosis. *Emerg Radiol.* 2012 Dec;19(6):513-7. Jun 29.

[158] Wood BP. Cystic fibrosis: 1997. *Radiology.* 1997 Jul;204(1):1-10.

[159] Weiser G, Kerem E. Early intervention in CF: how to monitor the effect. *Pediatr Pulmonol.* 2007 Nov;42(11):1002-7.

[160] Que C, Cullinan P, Geddes D. Improving rate of decline of FEV1 in young adults with cystic fibrosis. *Thorax.* 2006 Feb;61(2):155-7.

[161] De Jong PA, Lindblad A, Rubin L, et al. Progression of lung disease on computed tomography and pulmonary function tests in children and adults with cystic fibrosis. *Thorax.* 2006 Jan;61(1):80-5.

[162] Judge EP, Dodd JD, Masterson JB, Gallagher CG. Pulmonary abnormalities on high-resolution CT demonstrate more rapid decline than FEV1 in adults with cystic fibrosis. *Chest.* 2006 Nov;130(5):1424-32.

[163] De Jong PA, Nakano Y, Lequin MH, et al. Progressive damage on high resolution computed tomography despite stable lung function in cystic fibrosis. *Eur Respir J.* 2004 Jan;23(1):93-7.

[164] Maisonneuve P, Marshall BC, Knapp EA, Lowenfels AB. Cancer risk in cystic fibrosis: a 20-year nationwide study from the United States. *J Natl Cancer Inst.* 2013 Jan 16;105(2):122-9.

[165] MacKenzie T, Gifford AH, Sabadosa KA, et al. Longevity of patients with cystic fibrosis in 2000 to 2010 and beyond: survival analysis of the Cystic Fibrosis Foundation patient registry. *Ann Intern Med.* 2014 Aug 19;161(4):233-41.

[166] Huda W. Radiation doses and risks in chest computed tomography examinations. *Proc Am Thorac Soc.* 2007 Aug 1;4(4):316-20.

[167] Allen BC, Baker ME, Einstein DM et al. Effect of altering automatic exposure control settings and quality reference mAs on radiation dose, image quality, and diagnostic efficacy in MDCT enterography of active inflammatory Crohn's disease. *AJR. American journal of roentgenology.* 2010;195(1):89–100.

[168] Li J, Udayasankar UK, Toth TL, Seamans J, Small WC, Kalra MK. Automatic patient centering for MDCT: effect on radiation dose. *AJR Am J Roentgenol.* 2007 Feb;188(2):547-52.

[169] Mettler FA Jr, Huda W, Yoshizumi TT, Mahesh M. Effective doses in radiology and diagnostic nuclear medicine: a catalog. *Radiology.* 2008 Jul;248(1):254-63.

[170] Ramsey BW, Davies J, McElvaney NG, et al; VX08-770-120 Study group. A CFTR potentiator in patients with cystic fibrosis and the G551D mutation. *N Engl J Med.* 2011 Nov 3;365(18):1663-72.

[171] Davies JC, Wainwright CE, Canny GJ, et al; VX08-770-103 (ENVISION) Study Group. Efficacy and safety of ivacaftor in patients aged 6 to 11 years with cystic fibrosis with a G551D mutation. *Am J Respir Crit Care Med.* 2013 Jun 1;187(11):1219-25.

[172] Barry PJ, Plant BJ, Nair A, et al. Effects of ivacaftor in patients with cystic fibrosis who carry the G551D mutation and have severe lung disease. *Chest.* 2014 Jul;146(1):152-8.

[173] Cystic Fibrosis Foundation. Cystic Fibrosis Foundation Patient Registry. Bethsesda, MA: Cystic Fibrosis Foundation; 2013.

[174] Qi LP, Li Y, Tang L, et al. Evaluation of dose reduction and image quality in chest CT using adaptive statistical iterative reconstruction with the same group of patients. *Br J Radiol.* 2012 Oct;85(1018):e906-11.

[175] Prakash P, Kalra MK, Ackman JB, et al.Diffuse lung disease: CT of the chest with adaptive statistical iterative reconstruction technique. *Radiology.* 2010 Jul;256(1):261-9.

[176] Miéville FA, Berteloot L, Grandjean A, et al. Model-based iterative reconstruction in pediatric chest CT: assessment of image quality in a prospective study of children with cystic fibrosis. *Pediatr Radiol.* 2013 Mar;43(5):558-67.

[177] Neroladaki A, Botsikas D, Boudabbous S, Becker CD, Montet X. Computed tomography of the chest with model-based iterative reconstruction using a radiation exposure similar to chest X-ray examination: preliminary observations. *Eur Radiol.* 2013 Feb;23(2):360-6.

[178] Bhalla M, Turcios N, Aponte V, et al. Cystic fibrosis: scoring system with thin-section CT. *Radiology.* 1991 Jun;179(3):783-8.

[179] Carmichael JHE, Maccia C, Moores BM, et al. European Guidelines on Quality Criteria for Diagnostic Radiographic Images (1996). EUR16260. Luxembourg.

[180] Donadieu J, Roudier C, Saguintaah M, Maccia C, Chiron R. Estimation of the radiation dose from thoracic CT scans in a cystic fibrosis population. *Chest.* 2007 Oct;132(4):1233-8.

[181] Sanders DB, Zhanhai Li, Brody AS, Farrell PM. Chest computed tomography scores of severity are associated with future lung disease progression in children with cystic fibrosis. *Am J Respir Crit Care Med.* 2011 Oct 1; 184(7): 816–821.

[182] Assael BM, Castellani C, Ocampo MB, Iansa P, Callegaro A, Valsecchi MG. Epidemiology and survival analysis of cystic fibrosis in an area of intense neonatal screening over 30 years. *Am J Epidemiol*. 2002 Sep 1;156(5):397-401.

[183] Itoh S, Ikeda M, Arahata S, Kodaira T, Isomura T, Kato T, et al. Lung cancer screening: minimum tube current required for helical CT. *Radiology* 2000; 215: 175-183

[184]Laqmani A, Buhk JH, Henes FO, Klink T, Sehner S, von Schultzendorff HC, et al. Impact of a 4th generation iterative reconstruction technique on image quality in low-dose computed tomography of the chest in immunocompromised patients. *Rofo* 2013; 185: 749-757.

[185] Kalra MK, Woisetschläger M, Dahlström N, Singh S, Digumarthy S, Do S, Pien H, Quick P, Schmidt B, Sedlmair M, Shepard JA, Persson A. Sinogram-affirmed iterative reconstruction of low-dose chest CT: effect on image quality and radiation dose. *AJR Am J Roentgenol* 2013; 201: W235-W244.

[186] Katsura M, Matsuda I, Akahane M, et al. Model-based iterative reconstruction technique for radiation dose reduction in chest CT: comparison with the adaptive statistical iterative reconstruction technique. *Eur Radiol.* 2012 Aug;22(8):1613-23.

[187] Loeve M, Lequin MH, de Bruijne M, et al. Cystic fibrosis: are volumetric ultra-low-dose expiratory CT scans sufficient for monitoring related lung disease? *Radiology.* 2009 Oct;253(1):223-9

[188] Li AM, Sonnappa S, Lex C, et al. Non-CF bronchiectasis: does knowing the aetiology lead to changes in management*? Eur Respir J.* 2005 Jul;26(1):8-14.

[189] ESR statement on radiation protection: globalisation, personalised medicine and safety (the GPS approach). *Insights Imaging.* 2013 Dec;4(6):737–9.

[190] McCollough CH, Chen GH, Kalender W, Leng S, Samei E, Taguchi K, et al. Achieving routine submillisievert CT scanning: report from the summit on management of radiation dose in CT. *Radiology.* Radiological Society of North America, Inc.; 2012 Aug 1;264(2):567–80.

[191] CORK Study in Cystic Fibrosis: Sustained Improvements in Ultra-Low-Dose Chest CT Scores After CFTR Modulation With Ivacaftor. Ronan NJ, Einarsson GG, Twomey M, et al. *Chest.* 2017 Oct 14. pii: S0012-3692(17)32896-9.

[192] Patino M, Fuentes JM, Hayano K, Kambadakone AR, Uyeda JW, Sahani D V. A quantitative comparison of noise reduction across five commercial (hybrid and model-based) iterative reconstruction techniques: an anthropomorphic phantom study. *AJR Am J Roentgenol.* 2015 Feb;204(2):W176–83.

[193] Tilley S, Siewerdsen JH, Stayman JW. Model-based iterative reconstruction for flat-panel cone-beam CT with focal spot blur, detector blur, and correlated noise.

Phys Med Biol. 2016 Jan 7;61(1):296-319

[194] Padole A, Singh S, Lira D, Blake MA, Pourjabbar S, Khawaja RDA, et al. Assessment of Filtered Back Projection, Adaptive Statistical, and Model-Based Iterative Reconstruction for Reduced Dose Abdominal Computed Tomography. *J Comput Assist Tomogr.* 2015 Mar 27;39(4):462–7.

[195] Lönnroth N, Hirvonen-Kari M, Timonen M, Savolainen S, Kortesniemi M. Transition in occupational radiation exposure monitoring methods in diagnostic and interventional radiology. *Radiat Prot Dosimetry.* 2012 Aug;151(1):58-66.